Universidad del País Vasco
Euskal Herriko Unibertsitatea

Cosmology in an accelerated universe: observations and phenomenology

Irene Sendra Server

Ph.D. Thesis
Department of Theoretical Physics and History of Science
University of the Basque Country (UPV/EHU)
Leioa, May 2012

eman ta zabal zazu

Universidad del País Vasco
Euskal Herriko Unibertsitatea

Department of Theoretical Physics and History of Science

Cosmology in an accelerated universe: observations and phenomenology

Supervised by Professor Ruth Lazcoz Sáez
from the University of the Basque Country

Submitted by Irene Sendra Server
for the degree of Doctor of Physics

Als meus pares.

... i endevinar cavalls i temporals llunyans;
aclarir, destriar, amb l'orella apegada,
aplicada a la terra, la pobra i bruta terra,...

Vicent Andrés Estellés
Llibre de meravelles

"Bon guaret, fa bona collita"

Dita popular

ACKNOWLEDGEMENTS

This thesis is based on the research carried out at the Department of Theoretical Physics and History of Science at the University of the Basque Country during the years 2008-2012 with the financial support of the Ph.D. FPI fellowship contract from the Spanish Ministry of Economy and Competitiveness (BES-2008-005967) linked to the research project FIS2007-61800.

It is almost four years since I began to work on this Ph.D. thesis. It has been a long journey through the bizarre world of cosmology. During these years, I have had the chance to meet many people who have helped me in many different ways towards the completion of this thesis. Their encouragement and advice have allowed me to find the correct way and go ahead all the time. For that reason, I would like to express my deepest gratitude to each of them and make them participate in this moment.

First of all, I want to thank the person who has really made this possible, my supervisor **Ruth Lazkoz**. She has became an irreplaceable guide and friend during these years. Thanks Ruth for the patience, support and all the confidence and faith you have put on me. We both know that a PhD is not exactly a bed of roses, but with your courage you have taught me how to *break the back of the beast*.

I thank all members of the Department for their support and pleasant working atmosphere: **Juan M. Aguirregabiria**, **Igor Bandos**, **Montserrat Barrio**, **Alberto Chamorro**, **Iñaki Garay**, **Luis Herrera**, **Philipp Hyllus**, **Michele Modugno**, **Martín Rivas**, **Gunar Schnell**, **José M. Martín Senovilla**, **Géza Tóth**, **Manuel Á. Valle** and **Lianao Wu**. Specially, I would like to thank **Jon Urrestilla** for his good advices and fruitful discussions in the last stages of this thesis, and for giving me the opportunity to collaborate with him and his student **Joanes Lizarraga**; I thank **Raül Vera** because without his master classes on Linux this Ph.D. would not be the same. I am also grateful to **Alexander Feinstein** and **Íñigo L. Egusquiza** for their assistance with my teaching duties and to **Jesús Ibáñez** for his help with my fellowship. Finally, my most sincere thanks to **Vincenzo Salzano** who has been like an *elder brother* to me.

An special mention to **Tom Broadhurst**, **Jose Maria Diego** and **Adi Zitrin** who have introduced me to the field of Gravitational Lensing and specially for their patience during these last months, when I had no choice but to leave our collaborations aside for a while to focus on writing up the present thesis.

I am also grateful to the **Astrophysics Department** of the **University of Oxford**, specially to **Joseph Silk** and **Johanna Dunkley**, for giving me the chance of visiting them and for their help during and after my stay there. I would also like to mention my collaborators: **Luis. P. Chimento** and **Tristan L. Smith**.

I thank the referees of this thesis, **Roy Marteens** and **Jailson Alcaniz**, for the careful reading of the manuscript, and the members of the jury for accepting to come at the end of July when everybody is thinking of summer holidays.

On the other hand, I would like to express my deepest gratitude to my Ph.D. comrades-in-arms who have accompanied me along this adventure. In descending order of seniority I would like to mention **Iñigo Urizar**, **Giussepe Vitagliano**, **Carlos Meliveo**, **Borja Reina** and our last signings **Kepa Sousa** and **Lluc García**, for their comprehension in my moments of rush, for encouraging me during the hard times, for the *forced* breaks, for our countless, enjoyable and enlightening discussions and confessions and basically, for all the complicity. I will miss our music lists, *cierra la puerta, tengo algo que contar*, our battles to open or close the window and to decide where we should go for lunch. For all these and many other things, thank you very much, you have became really good friends. At this point, I would also like to name my colleagues **Cristina Fernández**, **Sebastian Pérez** and **Daniel Albornoz** for our good times together in Oxford.

També voldria agrair als majors "responsables" del meu interès en la física i la ciència: els meus professors de l'institut: Ferran i Mila; i aquells que a través del entusiasme pel seu treball, augmentaren la meva curiositat i les ganes d'aprendre, i m'introduïren en el món de la investigació, els meus **professors de la Universitat de València***: Vicent Martínez-Sancho, Ramon Lapiedra, Núria Rius, Toni Font, Joan Josep Ferrando, Miguel Portilla i Antonio Morales entre d'altres.*

I com no, no vull deixar d'agrair el suport incondicional de les meves amigues i els meus amics, **Rosa**, **Mònica**, **Àngela**, **David** *i* **Sergi**, *que malgrat estar lluny, la nostra amistat no s'ha perdut i sempre han estat al meu costat, tant els bons com no tan bons moments.*

Finalment, vull donar les gràcies a aquells que porten més temps aguantant-me i animant-me en tot allò que he fet, la **meva família***: els meus avis, cosins, oncles, i al* **meu germà Vicent**, *que ha demostrat tindre una paciència enorme amb mi. Ell sap ben bé "lo pudenta" que puc arribar a ser. I especialment,* **als meus pares, Vicent i Mari**, *que m'han donat tota l'educació, suport i força necessaris per a arribar on sóc. I que sobretot, m'han transmès a través del seu exemple, principis com l'esforç i la constància. A més, han sabut mostra-me allò que és important en cada moment. Es per això i molt més els dedique aquesta tesi, s'ho mereixen. I a tu* **Iker**, *que durant aquests 4 anys de tesis, has estat un pilar fonamental en el que recolzar-me. Has estat al meu costat de manera incondicional, has rellegit els meus treballs, m'has acompanyat allà on fora i m'has animat en aquells moments que més ho he necessitat, gràcies.*

RESUMEN

El término cosmología que proviene del griego *cosmos* (orden), y *loguía* (tratado, estudio), abarca el estudio del universo en su totalidad: su origen, su evolución y su estructura actual. En sus orígenes, se trataba de una ciencia prácticamente especulativa, ya que las limitaciones instrumentales reducían las observaciones a unas pocas. En esos primeros pasos hacia un primer modelo cosmológico, se adoptaron unos principios para que sirvieran de guía. Actualmente, la cosmología moderna, también se basa en la asunción de dos principios básicos: el Principio Cosmológico y el Principio Copernicano. Estos principios ayudan a simplificar el problema y establecen que a escalas suficientemente grandes el universo es homogéneo e isótropo, es decir, el universo es idéntico en todas partes y en todas las direcciones del espacio. Aunque a pequeña escala sabemos que no es así, ya que gran parte de la materia del universo se encuentra agrupada en planetas, estrellas, galaxias y otras estructuras más grandes, cuando se considera en promedio, a escalas grandes, la distribución de las galaxias y las agrupaciones de éstas es uniforme.

Con el tiempo y debido al progreso tecnológico, el número y la calidad de las observaciones aumentó, dando lugar a notables descubrimientos que cambiaron por completo la concepción del universo y revolucionaron el campo de la cosmología, como:

- El descubrimiento por parte de E. Hubble en 1929 de la expansión del universo.
- La primera medición del fondo cósmico de microondas (FCM) que obtuvieron de manera accidental Penzias y Wilson en 1965 y que ayudó a probar la isotropía del universo y la idea de Big-Bang.
- La observación de la reciente expansión acelerada del universo a través de la observación de las Supernovas en 1998 por parte de los grupos *Supernova Cosmology Project* y *High-Z Supernova Search Team* liderados por Saul Perlmutter, Brian P. Schmidt y Adam G. Riess, galardonados con el Premio Nobel de Física en 2011.

En las últimas décadas la cosmología ha experimentado notables avances como consecuencia del desarrollo de nuevos experimentos que nos han abastecido con precisos datos observacionales. La calidad de estos datos ha permitido construir una imagen global del universo actual; un universo acelerado compuesto principalmente por materia oscura ($\sim 23\%$),

distinta a la materia ordinaria ($\sim 5\%$), y energía oscura ($\sim 70\%$), la componente del universo que contrarrestaría el efecto gravitatorio y explicaría la expansión acelerada de éste. Con la existencia de estas dos principales componentes se puede explicar la situación actual del universo y los fenómenos que tienen lugar en él. Sin embargo, su naturaleza es todavía un misterio, por lo que nos encontramos ante un largo y apasionante camino que recorrer.

Después de la evidencia empírica acerca de la expansión acelerada del universo y de la necesidad de un modelo teórico que la explicara, se introdujo una constante, llamada constante cosmológica, en las ecuaciones de Einstein para poder dar una explicación a esta aceleración reciente. Por lo tanto, este modelo, conocido como ΛCDM, que corresponde a un universo compuesto principalmente por materia oscura y que explica la aceleración con la presencia de una constante cosmológica Λ, se ha convertido en el modelo estándar debido a su simplicidad y concordancia con los datos observacionales. Sin embargo, hay algunos puntos que todavía no puede explicar. Estas deficiencias teóricas han dado lugar a la aparición de modelos alternativos, como puede ser una energía oscura dinámica, es decir, que pueda evolucionar lentamente con el tiempo.

Es en este contexto donde se enmarca el trabajo presentado en esta tesis, cuyo principal objetivo es ir más allá y obtener algunas pistas nuevas sobre la naturaleza de la energía oscura. Las investigaciones llevadas a cabo durante esta tesis tratan de hacer frente a este sector 'oscuro" desde varias perspectivas, combinando la teoría y el análisis de datos astronómicos.

En el primer capítulo se presenta una introducción detallada a la cosmología en un universo acelerado, tanto desde un punto de vista teórico como observacional. Esta introducción se basa en diferentes libros de texto y artículos que se detallan en cada uno de los apartados.

Como primera aproximación al sector "oscuro", en el capítulo 2 se describe un nuevo modelo basado en una acción de Dirac-Born-Infeld para la unificación de la materia oscura y energía oscura. El estudio de este nuevo modelo se aborda tanto desde el punto de vista teórico como observacional. En primer lugar, se investiga su comportamiento de fondo a tiempos tempranos y tardíos. En este sentido, se demuestra que el modelo propuesto imita la materia a tiempos tempranos y que se recupera un régimen de Sitter en los últimos momentos. La validez de este modelo unificado se ve reforzada por su capacidad para crear estructuras, estudio que se lleva a cabo a través de un análisis perturbativo. Seguidamente, se presentan los resultados obtenidos a partir del análisis bayesiano. Éste nos permite establecer las restricciones observacionales sobre los parámetros del modelo que imponen las Supernovas de tipo Ia, el fondo de microondas y las oscilaciones acústicas de los bariones. Desde el punto de vista observacional, este modelo se ajusta mejor a las observaciones que el más popular de los modelos que unifican el sector oscuro: el gas de Chaplygin . Los resultados obtenidos en este trabajo indican una preferencia del modelo respecto al modelo tan ampliamente aceptado como es ΛCDM (constante cosmológica). El resultado más sorprendente es que el mejor ajuste corresponde un comportamiento fantasma, $w \leq -1$, conseguido sin añadir, explícitamente, una componente fantasma en el modelo. Finalmente, los resultados obtenidos del estudio del modelo desde diferentes ángulos demuestran que este modelo representa una buena alternativa para la unificación de la materia y la energía oscura y, sugiere que debe explorarse para su generalización. Probablemente, relajando la suposición que se ha hecho de que el lagrangiano sea puramente cinético e introduciendo algunos

grados de libertad más, se obtendría un modelo aún más acorde con las observaciones astronómicas. El trabajo presentado en este capítulo está basado en el siguiente artículo:

- **DBI models for the unification of dark matter and dark energy**
  L. P. Chimento, R. Lazkoz, I. Sendra, *Gen. Rel. Grav. 42 (2010) 1189-1209*.

En los capítulos 3 y 4 se detallan los resultados obtenidos cuando realizamos un análisis observacional de diferentes parametrizaciones de la ecuación de estado de la energía oscura. En concreto, en el capítulo 3, se estudia la posibilidad de detectar patrones oscilantes en la ecuación de estado de la energía oscura haciendo uso de distintos conjuntos de datos cosmolgicos. Para ello se da enfoque fenomenológico a la situación de manera que se estudian tres modelos distintos de oscilación de la ecuación de estado: uno de ellos periódico y los otros dos, propuestos aquí por primera vez, con una cierta amortiguación. Todos estos modelos se caracterizan por su amplitud, su valor central, y la frecuencia de las oscilaciones. Al contrario de lo que ocurre en otros trabajos anteriores, el valor del frecuencia no se fija a un valor fiduciario en relación con la extensión de tiempo de los conjuntos de datos elegidos, sino que se considera un conjunto discreto de valores con la intención de evitar cualquier arbitrariedad y, de esa manera, tratar de detectar cualquier período de tiempo posible en la ecuación de estado. Los modelos se prueban con una colección reciente de Supernovas de tipo Ia, mediciones directas de la constante de Hubble y de datos observacionales pertenecientes a explosiones de rayos gamma. Estas dos últimas mediciones, representan un novedad en este tipo de trabajos, ya que amplían el rango de distancias en las que detectar el comportamiento oscilatorio. Los principales resultados obtenidos son los siguientes:

I Aunque las restricciones sobre la amplitud no son demasiado fuertes, se detecta una tendencia de la misma en comparación con la frecuencia, es decir, una disminución de las amplitudes a medida que las frecuencias crecen.

II El centro de oscilación (que corresponde al valor actual de la ecuación de estado) está muy bien delimitado, además, de que el comportamiento fantasma queda excluido en 1σ, aparece la misma tendencia que muestra la amplitud con la frecuencia.

III Resulta difícil acotar el mejor valor para la frecuencia, ya que todos los valores de la serie discreta elegida muestran la misma validez estadística. Sin embargo, el mejor ajuste corresponde a un período que se encuentra en el rango de *redshifts* cubierto por los datos cosmológicos usados. Si comparamos los "mejores" modelos de oscilación obtenidos con ΛCDM haciendo uso de un criterio de información basado en la estadística bayesiana, la conclusión que se obtiene es que no existe ninguna evidencia significativa que se oponga a un modelo de energía oscura oscilante.

Los resultados obtenidos en este capítulo han sido publicados en:

- **Oscillations in the dark energy EoS: new MCMC lessons**
  R. Lazkoz, V. Salzano, I. Sendra, *Phys. Lett. B694 (2010) 198-208*.

Siguiendo la misma línea que el capítulo anterior, en el capítulo 4 con el fin de sacar el máximo provecho de los parámetros que nos definen la ecuación de estado de la energía oscura y de los datos observacionales de los que disponemos, se sugieren dos nuevas parametrizaciones de la ecuación de estado de la energía oscura. Esta vez, el principal objetivo es obtener una ecuación de estado cuyos parámetros estén mínimamente correlacionados y que, al mismo tiempo, representen una modificación mínima de ΛCDM. Las parametrizaciones propuestas se basan en una expansión a segundo orden de los polinomios convencionales y los de Chebyshev escritas en términos de los valores de la ecuación de estado en $z = 0$ y $z = 0.5$, que tienen una correlación baja y que, naturalmente, han mostrado ya ha mejora respecto a la popular parametrización de Chevallier-Polarski-Linder (CPL). Las pruebas astronómicas usadas en este trabajo corresponden a las observaciones recientes de Supernovas y las escalas típicas de las oscilaciones barionicas. Sin embargo, con la intención de deducir cuál será la mejora que nos darán los futuros experimentos, se han obtenido datos simulados del experimento EUCLID. De acuerdo con el criterio de desviación de información bayesiano (DIC), que penaliza los errores grandes y las correlaciones entre los parámetros, los nuevos modelos propuestos funcionan mejor que la famosa parametrización de la ecuación de estado, CPL, y su re-parametrización propuesta por Wang (en términos de $z = 0$ y $z = 0.5$). Esto es debido a la combinación de una correlación más baja y de unos errores relativos en los parámetros más pequeños. Lo mismo ocurre desde el punto de vista frecuentista, que muestra una Figura de Mérito mayor para las nuevas parametrizaciones. El trabajo presentado en este capítulo se basa en el publicado en:

- **SN and BAO constraints on (new) polynomial dark energy parametrizations: current results and forecasts**
  I. Sendra and R. Lazkoz, *Mont. Not. Roy. Astron. Soc. 422 (2012) 776-793*.

Otro reto emocionante en cosmología es descifrar cómo era el universo en sus primeras etapas. El FCM nos proporciona un ventana directa a esta época, ya que nos permite obtener información detallada de cada uno de los componentes del universo en esos primeros instantes de su historia. Este conocimiento, nos ayuda en gran medida a mejorar la comprensión sobre la evolución posterior del universo. Por lo tanto, es extremadamente importante conseguir una explicación detallada de cada uno de los componentes en estas primeras etapas. Y es justo éste uno de los propósitos del último trabajo presentado en esta tesis.

El FCM es la reliquia que nos llega de la radiación del universo temprano, y nos proporciona información sobre la densidad total de radiación alrededor del momento de desacoplo de los fotones, cuando se produjo el FCM. En esa época, los neutrinos representaban una fracción significativa de la densidad de energía de la radiación. Si asumimos que hay tres tipos de neutrinos, cualquier exceso en la medida del número efectivo de neutrinos, $N_{\rm eff}$, nos indicaría la existencia de una componente relativista adicional. Las medidas actuales del FCM muestran una ligera preferencia por $N_{\rm eff} > 3$ a un 95% de intervalo de confianza (I.C).

Este exceso en el número efectivo de neutrinos, se puede interpretar como la contribución de ondas gravitacionales primordiales con frecuencias superiores a $\sim\ 10^{-15}$Hz al FCM. Si consideramos que este fondo cosmológico de ondas gravitatorias se produjo bajo condiciones iniciales adiabáticas, sus efectos sobre el FCM y el espectro de potencias de materia imitaría

al producido por neutrinos sin masa. Sin embargo, con condiciones iniciales homogéneas, tal y como uno podría esperar de ciertos modelos de la inflación, modelos de pre Big-Bang, transiciones de fases u otros escenarios, el efecto sobre el FCM sería distinto. En el último capítulo de esta tesis, establecemos restricciones observacionales sobre el número efectivo de neutrinos. Para ello hemos utilizado los últimos datos del FCM procedentes de *WMAP7-year* y del *South Pole Telescope*. Estos límites se convierten en restricciones sobre la densidad energía del fondo cosmológico de ondas gravitacionales para los dos conjuntos de condiciones iniciales: adiabáticas y homogéneas. Incluyendo los datos de *South Pole Telescope* a pequeñas escalas se obtiene, en el caso adiabático, una mejora sobre la densidad de energía del fondo cosmológico de ondas gravitacionales de un factor 1.7 respecto $10^6\Omega_{gw} < 8.7$ a un 95% de I.C. Bajo estas condiciones iniciales, las cuerdas cósmicas podrían generar esta componente de las ondas gravitacionales, de manera que el límite sobre Ω_{gw} se puede convertir en un límite superior sobre la tensión de la cuerda, obteniendo $G_\mu < 2 \times 10^{-7}$ en 95% de I.C. En el caso homogéneo, la mejora es de un factor 3.5 sobre $10^6\Omega_{gw} < 1.0$ en 95% de I.C., esta vez, sin ninguna evidencia observacional sobre la existencia de un componente extra en la radiación. Este trabajo representa la primera vez en que se establece un límite sobre la tensión de las cuerdas cósmicas, G_μ, a partir de las restricciones obtenidas sobre el fondo cosmológico de ondas gravitacionales provenientes del exceso en el número efectivo de neutrinos. Como las cuerdas cósmicas también contribuyen al espectro de potencias del FCM, una extensión interesante de este trabajo sería investigar cuáles serían las nuevas limitaciones sobre $N_{\rm eff}$ o Ω_{gw} teniendo en cuenta tanto la contribución de cuerdas y como el número efectivo de neutrinos. Este capítulo se basa en el trabajo descrito en el artículo:

- **Updated constraints on the primordial GW background using the latest CMB data**
  I. Sendra and T. Smith, *Aceptado en Phys. Rev. D, para ser publicado en Junio del 2012 (arXiv:1203.4232)*.

PROLOGUE

Cosmology has experienced remarkable advances in the last decades as a consequence of the development of new experiments which have provided very accurate observations. The quality of these data has allowed to construct a global concordance picture of the Universe: an accelerated universe with a sub-critical mass content. This speed up of the Universe can be explained with the presence of an exotic component (dark energy) which counteracts the attractive effect of gravity. However, its nature is still unknown and progress has to be done to uncover it. Thus, the work carried out in this thesis tries to address this dark sector from several perspectives, combining the theory on cosmology and the analysis of astronomical data.

In the first chapter I present a detailed introduction to the cosmology in an accelerated universe, both on the theoretical and observational context. This introduction is based on different books, articles and reviews as it will be detailed.

Chapter 2 describes a model based on a Dirac-Born-Infeld action for the unification of dark matter and dark energy which is supported by the results of the study of its background behaviour at early and late times, and reinforced by the analysis of the evolution of perturbations. A Bayesian analysis is performed to set observational constraints on the model parameters using Type Ia Supernovae, Cosmic Microwave Background shift and Baryon Acoustic Oscillations data. Finally, to complete the study, the model kinematics, such as the effective equation of state parameter, the acceleration parameter and the transition redshift, are also investigated. This chapter is based on the article:

- **DBI models for the unification of dark matter and dark energy**
  L. P. Chimento, R. Lazkoz, I. Sendra, *Gen. Rel. Grav. 42 (2010) 1189-1209*.

The possibility of detecting oscillating patterns in the dark energy equation of state is studied in Chapter 3 using different cosmological datasets. A phenomenological approach is followed and three different oscillating models for the EoS are studied: one of them periodic and the other two, proposed here for the first time, with a certain damping. All these models are characterised by the amplitude value, their central value, and the frequency of the oscillations. In contrast to previous works in literature, the value of the frequency is not

fixed to a fiducial value related to the time extension of chosen datasets, but a discrete set of values is considered instead to avoid arbitrariness and try to detect any possible time period in the EoS. The models are tested using a recent collection of Type Ia Supernovae, direct Hubble data and Gamma Ray Bursts data. The results obtained in this chapter have been published in:

- **Oscillations in the dark energy EoS: new MCMC lessons**
  R. Lazkoz, V. Salzano, I. Sendra, *Phys. Lett. B694 (2010) 198-208*.

Then two new polynomial parametrizations of dark energy and their informative properties are presented in Chapter 4. The parameters to fit are the equation of state values at $z = 0$ and $z = 0.5$, which have naturally low correlation and have already been shown to improve the popular Chevallier-Polarski-Linder (CPL) parametrization. These models are tested with low redshift astronomical probes: Type Ia Supernovae and Baryon Acoustic Oscillations (BAO), in the form of both current and synthetic data. Specifically, simulations of measurements of the radial and transversal BAO scales similar to those expected in a BAO high precision spectroscopic redshift survey similar to EUCLID are disussed. The work presented in this chapter is based in that published in:

- **SN and BAO constraints on (new) polynomial dark energy parametrizations: current results and forecasts**
  I. Sendra and R. Lazkoz, *Mont. Not. Roy. Astron. Soc. 422 (2012) 776-793*.

Another exciting challenge in Cosmology is to decipher how the Universe was in its first stages. The Cosmic Microwave Background (CMB) provides a clear window into this epoch, and allows us to obtain information of each of the components of the Universe. This may impove our understanding of later evolution. Therefore, it is crucial at this stage to have a detailed explanation of each of the components, being it one of the purposes of the last work presented in this thesis.

The CMB is the relic of the radiation of the early stages of the Universe that reaches us. It is affected by the total radiation density around the time of decoupling, when it was produced. At that epoch, neutrinos comprised a significant fraction of the radiative energy, but there could also be a contribution from primordial gravitational waves with frequencies greater than $\sim 10^{-15}$Hz. If this Cosmological Gravitational Wave Background were produced under adiabatic initial conditions, its effects on the CMB and matter power spectrum would mimic non-interacting massless neutrinos. However, with homogenous initial conditions, as one might expect from certain models of inflation, pre big-bang models, phase transitions and other scenarios, the effect on the CMB would be distinct. In Chapter 5 updated observational bounds are presented for both sorts of initial conditions using the latest CMB data at small scales from the South Pole Telescope (SPT) in combination with that provided by the Wilkinson Microwave Anisotropy Probe (WMAP), current measurements of the BAO, and the Hubble parameter. For the adiabatic case, the constraint obtained is converted into an upper limit on the tension of horizon-sized cosmic strings that could explain the production

of this primordial gravitational wave component. This chapter is based on the work detailed in the recently accepted article:

- **Updated constraints on the primordial GW background using the latest CMB data**
  I. Sendra and T.Smith, *Accepted in Phys. Rev. D, to be publish in June 2012 (arXiv:1203.4232)*.

LIST OF PUBLICATIONS

Published Papers

DBI models for the unification of dark matter and dark energy
L. P. Chimento, R. Lazkoz, I. Sendra, *Gen. Rel. Grav. 42 (2010) 1189-1209*.

Oscillations in the dark energy EoS: new MCMC lessons
R. Lazkoz, V. Salzano, I. Sendra, *Phys. Lett. B694 (2010) 198-208*.

Tension between SN and BAO: current status and future forecasts
C. Escamilla-Rivera, R. Lazkoz, V. Salzano, I. Sendra, *JCAP 1109 (2011) 003*.

SN and BAO constraints on (new) polynomial dark energy parametrizations: current results and forecasts
I. Sendra and R. Lazkoz, *Mont. Not. Roy. Astron. Soc. 422 (2012) 776-793*.

Measuring large-scale structure with quasars in narrow-band filter surveys
L. R. Abramo, M. A. Strauss, M. Lima, C. Hernandez-Monteagudo, R. Lazkoz, M. Moles, C. M. de Oliveira, I. Sendra, L. Sodre, *Accepted in Mont. Not. Roy. Astron. Soc. (arXiv:1108.2657)*.

Updated constraints on the primordial GW background using the latest CMB data
I. Sendra and T. Smith, *Accepted in Phys. Rev. D (arXiv:1203.4232)*.

Submitted Papers

Revisiting a model-independent reconstruction method of dark energy
R. Lazkoz, V. Salzano, I. Sendra, *Submitted to Phys. Lett. B (arXiv:1202.4689)*.

CLASH: Mass Distribution in and around MACS J1206.2-0847 from a Full Cluster Lensing Analysis
K. Umetsu, E. Medezinski, M. Nonino, J. Merten, A. Zitrin, A. Molino, C. Grillo, M. Carrasco, M. Donahue, A. Mahdavi, D. Coe, M. Postman, A. Koekemoer, N. Czakon, J. Sayers, T. Mroczkowski, S. Golwala, P. M. Koch, K. Lin, S. M. Molnar, P. Rosati, I. Balestra, A. Mercurio, M. Scodeggio, A. Biviano, T. Anguita, L. Infante, G. Seidel, **I. Sendra**, S. Jouvel, O. Host, D. Lemze, T. Broadhurst, M. Meneghetti, L. Moustakas, M. Bartelmann, N. Benitez, R. Bouwens, L. Bradley, H. Ford, Y. Jimenez-Teja, D. Kelson, O. Lahav, P. Melchior, J. Moustakas, S. Ogaz, S. Seitz, W. Zheng, *Submitted to Astroph. Journal (arXiv:1204.3630)*.

Proceedings

DBI models for the unification of dark matter and dark energy
L.P. Chimento, R. Lazkoz, I. Sendra, *J. Phys. Conf. Ser. 229 (2010) 012068*.

DBI models for the unification of dark matter and dark energy
L. P. Chimento (Buenos Aires U.), R. Lazkoz, I. Sendra, *AIP Conf. Proc. 1241 (2010) 776-783*.

CONTENTS

LIST OF FIGURES

LIST OF TABLES

CHAPTER 1

INTRODUCTION

1.1 An expanding homogeneous and isotropic universe

Whenever a new field is explored in Science without any previous hints from observations or experiments that can provide a guide, some principles need to be adopted in the first trail towards a compelling theory that will give us the demanded understanding of the new phenomenon. These principles will be of help if they simplify the problem, reducing the numbers of degree of freedoms as it occurs with postulates related to symmetries. This is exactly what happened at the beginning of the last century with the first attempts to construct a cosmological model. One of the central pillars of these models was the "Cosmological Principle", which states that at sufficiently large scales, the Universe is homogeneous and isotropic. Homogeneity concerns an identical universe everywhere in space, while with isotropy one understands that the Universe looks the same in every direction. This principle is not exact, since much of the Universe's matter is found clustered together in planets, stars, galaxies, and larger structures, but when considered on average, the distribution of galaxies and clusters is uniform on large scales.

A good evidence of isotropy in the Universe was obtained in 1965, when Penzias and Wilson [204] observed a microwave radiation coming from all directions of the sky with a black body spectrum at a temperature around 3.5K. This accidental discovery became one of the most powerful pieces to support not only the hot Big Bang origin of the Universe, but also the best evidence for the Cosmological Principle. Even so, isotropy does not necessarily imply homogeneity without the previous assumption of the "Copernican Principle". Named after N. Copernicus, this principle postulates that there is no special location in the Universe. In this case, isotropy also involves homogeneity. As our location in the Universe is not privileged, if we obtain the same observations in every direction we look, we will do so in any other location, thus the Universe is also homogeneous. Later observations of the Universe at large scales such as galaxy distribution are also consistent with an homogeneous and isotropic structure.

Another breakthrough of the last century for cosmology was the observation of the

universe expansion. In 1914, V. M. Slipher, through his observations of the radial velocities of galaxies by measuring their Doppler shift of the spectral lines, discovered that most of them were redshifted. In his work "Spectrographic observations of nebulae" [250] he announced that almost all the galaxies he had observed where moving away from Earth, except for Andromeda, that was moving toward us.

If almost all the galaxies are moving away from Earth, we will observe a certain redshift between the wavelength of the radiation emitted by them, λ_{em} and the observed one, λ_{obs}:

$$z = \frac{\lambda_{obs} - \lambda_{em}}{\lambda_{em}}. \tag{1.1}$$

According to the Doppler shift phenomenon, for the non-relativistic case, if a nearby source is moving with velocity v, the measured redshift is $z = v/c$ with c the speed of light.

However it was E. Hubble who in 1929 combined his measurements on distances to galaxies through Cepheids, and discovered that the galaxy recessional velocity increases with its distance [126], obtaining the now called Hubble's law:

$$H_0 d = v, \tag{1.2}$$

where H_0 is known as the Hubble constant and d is the physical distance between the observer and the galaxy. This law was the cornerstone of the idea of an expanding universe. The light from distant galaxies is redshifted because their separation distance increases due to the expansion of the Universe.

At the same time, if everything is moving away from everything else, it is a sign of that at some point in the past, everything in the Universe was closer. So there was an event in the past where all matter was as close as possible and after some kind of explosion everything started to separate, thus, giving another probe for the Big-Bang model of cosmology.

1.1.1 Expansion, the scale factor and the cosmological redshift

Assuming an homogeneous and isotropic universe, we can define a "comoving coordinates system", in which the coordinates of a point are carried along the expansion, i.e, they remain constant. In a universe with such properties, the expansion will be also uniform, allowing us to relate the physical distance, d, between two different points with the comoving coordinate distance, x, through a scale factor $a(t)$ that depends only on time to ensure homogeneity, and accounts for the relative expansion of the Universe:

$$d(t) = a(t)x. \tag{1.3}$$

The wavelength of the photons crossing an expanding universe, will also scale with $a(t)$, thus the measured redshift of the light of a distant object will give us an indication of the relative size of the Universe at that time:

$$1 + z = \frac{\lambda_{obs}}{\lambda_{em}} = \frac{a(t_0)}{a(t)}. \tag{1.4}$$

With the relation given by Eq. (1.3) and the expression of the recessional velocity $v = \dot{d}$,

we can recover Hubble's law at any time, t:

$$v = \dot{d} = \frac{\dot{a}}{a} d = Hd, \tag{1.5}$$

where $H \equiv \dot{a}/a$ is the Hubble parameter and accounts for the expansion rate of the Universe. Its value at present can be expressed as $H_0 = 100h$km s^{-1}Mpc^{-1}, h being a dimensionless parameter.

1.2 General Relativity and FLRW equations

Now we require a mathematical framework which can provide the tools to describe and study the evolution of the Universe. On one hand, we need a metric which can encapsulate the geometric properties of a spatially homogeneous and isotropic Universe. Between 1922 and 1924, A. Friedman derived a metric with these characteristics. Some years later, G. Lemaître arrived independently at similar results as Friedmann; and finally, in 1935, Robertson and Walker rigorously proved that this metric is the only one on a spacetime that is spatially homogeneous and isotropic. The line element of this metric, known as the Friedmann-Lemaître-Robertson-Walker (FLRW) metric, can be written as follows in reduced-circumference polar coordinates:

$$ds^2 = g_{\mu\nu} dx^\mu dx^\nu = -c^2 dt^2 + a^2(t) \left(dr^2 + \chi^2(r) \left(d\theta^2 + r^2 \sin^2\theta d\phi^2 \right) \right), \tag{1.6}$$

where $a(t)$ is the scale factor introduced in the previous section. For the function $\chi(r)$ there are three possible choices, each one corresponding to a different spatial curvature $\mathcal{K}$:

$$\chi(r) = \begin{cases} r & \text{if } \mathcal{K} = 0 \text{ (flat universe)}, \\ \sin r & \text{if } \mathcal{K} = +1 \text{ (closed universe)}, \\ \sinh r & \text{if } \mathcal{K} = -1 \text{ (open universe)}. \end{cases} \tag{1.7}$$

On the other hand, it is well known that the strongest force at very large scales is gravity, so a theory describing this interaction will give us the best description of picture of the Universe at these scales. In that case Einstein's General Relativity is the best description we have, and it is captured in the so called Einstein equations:

$$G_{\mu\nu} \equiv \mathcal{R}_{\mu\nu} - \frac{1}{2}\mathcal{R} g_{\mu\nu} = 8\pi G T_{\mu\nu}. \tag{1.8}$$

Here $G_{\mu\nu}$ is the Einstein tensor; $\mathcal{R}_{\mu\nu}$ the Ricci Tensor, which depends on the metric and its derivatives; $\mathcal{R}$ the Ricci Scalar ($\mathcal{R} \equiv g^{\mu\nu} R_{\mu\nu}$); G stands for Newton's Constant of Gravitation and $T_{\mu\nu}$ is the energy-momentum tensor, which describes the background matter content. These equations give us now the relation between the geometry and the energy density content of the Universe.

The energy-momentum tensor, which describes the energy content of an homogeneous and isotropic universe, can be bound to the perfect fluid form:

$$T_{\mu\nu} = (-\rho + p) u_\mu u_\nu + p g_{\mu\nu}, \tag{1.9}$$

where the $4-$velocity is the time-like $4-$vector, $u^\mu = (\frac{1}{a}, 0, 0, 0)$ and $u_\mu u^\mu = -1$ while ρ and p are the fluid energy density and pressure respectively that can be related through the equation of state [1],

$$w = \frac{p}{\rho}. \tag{1.10}$$

Now if we solve the Einstein equations (1.8) for the FLRW metric under the assumption of a perfect fluid, we obtain the equations for the scale factor, $a(t)$, that describe how an homogeneous and isotropic universe evolves in the context of General Relativity. For generalized theories a similar treatment would have to be done. Those equations are called Friedmann equations:

$$\dot{H} = \frac{\ddot{a}}{a} = -\frac{4\pi G}{3}(\rho + 3p), \tag{1.11}$$

$$H^2 \equiv \left(\frac{\dot{a}}{a}\right)^2 = \frac{8\pi G}{3}\rho - \frac{k}{a^2}. \tag{1.12}$$

The first one is a first order differential equation for the Hubble parameter H, which gives us the evolution of the scale factor. The second one is a continuity equation which expresses the conservation of the energy.

From the 0-th component of the energy conservation equation $\nabla_\mu T^{\mu\nu} = 0$, an evolution equation for the energy density of the fluid can be obtained:

$$\dot{\rho} + 3H(\rho + p) = 0. \tag{1.13}$$

Integrating this equation for a constant equation of state and using Eq. (1.12), it is possible to obtain the variation of the energy density with the scale factor:

$$\rho = \rho_0 a^{-3(1+w)}, \tag{1.14}$$

with ρ_0 being the energy density at present time.

A universe filled with radiation, i.e. relativistic particles, can be described with a fluid with an equation of state $w_r = 1/3$. This value can be obtained from the fact that the trace of the energy momentum tensor (1.9) has to be zero for relativistic matter. For a non-relativistic matter universe which includes both dark matter and baryons, the effect of the pressure is almost negligible and we have $w_m \simeq 0$. Thus summarizing:

$$\text{Matter dominated: } \rho \propto a^{-3}, \tag{1.15}$$

$$\text{Radiation dominated: } \rho \propto a^{-4}. \tag{1.16}$$

[1] This is the usual factor which relates pressure and density of any given component through the relation $w_X \doteq p_X/\rho_X$.

At this point, it is convenient to define the critical energy density:

$$\rho_c(a) = \frac{3H^2}{8\pi G}, \tag{1.17}$$

and the dimensionless density parameter:

$$\Omega(a) = \frac{\rho(a)}{\rho_c(a)}. \tag{1.18}$$

With these two parameters we can rewrite Eq. (1.12) in the form

$$\Omega(a) - 1 = \frac{k}{(aH)^2}, \tag{1.19}$$

which allows us to relate the total energy density of the Universe to its local geometry, showing that the matter distribution clearly determines the spatial geometry of the Universe:

$$\Omega > 1 \quad \rightarrow \quad k = +1, \tag{1.20}$$
$$\Omega = 1 \quad \rightarrow \quad k = 0, \tag{1.21}$$
$$\Omega < 1 \quad \rightarrow \quad k = -1. \tag{1.22}$$

Current observations from the CMB give a value of $\Omega_k = -k/(a^2H^2) = -0.080^{+0.071}_{-0.093}$ [147], therefore the spatial flatness of the Universe is commonly assumed in order to simplify calculations.

If observations indicate that we are in an almost flat universe, and from Eq. (1.15) and (1.16) we see that at present the energy density of radiation is negligible compared to matter, we find we are in a purely matter dominated universe, $\Omega_m \sim 1$. This model is called Einstein-de Sitter (EdS) universe, and until the discovery of the current acceleration of the Universe, as we will see in the next section, was the most accepted one by theoretical cosmologists. Since 1932, different observations have indicated that a large fraction of this matter component is not visible, i.e. does not interact with light. J. H. Oort was the first to find an observational evidence for non visible matter in our Galaxy [197, 198]. Then, F. Zwicky [300, 301] found that the total mass inside the Coma cluster was larger than expected. These observations were based on the study of the motion of the astronomical objects: stars in a galaxy or galaxies in a cluster. They tried to check if the visible matter, that coming from stars and dust, was enough to generate the observed motion through gravitational attraction. And what they found was that extra matter should be taken into account to explain the observed movements. This extra component is known as **dark matter**, see [38, 228] for good reviews. The most evident application of this procedure is to their galaxy rotation curves. Other indirect observational evidences for dark matter have been found over the years. Maybe the most noticeable one are the galaxy rotation curves; but the existence of dark matter has been also proved with gravitational lensing or other observational probes that involve physics of the early universe as the Big Bang Nucleosynthesis or the Cosmological Microwave Background. All of them have shown that

dark matter does not interact electromagnetically, only gravitationally. Many candidates have been proposed, but the its exact nature is still unknown as we lack of a direct detection of the dark matter particle. The most promising candidate is a particle that behaves like a non-relativistic collisionless fluid (Cold Dark Matter).

Cosmological Horizons

At this point it is convenient to introduce the concepts of *particle horizon*, *coordinate horizon* and *horizon distance*. These quantities are a consequence of the finite speed of light. See [93, 94, 224] for nice and clear explanations of these concepts. For a given observer, the **particle horizon** at a given time, t, is defined as the surface that divides particles that have been already seen by the observer from those that have not seen yet. Thus, the **coordinate distance** is the distance that the light has been able to travel to an observer at time, t, from the earliest time possible for its emission, t_0 (usually taken as zero)

$$r_H(t) = \int_{t_0}^{t} \frac{cdt'}{a(t')}. \tag{1.23}$$

Finally, the **horizon distance**, which is the maximum distance to which the observer can see, can be expressed as

$$d_H(t) = a(t) r_H(t) = a(t) \int_{t_0}^{t} \frac{cdt'}{a(t')}. \tag{1.24}$$

As H_0^{-1} represents a rough measure of the age of the Universe, it is common to call the Hubble radius cH_0^{-1} the *horizon* or *horizon length*. In a similar way, it is also possible to define the **sound horizon**, the distance that the sound has had time to travel during the age of the Universe:

$$r_s(z_\star) = \int_{t_0}^{t} \frac{c_s(t')dt'}{a(t')}. \tag{1.25}$$

1.3 The currently accelerated universe

The Hubble Diagram, as first presented by Hubble himself, relates the recessional velocity or redshift of distant objects with their distance, and gives the most direct evidence we have of the expansion of the Universe. Later observations have used the same principle: measure the distance and the redshift of every object under observation. The easiest task is to measure the redshift, it can be obtained through either spectroscopy or photometry. However, the measurement of the distances is more complicated. The most common technique requires the existence of a *standard candle*, an object whose luminosity is well known and can be predicted from some other measurement. Sources which are far away appear fainter because the light spreads out over a larger area in its way to the observer who will measure a flux

$$F = \frac{L}{4\pi d_L^2}, \tag{1.26}$$

where L and d_L are the luminosity and the luminosity distance respectively. The last one can be related to the Hubble parameter:

$$d_L = (1+z)\int_0^z \frac{dz'}{H(z')}, \tag{1.27}$$

and allows us to infer the geometry and dynamics of the Universe. There are several types of standard candles, Hubble in his measurements made use of Cepheids, stars whose luminosity varies within a regular cycle [126, 157]. This kind of standard candles can only be used out to about 30Mpc. Nevertheless, in 1993 [211] it was demonstrated that Type Ia Supernovae (SNeIa), stellar explosions at the end of massive stars life, are good candidates for standard candles, with the benefit that they can be seen at large distances given their extreme brightness.

Five years later, two independent groups of astronomers, the Supernova Cosmology Project and the High-Z Supernova Search Team, obtained a set of 42 and 10 supernovae respectively, up to the highest redshift measured by then, $z \sim 0.82$, that let them obtain the Supernovae Hubble diagram to larger distances than was previously possible [16, 210, 220, 221]. Making use of the distance modulus, μ:

$$\mu \equiv m - M = 5\log_{10}\left(\frac{d_L}{Mpc}\right) + 25, \tag{1.28}$$

with m the apparent and M the absolute magnitude of the sources respectively, both teams showed that distant SNeIa were dimmer than they would be in a decelerating universe, indicating not only that the Universe was expanding, but also that this expansion has been accelerating for the past 5Gyrs. This discovery opened a new era in Cosmology, and has been awarded with the Nobel Prize in 2011 [293].

Nowadays, the accelerated expansion of the Universe stands as confirmed by several independent observations as the already mentioned SNeIa [107, 115, 215, 262, 274], the measurements of cluster properties as the mass, the correlation function and the evolution with redshift of their abundance [17, 18, 91, 283]; the optical surveys of large scale structure [60, 90, 212]; the anisotropies in the Cosmic Microwave Background (CMB) [78, 147, 261], the cosmic shear measured from weak lensing [216, 282] and the Lyman$-\alpha$ forest absorption [68, 189].

Given that the accelerated cosmic expansion has been well proved, the main challenge is to understand which is the origin of this acceleration. So far, we can think of two possible solutions. One would be the existence of a new component, **dark energy** (DE), with negative pressure that would counteract the effects of the gravitational attraction, leading to the observed accelerated expansion of the Universe. The other possible way to explain these observations would be to consider that General Relativity breaks down at large scales, i.e, cosmological scales, and needs to be replaced with a broader theory of gravity. If we pay attention to Eq. (1.8), these two possibilities would respectively be translated into a modification of the right hand side of the equation, which takes into account the matter energy content of the Universe, either by adding a new one, or by introducing changes in the left side of the equation, which describes the geometry of the Universe.

1.4 Dark Energy

In Sec. 1.2 we have seen that Friedmann equations explain how an homogeneous and isotropic universe expands in the context of General Relativity. Considering the Universe is filled with several fluid components, matter, radiation and dark energy, the Friedmann equation becomes

$$H^2 = H_0^2 \left(\Omega_m a^{-3} + \Omega_r a^{-4} + \Omega_k a^{-2} + \Omega_{DE} a^{-3(1+w_{DE})}\right). \tag{1.29}$$

At the same time, we have already mentioned, observations are indicating that this expansion is accelerated, i.e. $(\ddot{a} > 0)$, which translates into a negative deceleration parameter:

$$q = -\frac{\ddot{a}}{aH^2}. \tag{1.30}$$

From Eqs. (1.11) and (2.4) we see that acceleration occurs when the equation of state for this new component satisfies $w < -1/3$. This means we are looking for a fluid with large negative pressure that causes the expansion. Although its existence is well established observationally, there is not an entirely compelling theoretical model which gives a theoretical physical framework within which dark energy can be understood. Moreover, models so far proposed are, in general, not compliant with all main observations.

1.4.1 ΛCDM model

In parallel to observational discoveries, new theories or models are being developed with the aim of explaining the new findings. This is what took place after Hubble's breakthrough on the Universe expansion. In 1917 when Einstein announced General Relativity, he introduced in the equations a constant to obtain a static and finite cosmological model. A couple of years later, the possible solutions to these equations were studied [79, 100, 161], and showed that the case with matter and a cosmological constant, Λ, leads to an expansion or contraction of the Universe. However, in 1929, with Hubble's discovery of the expansion of the Universe, Einstein retracted from his previous formulation and removed the constant to have a model coherent with the observations.

After the empirical evidence about the accelerated expansion of the Universe and the need of a compliant theoretical model to explain it, the cosmological constant was recovered and became a good candidate to explain the recent acceleration. Thus, it represents the simplest model for dark energy, as it gives the same results as a new component of the energy density of the Universe with constant equation of state parameter equal to -1. Einstein equations (1.8) in the presence of the cosmological constant read

$$G_{\mu\nu} \equiv \mathcal{R}_{\mu\nu} - \frac{1}{2}\mathcal{R}g_{\mu\nu} = 8\pi G T_{\mu\nu} + \Lambda g_{\mu\nu}, \tag{1.31}$$

and the Friedmann equations get modified as follows:

$$\frac{\ddot{a}}{a} = -\frac{4\pi G}{3}(\rho + 3p) + \frac{\Lambda}{3}, \tag{1.32}$$

$$H^2 = \frac{8\pi G}{3}\rho - \frac{k}{a^2} + \frac{\Lambda}{3}. \tag{1.33}$$

These equations clearly show that the cosmological constant represents a negative pressure term, becoming the needed repulsive effect.

The Λ Cold Dark Matter (ΛCDM) model, which accounts for a universe mainly filled with cold dark matter and puts down the acceleration to the presence of a cosmological constant Λ, has become the standard model of cosmology due to its simplicity and compliance with the data, but there are still some points that it cannot explain:

- **Fine tuning or cosmological constant problem**: In 1960's Zeldovich pointed out that the origin of the cosmological constant could be the vacuum energy density. If we consider it as the sum over all the zero-point energies of the quantum fields with mass m, it would be given by

  $$\frac{\Lambda}{8\pi G} = \rho_{vac} = \frac{1}{4\pi^2}\int_0^\infty k^2\sqrt{k^2+m^2}dk, \tag{1.34}$$

  which shows a divergence for high-frequencies. However, if one considers a cut-off at Planck scales, one finds $\rho_{vac} \simeq 10^{76}\text{GeV}^4$, which is over 123 orders of magnitude larger than the observed value $\rho_\Lambda \simeq 10^{-47}\text{GeV}^4$.

- **Coincidence problem:** Observations show that at the present epoch matter and dark energy dominate the Universe, i.e. $8\pi G\rho/3H_0^2$ and $\Lambda/3H_0^2$ are of the same order of magnitude. However, we know that in an expanding universe, these terms would have had different magnitudes at early times. At that stage, radiation dominated the Universe, thus

  $$\frac{\rho_\Lambda}{\rho_{rad}} \propto a^4, \tag{1.35}$$

  and the energy density corresponding to Λ was negligible. As Λ is constant, at some point in the future it will dominate. So, it seems we are in an special moment of the history of the Universe; the actual balance between these quantities benefits us, so in another epoch the Universe would be completely different, and the Universe would not exist as we know it. So, the problem is: why does this happen exactly now? Why are we so privileged?

1.4.2 Dynamical models of Dark energy

These theoretical shortcomings we have just discussed have lead to the proposal of other settings which admit a slightly time-variable dark energy as the agent producing the cosmic acceleration. There are good reasons to consider a dynamical dark energy as an alternative to the cosmological constant. First, it can evolve slowly to zero, giving a solution to the cosmological constant problem. Second, a dynamical dark energy can give us a hint of the

evolution of dark energy, allowing us to learn something more about the underlying physics. This fact also solves the coincidence problem, if the dynamics is such as to trigger the recent dominance of the dark energy.

Many such models have emerged along theoretical avenues: quintessence [299], Chaplygin gas [34, 138], modified gravity [195], holographic dark energy [168], braneworld models [182], $f(R)$ theories [257], theories with extra dimensions [158], and quite a few others. Unfortunately, none of them have emerged as definitive answers for the dark energy problem, so currently the situation is one of quick advances on the empirical front (regarding the quantity and quality of the data), whereas theory is somewhat mired in a jungle of alternatives.

1.4.3 Quintessence

The scalar fields which arise from particle physics are good candidates for dark energy. There has been proposed a wide variety of fields for this purpose, but Quintessence[2] has became the leading class, as its capability has been checked to also induce early cosmic inflation. These models are described by a scalar field, ϕ, minimally coupled to gravity whose action is given by

$$\mathcal{S} = -\int d^4x\, \sqrt{-g}\left[-\frac{1}{2}\left(\nabla\phi\right)^2 - V(\phi)\right] \tag{1.36}$$

with $\left(\nabla\phi\right)^2 = g^{\mu\nu}\partial_\mu\phi\partial_\nu\phi$ and $V(\phi)$ being the potential of the field. The corresponding energy-momentum tensor can be obtained varying the action with respect to $g_{\mu\nu}$:

$$T_{\mu\nu} = \frac{-2}{\sqrt{-g}}\frac{\delta\mathcal{S}}{\delta g^{\mu\nu}} = \partial_\mu\phi\partial_\nu\phi - g_{\mu\nu}\left[\frac{1}{2}g^{\alpha\beta}\partial_\alpha\phi\partial_\beta\phi + V(\phi)\right], \tag{1.37}$$

note that $\delta\sqrt{-g} = -(1/2)\sqrt{-g}g_{\mu\nu}\delta g^{\mu\nu}$. Comparing this expression with the corresponding one for a perfect fluid, see Eq. (1.9), we obtain an expression for the energy density and pressure of the field:

$$\rho = \frac{1}{2}\dot{\phi}^2 + V(\phi) \tag{1.38}$$

$$p = \frac{1}{2}\dot{\phi}^2 - V(\phi). \tag{1.39}$$

For these models, Eqs. (1.11) and (1.12) for a flat universe become

$$H^2 = \frac{8\pi G}{3}\left[\frac{1}{2}\dot{\phi}^2 + V(\phi)\right] \tag{1.40}$$

$$\frac{\ddot{a}}{a} = -\frac{8\pi G}{3}\left[\frac{1}{2}\dot{\phi}^2 - V(\phi)\right]. \tag{1.41}$$

From the last equation it is straightforward to see that the acceleration will take place when $\dot{\phi} < V(\phi)$, i.e. when we have a flat enough potential which ensures that the scalar field will slowly roll. The most used is the exponential potential, however the literature is full of

[2]The name "Quintessence" comes from the ancient philosophical fifth element.

other kinds of potentials that fulfil this condition, see [228] and references therein.

The expression for the equation of state is then

$$w_\phi = \frac{\dot{\phi}^2 - 2V(\phi)}{\dot{\phi}^2 + 2V(\phi)}, \tag{1.42}$$

which is bounded to $-1 \leq w_\phi \leq 1$.

Phantom Field

Current observational data gives us bounds on the dark energy equation of state in which the case with $w < -1$ is allowed at 68% confidence level: WMAP7-year provides $w = -1.20^{+0.57}_{-0.25}$ [147] and Type Ia Supernova data from Union2.1 $w = -1.001^{+0.348}_{-0.398}$ [270]. Therefore, a new type of scalar field needs to be taken into account in order to be able to recover these values. It is usually done with the so called "Phantom[3] fields" which are a modification of the previous scalar fields with a negative kinetic term [51, 52]

$$\mathcal{S} = -\int d^4x \, \sqrt{-g} \left[\frac{1}{2} (\nabla\phi)^2 - V(\phi) \right]. \tag{1.43}$$

This change in the sign of the kinetic term changes the equation of state, being now

$$w_\phi = \frac{\dot{\phi}^2 + 2V(\phi)}{\dot{\phi}^2 - 2V(\phi)} \tag{1.44}$$

allowing the case with $w_\phi < -1$ for $\dot{\phi}/2 < V(\phi)$.

As this kind of fields does not have a lower bound, they usually present Ultra Violet instabilities, this being one of its main shortcomings.

1.4.4 Chaplygin Gas

A special fluid motivated by Braneworld cosmology has emerged as a good candidate, not only to describe a dynamical dark energy equation of state, but also to unify in a single fluid dark matter and dark energy [34, 138]. The generalized form for the equation of state of this fluid is given by

$$p = -\frac{A}{\rho^\alpha}, \tag{1.45}$$

where A is a positive constant. The original Chaplygin gas is recovered with $\alpha = 1$. Inserting this expression in Eq. (1.13) for the conservation of the energy density we obtain

$$\rho = \left[A + \frac{B}{a^{3(1+\alpha)}} \right]^{1/(1+\alpha)}, \tag{1.46}$$

[3] This name is taken from Part I of Star Wars "The Phantom Menace"

with B a constant. This equation allows us to obtain the equation of state for the Generalized Chaplygin gas in terms of the redshift:

$$w = \frac{p}{\rho} = -\frac{A}{\rho^{\alpha+1}} = -\frac{1}{1+(B/A)(1+z)^{3(1+\alpha)}}. \tag{1.47}$$

From Eqs. (1.46) and (1.47) we see that at early times $(a \ll 1)$ the Chaplygin gas behaves as purely matter:

$$\rho \propto a^{-3} \quad \text{with } w \simeq 0. \tag{1.48}$$

However, at late times $(a \gg (B/A)^{1/[3(1+\alpha)]})$ it mimics the cosmological constant:

$$\rho \propto constant \quad \text{with } w \simeq -1. \tag{1.49}$$

1.4.5 Dark energy parametrizations

Since it is not fully clear what the observations should be compared with, in many of the phenomenological models for dark energy a try and tested approach is to define a parametrization of its equation of state (EoS) or energy density which, if well designed, allow to encapsulate all the observational information in a few numbers which can afterwards be compared with theoretical predictions (see [228] for a good reference on this topic). It is usually assumed that these quantities vary slowly with redshift and can be approximated by a fitting formula with a small number of free parameters. These parameters can be constrained comparing the ansatz with observations using an optimization procedure, as we will detail in Sec. 1.7. Choices are typically built upon intuition and prior information, but there is yet plenty of room for discussion and improvements.

At present, we recall that the two main fluids are the dark matter and dark energy, the last being the governor. As already discussed, dark energy can be described in an effective way in the sense we do not need to appeal to any fundamental theory to deduce its behaviour, and just let it be represented by a phenomenological equation of state:

$$w_{DE}(z) = \frac{p_{DE}}{\rho_{DE}}. \tag{1.50}$$

The importance of the EoS is significant, because it determines the form of the Hubble parameter $H(z)$ or any derivation of it which is necessary to obtain the observable quantities, as the luminosity distance $D_L(z)$. Under the spatial flatness assumption ($k = 0$), we can express the Hubble parameter as

$$\frac{H^2(z)}{H_0^2} = \Omega_m(1+z)^3 + \Omega_{DE}X(z) \tag{1.51}$$

with

$$X(z) = \frac{\rho_{DE}(z)}{\rho_{DE}(0)} = \exp\left(3\int_0^z \frac{1+w(z)}{1+z}dz\right), \tag{1.52}$$

the dark energy density function and $\Omega_{DE} = 1 - \Omega_m$. $H(z)$ will be completely determined once $w(z)$ or $X(z)$ are parametrized.

There are many parametrizations of $w(z)$ which have been proposed in the literature, in terms of redshift, scale factor or functions of them; see Table 1.1, where a list of the most used and some others is provided.

The last two parametrizations of the table involve more than two dark energy parameters. Nevertheless, it has been argued that, at present, not enough data are available so as to constrain more than two dark energy parameters [177, 269]. Therefore, although parametrizations with three or more parameters can recover a wider range of models with different variations with redshift or transitions, all of them cannot be well constrained at the same time. This shows how challenging it is to find a parametrization that can provide us as much information as possible about dark energy and its evolution with only two parameters.

The most natural way is to expand $w(z)$ in a Taylor series of the redshift, $w(z) = w_0 + w_1 z$ to first order, so that one has only two parameters. However, this clearly gives a divergence for high z. This problem can be solved if the expansions are carried out in terms of the scale factor a, giving place to the CPL parametrization, which we will discuss in what follows.

Chevallier-Polarski-Linder (CPL)

This parametrization was first discussed in [55] and reintroduced in [174], and defines the dark energy equation of state as

$$w_{CPL}(z) = w_0 + w_a \left(\frac{z}{1+z} \right), \tag{1.53}$$

where w_0 is the value of the dark energy equation of state today (i.e. at redshift $z = 0$) and $w_a + w_0$ the limit when $z \to \infty$. The corresponding dark energy density function takes the form:

$$X_{CPL}(z) = e^{-\frac{3w_a z}{z+1}} (z+1)^{3(w_0+w_a+1)}. \tag{1.54}$$

This parametrization has been widely used because of its simplicity, sensitivity to observational data and because it is well behaved and bounded at high redshifts. Its adoption by the Dark Energy Task Force [8] as a preferred parametrization has contributed to its popularity.

However, this parametrization has two shortcomings. Its flexibility to determine cosmological parameters for some dark energy models with rapid evolution has been put in doubt recently. On the other hand, the second parameter is typically very poorly constrained, thus losing power of conviction about the conclusions to be drawn from it.

Intuitively, in order to be able to discern which dark energy model is closest to reality and to offer a sensible interpretation of the results, it seems necessary to consider dark energy parameters which offer clear advantages. Apart from having a clear physical meaning, for a parameter to be eligible there should be previous hints or theoretical grounds forecasting reasonably tight constrains; and as it is well know, the parameter should be the least possibly correlated to others.

Most of the parametrizations listed suffer from quite a significant correlation, besides the fact that constraints on one of their parameters are typically large in percentual terms.

Authors	Parametrization	Special features	Refs.
Quiessence	$w = w_0$	• Constant EoS. • Derived from a scalar field.	[230]
Cooray-Huterer	$w_{CH}(z) = w_0 + w_1 z$	• Linear with z. • Valid for $z \ll 1$. • Diverges when $z \to \infty$.	[63, 108, 289]
Efstathiou	$w_E(z) = w_0 - \alpha w_a \ln(z+1)$	• Approximation to the EoS given by a wide range of dynamical scalar fields.	[86]
Barboza	$w_B(z) = w_0 - w_\beta \frac{(1+z)^{-\beta}-1}{\beta}$	• Generalization of CPL EoS and the previous 2 parametrizations for the limits $\beta = \pm 1, 0$ respectively.	[19]
Wetterich	$w_W(z) = \frac{w_0}{b\ln(z+1)+1}$	• Accounts for early dark energy.	[290]
Padmanabhan-Choudhury	$w_{PC}(z) = w_0 + \frac{w_1 z}{(z+1)^2}$	• Same EoS at present and at high redshift. • Rapid variation for low z.	[130]
Barboza-Alcaniz-Santos	$w_{BAS}(z) = w_0 + \frac{w_a z(z+1)}{z^2+1}$	• Well behaved for $z \in [-1, \infty)$. • Obtained from a scalar field. • Avoids divergences with z.	[20, 21]
Ma-Zhang	$w_{MZ}(z) = w_0 + w_a \left(\frac{\ln(z+2)}{z+1} - \ln(2)\right)$	• Can be extended to the future.	[181]
	$w_{MZo}(z) = w_0 + w_a \left(\frac{\sin(z+1)}{z+1} - \sin(1)\right)$	• Same as before in an oscillating form.	
Hannestad-Mortsell	$w_H M(z) = \frac{1+\left(\frac{1+z}{1+z_T}\right)^n}{\frac{1}{w_0}+\frac{1}{w_1}\left(\frac{1+z}{1+z_T}\right)^n}$	• Adaptability of transition.	[113]
Corasaniti	$w_C(a) = w_0 + (w_m - w_a)\Gamma(a, a_t, \Delta)$	• Adaptability of transition: – $\Gamma(a, a_t, \Delta) = \frac{1+e^{a_t/\Delta}}{1+e^{-(a+a_t)/\Delta}} \times \frac{1+e^{-(a+1)/\Delta}}{1+e^{1/\Delta}}$ – $\Gamma(z, z_t, \Delta) = \frac{-1}{1+e^{(z+z_t)/\Delta}}$	[65, 66] [24–26]

Table 1.1: *Parametrizations of the dark energy equation of state.*

This problem can be avoided with rewriting Eq. (1.53) in terms of a pivot scale factor a_p at which $w_p \equiv w(a_p)$ and w_a are uncorrelated [123, 127, 176, 186]:

$$w(a) = w_p + w_a(a_p + a). \tag{1.55}$$

Wang parametrization

The pivot technique we have just described was also used in [286], where a new dark energy EoS was given in terms of two parameters: $w_0 = w(z = 0)$ and $w_c = w(z_c)$,

$$w_w(a) = \left(\frac{a_c - a}{a_c - 1}\right) w_0 + \left(\frac{a - 1}{a_c - 1}\right) .w_c \tag{1.56}$$

This can be seen just as a rearrangement of the classic CPL parametrization with

$$w_c = w_0 + (1 - a_c)w_a. \tag{1.57}$$

The value of a_c can be then chosen as the scale factor at which the correlation between w_0 and w_a is lower. Using error propagation, from Eq. (1.57) one gets

$$\sigma(w_c)^2 = \sigma(w_0)^2 + (1 - a_c)\sigma(w_a)^2 + 2\|1 - a_c\|\sigma(w_0, w_a). \tag{1.58}$$

In the remainder we will drop the absolute value given that we are only interested in a $a_c < 1$ situation. In contrast, if one solves Eq. (1.57) for w_a and then applies on it error propagation, it results

$$\sigma(w_a)^2 = \frac{\sigma(w_0)^2 + \sigma(w_c)^2 - 2\sigma(w_0, w_c)}{(1 - a_c)^2}. \tag{1.59}$$

Combining our results above (Eqs. (1.58) and (1.59))

$$\sigma(w_0)^2 + (1 - a_c)\sigma(w_0, w_a) = \sigma(w_0, w_c) \tag{1.60}$$

is obtained, and then one deduces that total decorrelation ($\sigma(w_0, w_c) = 0$) is achieved for

$$a_c = 1 + \frac{\sigma^2(w_0)}{\sigma(w_0, w_a)}. \tag{1.61}$$

It depends on the observational data set, but in practice $a_c = 2/3 \leftrightarrow z_c = 0.5$ is used for current data. Note that, according to our notation, $\sigma(w_0, w_a)$ denotes in this case the non-diagonal element of the covariance matrix of w_0 and w_a, whereas $\sigma(w_0, w_c)$ denotes the non-diagonal element of the covariance matrix between w_0 and w_c. In this case, the EoS written in terms of the redshift takes the form

$$w_w(z) = 3w_{0.5} - 2w_0 + \frac{3(w_0 - w_{0.5})}{1 + z}, \tag{1.62}$$

with the corresponding dark energy density function:

$$X_w(z) = (1+z)^{3(1-2w_0+3w_{0.5})} \exp\left[9(w_0 - w_{0.5})\frac{z}{1+z}\right]. \tag{1.63}$$

The main gain of this reformulation is that it minorates the correlation between the parameters and allows us to obtain tighter constraints along with a more transparent interpretation of the parameter estimation results.

In contrast with the procedure described before, if one is just demanding a situation where $\sigma(w_0, w_c) < \sigma(w_0, w_a)$, it is very easy to deduce from Eq. (1.60) that such condition is met whenever

$$a_c > \sigma(w_0)^2/\sigma(w_0, w_a) \tag{1.64}$$

giving us other possible values of a_c.

1.5 Early Universe

The observed CMB radiation, together with the expansion of the Universe, indicate that there was a previous stage where the Universe was hotter and smaller. Simultaneously, from theory we can also see that there exists a singularity known as Big-Bang, which is reached when the scale factor tends to zero. A fundamental question at this point is: which was the state of the Universe at these early epochs? Which was the main constituent? Observations give us a general picture of the Universe at present mainly composed by matter, dark energy, photons and other relativistic species like neutrinos that contribute to the radiation in the form

$$\Omega_r = \Omega_\gamma \left[1 + \left(\frac{7}{8}\right)\left(\frac{4}{11}\right)^{4/3} N_{\text{eff}}\right], \tag{1.65}$$

where N_{eff} is the effective number of neutrino species, [179]. At present, the energy density corresponding to radiation is $\Omega_{r,0} \simeq 4.15 \times 10^{-5} h^{-2}$, which is negligible if one compares it with the matter energy density $\Omega_{m,0} \simeq 0.1134 h^{-2}$ [147]. In section 1.2, we studied how the energy density of both relativistic and non-relativistic matter vary with the the scale factor as the Universe expands. From Eqs. (1.15) and (1.16) we can find the ratio between these two quantities at any time in the past:

$$\frac{\Omega_r}{\Omega_m} = \frac{\Omega_{r,0}}{\Omega_{m,0}}\frac{a^3}{a^4} = \frac{\Omega_{r,0}}{\Omega_{m,0}}\frac{(1+z)^3}{(1+z)^4}. \tag{1.66}$$

However, from this equation we can see that although at present $\Omega_r \ll \Omega_m$, at earlier times, it was completely the reversal. The epoch at which both densities were the same is known as *matter-radiation equality*, and it took place at

$$1 + z_{eq} = \frac{1}{a_{eq}} = \frac{\Omega_{m,0}}{\Omega_{r,0}} \simeq 3200. \tag{1.67}$$

From Fig. 1.1(a) we can easily see that after equality the Universe became dominated by

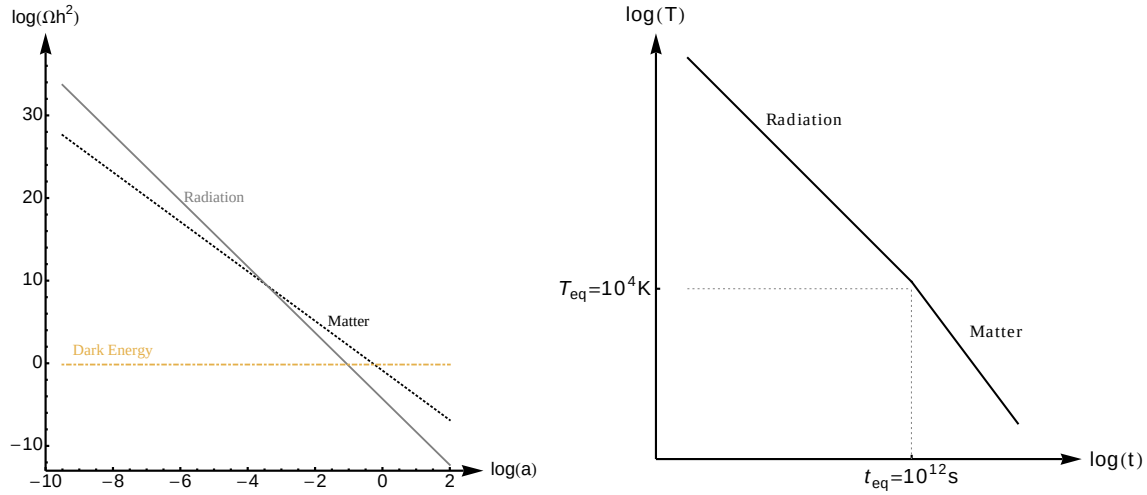

(a) Energy density evolution with the scale factor (b) Variation of the Universe temperature with time

Figure 1.1: *Schematic evolution in log-scale of the energy-density and temperature for the different components of the Universe: matter, radiation and dark energy*

non-relativistic matter until the moment the dark energy began to be dominant. However, before decoupling, the Universe was effectively dominated by radiation.

Around equality, different phenomena of crucial importance took place in the life of the Universe, and left an imprint on the CMB. Before matter-radiation equality, the speed of the expansion was so high that fluctuations on matter density could not collapse under their own gravity; only at later times cosmological structures were able to start to form. The age of the Universe at the equality epoch imprints a characteristic scale that can be measured in the galaxy clustering today, more details will be given in sections 1.6.3 and 1.6.4. For a universe dominated by radiation, we can use the relationship between the energy density of radiation and the temperature of a black body,

$$\rho_r c^2 = \alpha T_r^4, \tag{1.68}$$

$\alpha = \pi^2 k_B^4 / 15\hbar^3 c^3 = 7.565 \times 10^{-16} \mathrm{Jm}^{-3}\mathrm{K}^{-4}$ being the radiation constant, to find the equation that gives us the dependence of the temperature with the scale factor or redsfhit. Using this relation and Eq. (1.16), which gives us how the energy density of radiation evolves with the expansion, we have

$$T_r = T_0 \frac{a_0}{a} = T_0 \left(1 + z\right). \tag{1.69}$$

Before equality, in the radiation dominated universe, the concentration of electrons was equal to the density of protons, leading to a neutral situation. At that time, the temperature was high enough for the energy of any photon to be higher than the ionization energy of the simplest atoms, hydrogen atoms (H). So electrons could not bind to protons to form hydrogen because they would be immediately ionized by photons. So, the Universe was a ionized plasma of protons (free nuclei), electrons and photons interacting through

Thompson scattering. The mean free path of a photon (average distance the photon travels before Thomson scattering off a free electron) was short. As the Universe expanded, the temperature dropped, the photons lost energy and became less able to ionize. When the temperature was below ∼eV, protons began to capture electrons to form atoms of hydrogen, thus, descending the number of ionized particles. This stage of the early universe is called *recombination*, although it is the first time protons and electrons combine to produce hydrogen. While the temperature was high enough, there was a thermal equilibrium in the reactions of recombination and photo-dissociation of hydrogen. Over a short time interval, the photons were unable to interact with electrons and the Universe became transparent. The photons, which previously were unable to escape due to electron interaction, having not enough energy to ionize the atoms formed, were able to get away and travel through Universe in its evolution. This process, known as *decoupling*, produced the Cosmological Microwave Background that we can measure at present.

We have seen that two processes took place before the CMB was produced, if this processes were instantaneous they would have coincided, but it was not the case, both processes would have taken some time, and decoupling would have occurred after recombination. Taking $X \equiv n_e/n_B$ as the ionization fraction being, $n_e = n_p$ the concentration of free electrons (which in a neutral universe is equal to the density number of protons) and $n_B = n_p + n_H$ the concentration of baryons, one can write the so called Saha equation for the equilibrium ionization fraction, which in this case can be written as [179]:

$$\frac{1-X}{X^2} \simeq 3.8 \frac{n_B}{n_\gamma} \left(\frac{k_B T}{m_e c^2}\right)^{3/2} \exp\left(\frac{E_0}{k_B T}\right). \tag{1.70}$$

Here $E_0 = m_e + m_p - m_H = 13.6$ eV is the binding energy of hydrogen atoms. To obtain this relation we have used the distribution functions for protons, electrons and hydrogen:

$$n_x = g_x \left(\frac{m_x k_B T}{2\pi}\right)^{3/2} \exp\left(\frac{\mu_x - m_x}{k_B T}\right), \tag{1.71}$$

where $x = p, e, H$ denotes each of the species and g_x their degeneracy which is $4, 2, 2$ for hydrogen, protons and electrons. Focusing on Eq. (1.70), the case of full ionizations $X \sim 1$ corresponds to the case with a high temperature, T, larger than the binding energy E_0. Once the temperature drops, the right hand side of the equation becomes larger, and the ionization fraction approximates to zero. It is defined as the epoch of recombination, when the process is almost complete, and the photoionization reactions cannot balance hydrogen production. At this point, the ionization fraction is $X_{\rm rec} \simeq 0.1$. In this case, the Saha equation can be solved numerically and $T_{\rm rec} \simeq 3600$K is obtained, which corresponds to $z_{\rm rec} \simeq 1300$ [105]. Decoupling took place a little bit later, when $X_{dec} \simeq 0.0001$, which implies $T_{dec} \simeq 3000$K which in turn corresponds to a $z_{dec} \simeq 1100$. At this stage, the drop in the ionization fraction means an increase of the photon mean free path:

$$\lambda_{Th} \simeq \frac{1}{n_e \sigma_{Th}}. \tag{1.72}$$

Before decoupling this is of ∼Mpc and after that it raises to $\sim 10^4$Mpc, so the photons can

reach us without being scattered, and the Universe becomes transparent to radiation.

But, what happened before equality, in earlier times when the Universe was radiation dominated? As the Universe is expanding it gets cooler and cooler, see Fig. 1.1(b). But in the opposite direction, when the Universe was mainly composed by radiation, the temperature was inversely proportional to the scale factor. Thus, as the scale factor approaches zero, the temperature increases infinitely, but there is a point in the extrapolation where classical physics does not work any more, and the Universe begins to be dominated by quantum effects or strings. This point is known as *Planck era* and it is the stage at which the De Broglie wavelength of the particles in thermal equilibrium gets smaller than the corresponding Schwarzschild radius. The characteristic mass for this effects is known as Planck mass,

$$m_P = \sqrt{\frac{\hbar c}{G}} \simeq 10^{19}\text{GeV}. \tag{1.73}$$

In a similar way, the corresponding Planck length and Planck time are also defined:

$$l_P = \sqrt{\frac{\hbar G}{c^3}} \simeq 10^{-35}\text{m} \tag{1.74}$$

$$t_P = \sqrt{\frac{\hbar G}{c^5}} \simeq 10^{-43}\text{s} \tag{1.75}$$

This is the earliest stage in the Universe history which can be described with standard physics. As these first stages of the Big-Bang involve high energies, the main processes that took place were those involving elementary particles. As the Universe cools down different phase transitions occur. In these transitions a disordered phase in a many-particle system characterized by a certain symmetry disappears and a new ordered phase with less degrees of symmetry appears. The *era of phase transitions* which extends from $T_P \simeq 10^{19}$GeV to $T_{QH} \simeq 10^2$ MeV (when the quarks get confined in hadrons) can be divided into several stages:

- $T_P > T > T_{GUT} \simeq 10^{15}$ GeV $(t_P < t < t_{GUT} \simeq 10^{-37}\text{s})$: At this point, the Universe was a plasma of relativistic particles; quarks, leptons and gauge and Higgs bosons in thermal equilibrium under interactions described by Grand Unification Theory (GUT) which unifies electroweak and strong forces. At T_{GUT} there is a symmetry breaking giving place to the GUT transition and origin to the matter-antimatter asymmetry and magnetic monopoles.

- $T_{GUT} > T > T_{EW} \sim 10^2$ GeV $(t_{GUT} < t < t_{EW} \simeq 10^{-11}\text{s})$: After the GUT transition, the unification force of strong and electroweak interactions splits into two different forces. When temperature reaches 10^2 GeV the electroweak unification ends, and the electromagnetic and weak interactions appear as a consequences of different forces. During this electroweak transition, some gauge bosons and other particles acquire mass via the Higgs mechanism and the full symmetry is broken (end of Supersymetry).

- $T_{EW} > T > T_{QH} \sim 200 - 300$ MeV ($t_{EW} < t < t_{QH} \simeq 10^{-5}$s): At this stage the last phase transition takes place: the quark-hadron phase transition. The strong interactions become stronger and the quarks get confined into hadrons, beginning the hadron era.

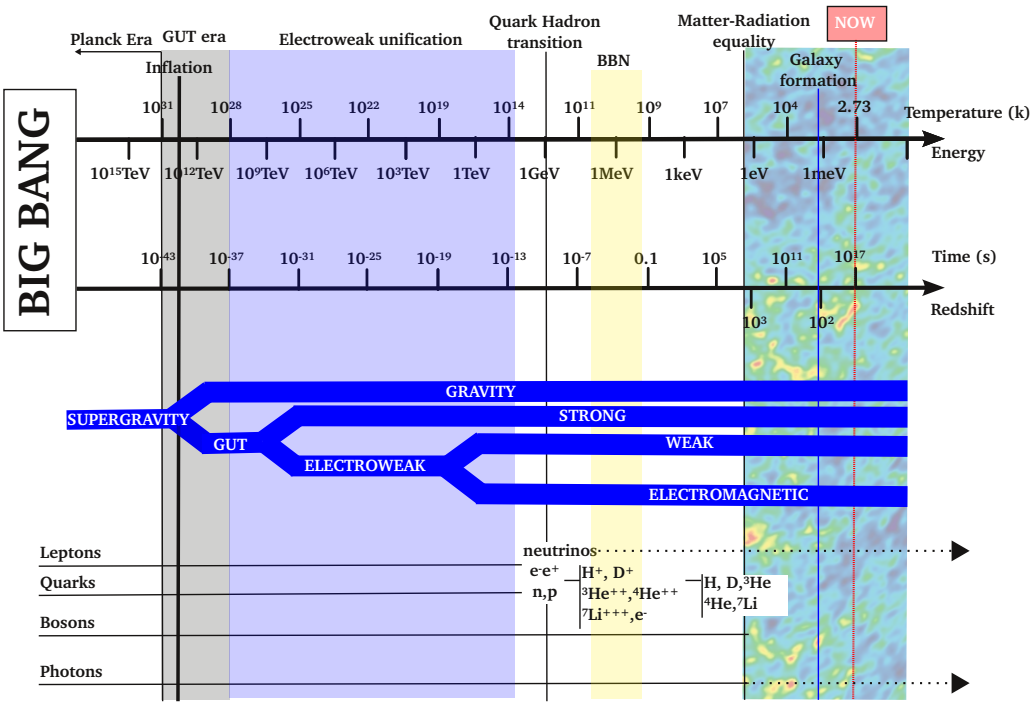

Figure 1.2: *Early universe History*

Hadrons are short lived, except for protons and neutrons, so when the Universe cools to $T \simeq 10^2$MeV, the pions pairs $\pi^+ - \pi^-$ annihilate, remaining only leptons, antileptons, photons, protons and neutrons. At $T \simeq 10 - 0.1$MeV began the primordial nucleosynthesis, at these temperatures practically all of the neutrons bound into ^4He nuclei, a small fraction produced deuterium ^3He even ^7Li. When the temperature reached the $\sim$ MeV neutrino interactions are too weak to keep them in thermal equilibrium and they decoupled. Later on, the matter density becomes equal to radiation, leading to the reionization, decoupling and the Cosmological Microwave Background as it has been described before.

1.5.1 Cosmological Perturbations

Although the Universe on average is homogeneous and isotropic, it has developed nonlinear structures which take the form of galaxies, clusters and superclusters, and large structures of voids and filaments of galaxies of size exceeding 100 Mpc. The CMB reveals us that at the time of recombination the Universe was very homogeneous and isotropic, with

inhomogeneities at very small scales. The most natural mechanism through which these small initial perturbations developed the large structures we observe is gravitational instabilities. Matter was attracted to regions with higher density which became more dense and amplified the existing inhomogeneities. To understand these processes and relate the physics of the early universe to the CMB anisotropies and large-scale structure, one needs to study the evolution of the perturbations in the context of the cosmological perturbation theory. The physics that took place in the early universe and seeded the nonlinear gravitational collapse concerns complex relativistic effects. It can accurately be described with a study of the evolution of relativistic perturbations. For a wider view of this topic refer to [180].

Metric Perturbation

Starting with the metric of the Friedmann-Robertson-Walker Universe,

$$\bar{g}_{\mu\nu} = a^2(\tau)\eta_{\mu\nu}, \tag{1.76}$$

where $\tau = dt/a(t)$ denotes conformal time (derivatives respect to τ will be indicated with ') and $\eta_{\mu\nu} = \begin{pmatrix} -1 & 0 \\ 0 & \boldsymbol{\delta}_{ij} \end{pmatrix}$, one can perturb it in the following way:

$$g_{\mu\nu} = \bar{g}_{\mu\nu} + \delta g_{\mu\nu} = a^2(\tau)\left(\eta_{\mu\nu} + h_{\mu\nu}\right). \tag{1.77}$$

Here $\bar{g}_{\mu\nu}$ is the unperturbed metric and $\delta g_{\mu\nu}$ the perturbation, which can be written as

$$[h_{\mu\nu}] = \begin{pmatrix} -2A & -B_i \\ -B_i & -2D\delta_{ij} + 2E_{ij} \end{pmatrix}. \tag{1.78}$$

Thus, the perturbed metric takes the form

$$ds^2 = a^2(\tau)\left\{-(1+2A)d\tau^2 - 2B_i d\tau dx^i + \left[(1-2D)\delta_{ij} + 2E_{ij}\right]dx^i dx^j\right\}. \tag{1.79}$$

As one can see from Eq. (1.78), the metric perturbation is characterized by a $(0,2)$ symmetric tensor. Its 00-component, A, is a scalar and relates the conformal time, τ, with the proper time, t. B_i is a vector which corresponds to the $0i$-component of the metric perturbation tensor, and it is known as the *shift function*; it specifies the relative velocity between the direction of motion and the wordlines orthogonal to the slicing. The term inside the brackets is a tensor, and it represents the spatial metric perturbation. This spatial tensor can be decomposed into a trace, $(1-2D)$, and and traceless, $E_{i,j}$ part. The last one is known as *strain*, and will happen to contain radiation, the so called *Gravitational Waves*.

If we pay attention to Eq. (1.79), we see it is a symmetric tensor with a total of 10 degrees of freedom for the possible perturbations of the metric: 2 from the scalar fields (A, D), 3 given by the vector field B_i and 5 for the symmetric tensor E_{ij}. Thus, one can distinguish three classes of perturbations, see [39]:

- **Scalar mode:** this kind of perturbations are described with scalar functions, and correspond to the growing density and pressure perturbations. They are the most important for structure formation, and we will discuss them in detail later.

- **Vector mode:** it corresponds to the vector parts of the metric, and is related to vorticity perturbations. In the absence of sources, these modes decay on large scales.

- **Tensor mode:** these perturbations involve the traceless part of the spatial tensor h_{ij} that cannot been obtained as a gradient of a scalar or vector, namely E_{ij}. This mode is completely gauge invariant, and has two degrees of freedom. Einstein equations for the spatial tensor perturbation to the metric result in a wave equation for h_{ij}: $\partial^\sigma \partial_\sigma h_{\mu\nu} = 0$ in a flat empty spacetime. Thus, as it has been pointed before, it can be interpreted as transverse gravitational radiation; the two degrees of freedom being the two possible polarizations of gravitational waves.

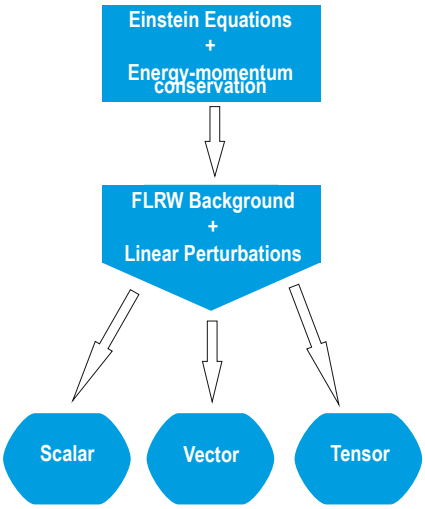

Figure 1.3: *Scalar, vector, tensor decomposition of linear perturbations. At the top of the tree of possibilities for structure formation models we have the assumption that general relativity holds and that the Universe is homogeneous and isotropic on average.*

The points of the unperturbed background space-time and those corresponding to the perturbed one can be related with a proper coordinate system x^α. Nevertheless, given a coordinate system in the background space there exist a huge amount of them in the perturbed spacetime. So, the choice of one among them is known as a *gauge choice*.

In what follows, to describe the scalar mode perturbations we are interested on, we will make use of the "Synchronous Gauge", which leaves the components $\bar{g}_{00}$ and $\bar{g}_{0i}$ of the metric tensor unperturbed $(A = B = 0)$, so, the line element is given by

$$ds^2 = a^2(\tau)\left[-d\tau^2 + (\delta_{ij} + h_{ij})\, dx^i dx^j\right]. \tag{1.80}$$

This gauge is related to a coordinate system where the cosmic time is comoving with the fluid and it becomes advantageous for the study of perturbations with a wavelength larger that the Hubble radius ($\lambda \gg 1/H$); conditions satisfied by any mode at early epochs. In fact, it is the natural coordinate system for free falling observers.

Energy-momentum tensor perturbations

In cosmological perturbation theory, all energy density components fluctuate and give a contribution to the growth of inhomogeneities that produce the large scale structures. In addition to the metric perturbations, we have to consider density and pressure perturbations:

$$\delta\rho = \rho - \bar{\rho} \tag{1.81}$$
$$\delta p = p - \bar{p} \tag{1.82}$$

which are of the same order of the coordinate velocity, $v^i \equiv dx^i/d\tau$, the perturbation to the 4-velocity of a fluid, $u^\mu = \frac{1}{a[1-v^2]^{1/2}}\{1, v^i\}$.

In order to obtain the perturbation equations, the starting point are Einstein equations (1.8), which have to be satisfied by the background and the perturbed metric, and the energy-momentum tensor of the fluid that describes each of the components of the Universe. The components of the energy-momentum tensor, if we consider perturbations to the first order, are:

$$T^0_0 = p - (\rho + p) = -\rho = -(\bar{\rho} + \delta\rho), \tag{1.83}$$
$$T^0_i = p g^0_i + (\rho + p) u^0 u_i = (\rho + p)\frac{d\tau}{(-ds^2)^{1/2}}\frac{dx_i}{(-ds^2)^{1/2}} \approx (\bar{\rho} + p) v_i = -T^i_0, \tag{1.84}$$
$$T^i_j = p g^i_j + (\rho + p) u^i u_j = (\bar{p} + \delta p)\delta^i_j + \Sigma^i_j. \tag{1.85}$$

Here, Σ^i_j is the traceless component of T^i_j, defined as

$$\Sigma^i_j \equiv T^i_j - \delta^i_j \frac{T^k_k}{3}. \tag{1.86}$$

Scalar perturbation equations

As tensor and vector modes do not produce density perturbations, they are not as important as the scalar modes for structure formation. Thus, we will not discuss them in detail here. From Einstein equations it is possible to obtain a complete set of equations for all the modes together with the corresponding constrain equations. However, to obtain the evolution of the scalar perturbations, it is easier to start form the energy-momentum conservation equations, which at the same time are a consequence of Einstein equations:

$$\begin{aligned} T^{\mu\nu}_{;\nu} &= \partial_\mu T^{\mu\nu} + \Gamma^\nu_{\alpha\beta} T^{\alpha\beta} + \Gamma^\alpha_{\alpha\beta} T^{\nu\beta} \\ &= \frac{1}{\sqrt{-g}}\frac{\partial\left(\sqrt{-g}\right) T^\mu_\nu}{\partial x^\mu} - \frac{1}{2} g_{\mu\alpha,\nu} T^{\mu\alpha} = 0. \end{aligned} \tag{1.87}$$

In this formulation $_{;\mu}$ denotes the covariant derivative.

From each of the components we will obtain a different evolution equation for the perturbations. Considering in the first place the component $\nu = 0$ of Eq. (1.87), one gets the continuity equation, $T^{\mu}_{;\mu}$, which at first order of perturbations reads:

$$\begin{aligned}
T^{\mu}_{0;\mu} &= \frac{1}{\sqrt{-g}}\frac{\partial\left(\sqrt{-g}T^{\mu}_{0}\right)}{\partial x^{\mu}} - \frac{1}{2}g_{\mu\alpha,0}T^{\mu\alpha} \\
&= \frac{1}{\sqrt{-g}}\left\{\frac{-g'}{2\sqrt{-g}}T^{0}_{0} + \sqrt{-g}T'^{0}_{0} - \frac{g_{,i}}{2\sqrt{-g}}T^{i}_{0} + \sqrt{-g}T^{i}_{0,i}\right\} - \frac{g^{00}}{2}g_{00,0}T^{0}_{0} - \frac{g^{ki}}{2}g_{jk,0}T^{j}_{i} \\
&\approx \frac{g'}{2g}T^{0}_{0} + T'^{0}_{0} - \frac{g_{,i}}{2g}T^{i}_{0} + T^{i}_{0,i} + \frac{2aa'}{2a^{2}}\left(\bar{\rho}+\delta\rho\right) - \frac{g^{ki}}{2}g_{jk,0}\left(\bar{p}+\delta p\right)\delta^{i}_{j} \\
&\approx -\frac{4a'}{a}\delta\rho - \frac{h'}{2}\bar{\rho} - \delta\rho' + \frac{a'}{a}\delta\rho - \frac{3a'}{a}\delta p + \frac{h'}{2}p - \left(\bar{\rho}+\bar{p}\right)\theta \\
&= -\left(\bar{\rho}+\bar{p}\right)\left(\theta + \frac{h'}{2}\right) - \frac{3a'}{a}\left(\delta\rho+\delta p\right) - \delta\rho' = 0
\end{aligned} \tag{1.88}$$

with $\theta = ik_j v^j = \partial v^j/\partial x^j$ being the fluid divergence.

With the expression for the density fluctuation $\delta \equiv \delta\rho/\bar{\rho}$, we can obtain

$$\delta\rho' = \bar{\rho}'\delta + \bar{\rho}\delta' = -\frac{3a'}{a}\left(\delta\rho\right)\delta + \bar{\rho}\delta' = -\frac{3a'}{a}\left(1+w\right)\delta\rho + \bar{\rho}\delta' \tag{1.89}$$

where we have considered the fluid equation of state $w \equiv \bar{p}/\bar{\rho}$. Finally, combining Eqs. (1.88) and (1.89) we have the equation of the energy density fluctuations:

$$\delta' = -\left(\theta + \frac{h'}{2}\right)\left(1+w\right) - \frac{3a'}{a}\left(\frac{\delta p}{\delta\rho} - w\right)\delta. \tag{1.90}$$

The $\nu = i$ components of the energy-momentum conservation give Euler equations, which in the perturbed case take the form:

$$\begin{aligned}
T^{\mu}_{i,\mu} &= \frac{1}{\sqrt{-g}}\left\{\frac{\partial\left(\sqrt{-g}\right)}{\partial x^{0}}T^{\mu}_{i} + \sqrt{-g}\frac{\partial T^{\mu}_{i}}{\partial x^{0}} + \frac{\partial\left(\sqrt{-g}\right)}{\partial x^{j}}T^{\mu}_{i} + \sqrt{-g}\frac{\partial T^{\mu}_{i}}{\partial x^{j}}\right\} \\
&\quad -\frac{1}{2}g_{\mu\alpha,0}\left\{g^{\alpha 0}T^{\mu}_{0} + g^{\alpha i}T^{\mu}_{i}\right\} = \frac{a'}{a}\left(1+w\right)\bar{\rho}v_i\left(4-3\left(1+w\right)\right) \\
&\quad +w'\bar{\rho}v_i + \left(1+w\right)\bar{\rho}v'_i + \frac{h_{,i}}{2}\bar{p} + \frac{\partial}{\partial x_i}\left(\bar{\rho}+\delta p\right) + \Sigma^{j}_{i,j} + \frac{h_{,i}}{2}\left(\bar{p}+\delta p\right) \\
&= \frac{a'}{a}\left(1+w\right)\bar{\rho}v_i\left(4-3\left(1+w\right)\right) + w'\bar{\rho}v_i + \left(1+w\right)\bar{\rho}v'_i + ik^i\delta p + ik_j\Sigma^{j}_{i} = 0.
\end{aligned}$$

Multiplying this equation by ik_i we obtain an expression for θ',

$$\theta' = -\frac{a'}{a}\left(1-3w\right)\theta - \frac{w'}{\left(1+w\right)}\theta + \frac{\delta p/\delta\rho}{\left(1+w\right)}k^2\delta - k^2\sigma, \tag{1.91}$$

with σ the shear stress:

$$(\bar{\rho}+\bar{p})\,\sigma \equiv -\left(\hat{k}_i\cdot\hat{k}_j-\frac{1}{3}\delta_{ij}\right)\Sigma^i_j=-\hat{k}_i\cdot\hat{k}_j\Sigma^i_j=-\frac{k_ik_j}{k^2} \tag{1.92}$$

Eqs. (1.89) and (1.91) describe the evolution of the scalar modes for the energy density and pressure perturbations. These expressions can then be particularized for a given theoretical model to obtain the specific prediction for structure formation.

1.5.2 Inflation

In previous sections we have seen the success of the standard cosmology to explain the observations of the Cosmological Microwave Background, the expansion of the Universe and the framework within the formation of large structures can be understood. However, there are certain unexplained features connected to the first stages of the Universe History as the Big-Bang:

- **Horizon Problem:** This is probably the most outstanding problem of the Hot Big Bang model. We have already seen in the last part of section 1.2 that, given the finite age of the Universe, the light can have only traveled a finite distance in a certain time. Thus, the observable universe is the region inside the particle horizon which is causally connected. Observations have revealed that CMB radiation is very isotropic; the radiation we receive from all parts of the sky give us the same temperature. This feature is a consequence of a certain thermal equilibrium, and could be explained if all regions of the sky have been causally connected and have been able to interact. However, if we compute the horizon length at the last scattering surface, i.e. at the epoch the CMB was produced, we obtain that it is very small, and it covers only $\theta < 2^o$ of the sky. Thus, how is it possible that we observe the same variation of temperature from the CMB radiation coming from two opposite sides of the sky if they were causally disconnected when the radiation was produced?

- **Flatness Problem:** Eq. (1.19) gives us the relation of spatial curvature with the total energy density of the Universe. Taking into account Eqs. (1.15) and (1.16), we obtain:

$$|\Omega-1| \propto t \text{ for Matter dominated universe} \tag{1.93}$$
$$|\Omega-1| \propto t^{2/3} \text{ for Radiation dominated universe.} \tag{1.94}$$

  So, in both cases, if the total energy density, Ω, deviates from 1, this will increase with time very quickly, leading to an even more curved universe. At present, current observations give us a value of the total energy density really close to 1, which means that at very early times this deviation had to be smaller, giving place to an extremely flat universe. Thus, if the curvature term is not dominant at present, it must have had a very small initial value. We are again in front of another fine-tuning problem: why were the initial conditions so flat?

- **Initial perturbation problem:** One further problem is the origin of the primordial inhomogeneities. We know from perturbation theory that initial small perturbations can seed the gravitational instabilities that later will produce the large scale structures of the Universe we can observe at present. However, the origin of these initial perturbations is unknown.

- **Relic particle abundances or monopole problem:** GUT theories often predict the formation of extremely heavy particles at the very early in the history of the Universe. As the early universe was dominated by radiation with rapidly decreasing energy density, heavy particles would quickly come to dominate the universe leading to an evolution incompatible with the present observations.

In the 80's a possible solution to these problems was proposed: an initial short period in the Universe History of **Inflation** [7, 112, 173]. During inflation the universe experimented an evolution with an accelerating scale factor, $\ddot{a}(t) > 0$, i.e. a very rapid expansion. Looking at Eq. (1.11), it is easy to see that this acceleration occurs when $\rho + 3p < 0$, which implies an equation of state $w < -1/3$. During that period, the accelerated expansion is supposed to be driven by the vacuum energy of a scalar field ϕ with some self-interacting potential $V(\phi) \geq 0$, rolling slowly toward its ground state, so that its energy density is approximately constant in time and given by its potential energy $\rho \sim V(\phi)$.

Such a field is equivalent to a perfect fluid with energy density and pressure given by $\rho = 1/2\dot{\phi}^2 + V(\phi)$ and $p = 1/2\dot{\phi}^2 - V(\phi)$. If we insert these expressions into Eqs. (1.11) and (1.13), we see that to obtain the inflationary requirement, $\ddot{a}(t) > 0$, the condition $\dot{\phi}^2 < V(\phi)$ has to satisfied together with $|\ddot{\phi}| \ll H|\dot{\phi}|$, which has to be fullfield if we want the field, ϕ, to roll slowly down its potential (*slow-roll condition*). In the literature one can find a large amount of models for inflation where different types of scalar fields and potentials have been studied in detail. However, as it would deviate us from the main line of this work, we will not review them here; please see [28, 169] and references therein for a good review.

1.6 Observational cosmology

Initialy, Cosmology was practically a speculative science. In its origins, the instrumental limitations reduced observations to a few. With time, the number and quality of observations increased, giving place to remarkable discoveries that changed completely the conception of the Universe and revolutionized Cosmology. As we have seen in sections 1.1 and 1.3, observational discoveries have motivated theoreticians to develop a compelling cosmological model that could explain them. This is the case of the discovery of the expansion of the Universe, the first measurement of the Cosmic Microwave Background or the observation of the accelerated expansion in the early past.

In the last decades, there have been remarkable advances in observational cosmology as a consequence of the development of new experiments to observe the CMB, the large scale distribution of galaxies, distant Type Ia supernovae (SNeIa), baryon acoustic oscillations (BAO), gravitational lensing, etc. The quality of these data has allowed us to obtain a global

vision of the Universe, the so called concordance model; see Figs. 1.4 and 1.5. However, when one tries to explain observations in detail, i.e. when the cover-layer is peeled off, a lot of lower level complications arise, thus making the situation extremely challenging. Thus, at the same time that observational data became the seed of new physics, when observations give us inconsistencies with the concordance model; they also help us to determine the global geometry and dynamics of the Universe, comparing observations with theoretical predictions.

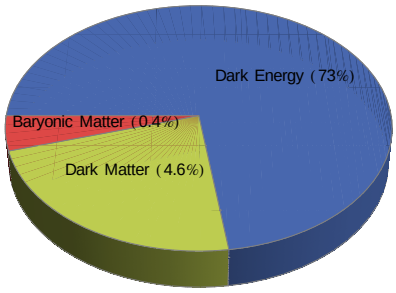

Figure 1.4: *The left panel show the percentual energy density content of the Universe.*

Any step forward in theoretical cosmology has to be able to be constrained with observational data, i.e. any cosmological model has to pass the exam of observations. Apart from explaining current data, they have to be able to give us the most accurate measure of the global geometry and dynamics of the Universe. At present we have a huge amount of precise data, so it is crucial to define the tools that will allow us to extract as much information as possible from it. In what follows we describe the main cosmological tests used in Cosmology at present, which relate the observational magnitudes with those parameters that define most precisely our cosmological model. Those quantities can be the energy density content, the equation of state of dark energy or any other parameter that can give us a hint of the dynamics of the Universe.

The essence of these tests is to correlate the redshifts measurements with some measurement of distances or magnitude that can be directly related to a distance. There are several types of cosmological tests:

- **Standard candles:** are luminous sources with a well known intrinsic luminosity. They are used to measure the luminosity distance which is connected to $H(z)$, as it is detailed in Eq. (1.98) in Section 1.3. The most common standard candles in cosmology are Type Ia Supernovae (Snela), as their luminosity is well known. Another kind of standard candles, far less accurate but more luminous, are Gamma Ray Bursts. So, in fact theri standard character is questionable.

- **Standard rulers:** objects whose length perpendicular to the line of sight is known *a priori*. These objects are used to measure the angular diameter distance, the ratio of an object physical transverse size to its angular size:

$$D_A = \frac{c}{(1+z)} \int_0^z \frac{dz'}{H(z)}. \tag{1.95}$$

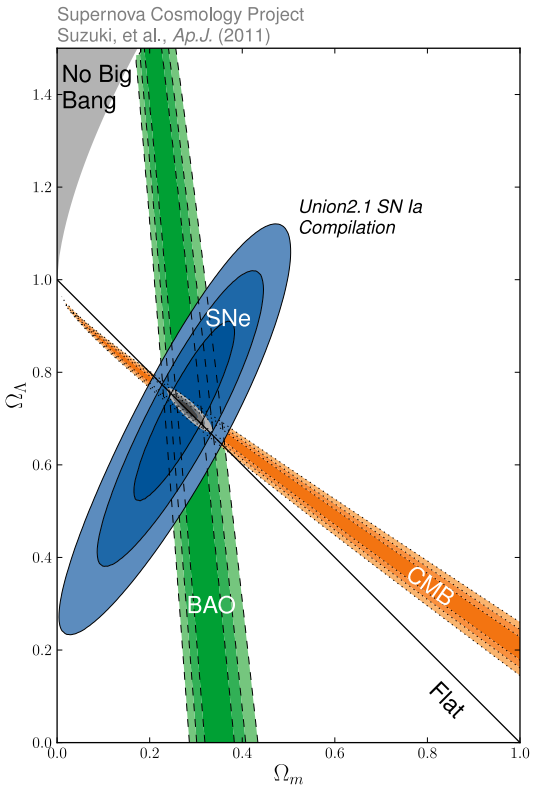

Figure 1.5: *68%, 95%, and 99.7% constraints on Ω_m and Ω_Λ obtained from CMB (orange), BAO (green), and the SNeIa Union Compilation 2.1 (blue). This figure is courtesy of the Supernova Cosmology Project [270]*

Some suggested candidates are the isophotal diameters of brightest cluster galaxies, the mean separation of galaxies in clusters, radio source lobe separations, etc [73, 90]. The last scattering horizon is also commonly used a standard ruler, this scale can be measured either directly at $z \simeq 1089$ through the CMB temperature power spectrum or indirectly through Baryon Acoustic Oscillations (BAO) on the matter power spectrum at low redshifts. Under certain assumptions clusters of galaxies and radio galaxies are also used as standard rulers, but they are less accurate than the CMB or BAO.

- **Standard populations:** Source number counts as a function of redshift, flux or magnitude of discrete populations such as galaxies, radio sources, quasars, etc. help to probe the evolution of a volume element. These tests require a population of sources with a constant comoving density which exhibit an evolution with the expansion of the Universe, [76, 219].

- **Standard clocks:** Indirect tests of age with redshift. Usually those measurements are highly model dependent, [72].

- **Direct measures of $H(z)$** [133, 134, 249, 266].

1.6.1 Type Ia Supernovae

Type Ia supernovae are the most used tool for studying cosmic acceleration, as it was discovered through their observation [210, 220]. These objects are detected observationally by the presence of silicion II and the absence of hydrogen in their spectra [99]. These evidences supported the idea that Type Ia supernovae are originated after a nuclear explosion of carbon/oxygen white dwarfs, the final stage of a star life cycle when the nuclear fusion which maintained the equilibrium has ended. There are two models for the progenitors. One in which the white dwarf accretes matter from a binary companion and exceeds the Chandrasekhar mass limit ($\sim 1.4M_{\odot}$), the mass above which the degenerate electrons composing the white dwarf became relativistic. In the second model, it is the gravitational radiation which forces the orbiting pair of white dwarfs to merge and transcend the Chandrasekar limit, [118]. Once this limit is achieved, there is a nuclear explosion in the core in which carbon or oxygen is converted to iron, and a nuclear flame propagates to the exterior. These events are the most energetic and bright of the Universe, they can provide us a measure of distances even though they are at high redshift. The other advantage is that those processes are detected not only in young but also old stellar populations. The excellent uniformity of their light-curves and their brightness peak, $\sim 10^{10}L_{\odot}$, with a characteristic decay time of about one month, provides a standard spectral template that can be used to infer cosmic expansion through the comparison of the peak of distant supernovae to those of closer ones that act as calibrators ($0.03 < z < 0.1$). Given the high correlation between the peak luminosity, L_{peak} and the decay time, an empirical relation is obtained between the peak absolute magnitude M_B and the observed change in apparent magnitude 15 days after the peak in the luminosity, Δm_{15}:

$$M_B \simeq 0.8(\Delta m_{15} - 1.1) - 19.5. \tag{1.96}$$

Supernovae events in a given galaxy are rare in human time scale. However, from the discovery of cosmic acceleration, supernovae surveys have became one of the main areas of research in observational cosmology over the last years. These surveys track thousands of galaxies in a regular way with the objective of detecting as many as possible events in the widest redshift range. The largest high-redshift data sets with over ~ 500 SNeIa are those from ESSENCE survey [77] and Supernova Legacy Survey [16, 61, 268], and at higher redshifts, $z > 1.0$, the data sets are provided by the Hubble Satellite Telescope (HST) [225, 270]. Given the high utility of SNeIa, several samples can be compiled to expand the redshift range. However, the samples have to been carefully chosen in order to reduce the systematic errors, so it is valuable to obtain a compiled sample as homogeneous as possible, as it has been done in Union and Union2.1 [10, 148, 270], "Gold" [221], Constitution [117] and the compilation of SNLS3 and HST sample [61].

Once a sample of SNeIa is compiled, the observed magnitudes are calibrated, providing us a measure of the distance modulus, μ, the best quantity to be related to the Hubble parameter $H(z)$ which describes the energy content of the Universe and its evolution. The distance modulus represents the difference between the apparent magnitude of the source, m, and the absolute magnitude, M. The expression for μ can be obtained from the logarithm

of Eq. (1.26). It has the form

$$\mu_{th}(z_i) = m - M = 5\log_{10}\left(d_L\left(z;\boldsymbol{\theta}\right)\right) + \mu_0, \tag{1.97}$$

and it is a function of the luminosity distance:

$$d_L\left(z;\boldsymbol{\theta}\right) = (1+z)\int_0^z \frac{dz'}{H\left(z';\boldsymbol{\theta}\right)}. \tag{1.98}$$

which at the same time depends on the N model parameters $\boldsymbol{\theta} = \{\theta_1, \theta_2, ..., \theta_N\}$.

In Fig. 1.6 observational data coming from the Union2 data set [10] are plotted together with the distance modulus predicted by three different cosmological models in order to show how SNeIa can help us to depict the composition of the Universe. Observational points from supernovae are completely in agreement with those values predicted in a universe with matter but dominated by dark energy. In a universe under matter domination the observed SNeIa should be fainter that they really are, just the opposite of what would happen in a universe without matter and completely filled with dark energy, where the SNeIa would actually be brighter than observed.

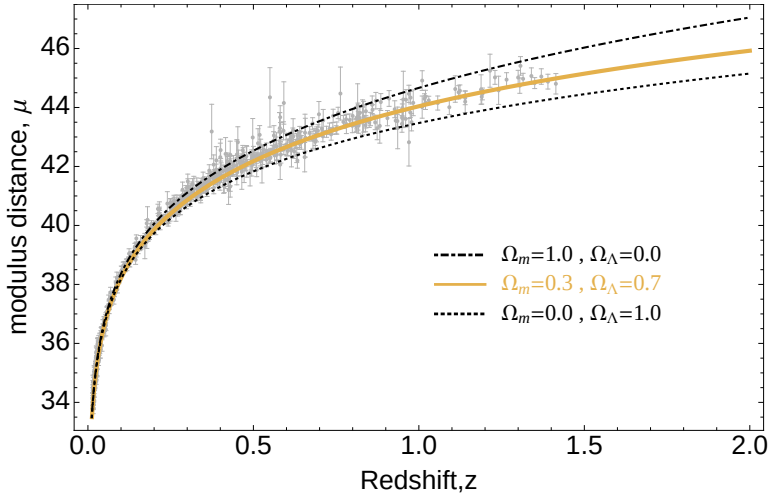

Figure 1.6: *Distance modulus, μ, versus redshift, z for a flat universe. The data points correspond to the Union2 data set given in [10]. The lines show three different cosmological models: (top) $\Omega_m = 0.0$ and $\Omega_\Lambda = 1.0$ (middle) $\Omega_m = 0.3$ and $\Omega_\Lambda = 0.7$ and (bottom) $\Omega_m = 1.0$ and $\Omega_\Lambda = 0.0$.*

Usually, when a theoretical model is proposed it has to be contrasted with observational data with two purposes: to see if it can give an explanation to them and to infer the values of model parameters that give us the best fit with observational data, i.e. set somehow constraints on these parameters. The last goal is obtained with a method of optimization wich considers the uncertainties they present. The most used method in these cases is the maximization of the likelihood, or what is the same, the χ^2 function minimization. This method will be explained in section 1.7, here we detail the general procedure to be applied to SNeIa. We say it is general because, depending on the the data set, it has to be adapted to the special way observational data are provided. Sometimes one has to minimize

over nuisance parameters that take into account the light-curve shape, the stretch of the luminosity relation, etc. It is common to provide observational data as the redshift, z, the distance modulus, μ_{obs}, and the error of the latter for each supernova. In this case, the strategy to follow is to define the χ^2 as the square of the differences of the theoretical and observed distance modulus divided by the uncertainties of the mesurements:

$$\chi^2_{\rm SN}(\mu_0, \boldsymbol{\theta}) = \sum_{j=1} \frac{(\mu_{\rm th}(z_j; \mu_0, \boldsymbol{\theta}) - \mu_{\rm obs}(z_j))^2}{\sigma^2_{\mu,j}}, \tag{1.99}$$

where $\sigma_{\mu,j}$ are the measurement variances. However, if we look at Eq. (1.97), we see that there is an extra parameter, μ_0, which encodes the absolute magnitude M and the Hubble parameter, H_0. The introduction of this parameter in the definition of χ^2 makes the minimization more intensive as this parameter has to be marginalized over, as the only parameters of interest are those that define the cosmological model. In order to proceed with the marginalization, we should integrate the χ^2 over μ_0, but depending on the cosmological model, this can be extremely complicated:

$$\tilde{\chi}^2 = -2 \log \left(\int \exp\left(-\chi^2_{SN}\right) d\mu_0 \right). \tag{1.100}$$

Nevertheless, an alternative way to marginalize is often used. It consists in maximizing the likelihood by minimizing χ^2 with respect to μ_0 [92]. In this case, one can rewrite Eq. (1.99) as

$$\chi^2_{\rm SN}(\boldsymbol{\theta}) = c_1 - 2c_2\mu_0 + c_3\mu_0^2, \tag{1.101}$$

where the new terms are:

$$c_1 = \sum_{j=1} \frac{(\mu_{\rm obs}(z_j) - 5\log_{10} d_L\left(z_j; \boldsymbol{\theta}\right))^2}{\sigma^2_{\mu,j}}, \tag{1.102}$$

$$c_2 = \sum_{j=1} \frac{\mu_{\rm obs}(z_j) - 5\log_{10} d_L\left(z_j; \boldsymbol{\theta}\right)}{\sigma^2_{\mu,j}}, \tag{1.103}$$

$$c_3 = \sum_{j=1} \frac{1}{\sigma^2_{\mu,j}}. \tag{1.104}$$

Now, it is easier to carry on with the minimization over μ_0, which gives us the value of the nuisance parameter that corresponds to the minimum value of χ^2:

$$\mu_0 = c_2/c_3. \tag{1.105}$$

Finally the χ^2 function after the minimization takes the form

$$\tilde{\chi}^2_{\rm SN}(\boldsymbol{\theta}) = c_1 - \frac{c_2^2}{c_3}. \tag{1.106}$$

This is an approximate method but it has negligible effects in the final results as it is

shown in [194].

1.6.2 Gamma Ray Bursts

Other suggested distance indicators and possible candidates to standard candles are Gamma Ray Bursts (GRBs). GRBs are the most intense explosions observed in the Universe, their duration varies from milliseconds to several minutes. They consist on an initial burst of gamma rays followed by an afterglow of radiation of larger wavelengths as X-ray, ultra violet, optical, infrared or radio emissions. These processes are so luminous that can be detected up to very high redshifts, $z > 8$. [69, 110, 232, 272]. The nature of their progenitors is still uncertain (see [190] for a review), depending on their duration, they are believed to be released by the collapse of a rapidly rotating massive star core into a black hole if they are long lived. For the case of short lived GRBs it is suspected that the scenario in which they are produced is completely different, and they are thought to be produced after the collisions of neutron stars in a binary system. Even their nature can be extremely diverse, GRBs show a correlation between equivalent isotropic energy and spectral properties as the energy peak or variability. These features make it possible to construct distance-redshift diagrams for systems whose redshift has been obtained via spectroscopy. Thus, they provide a new window to study the properties of the Universe in the redshift desert range given by SNeIa ($z \lesssim 2$) and CMB ($z = 1089$), inaccessible in other ways.

Even GRBs cannot be considered as standard candles at the moment, so they are not comparable to SNeIa, they contain a lot of information about high redshift properties of the Universe which cannot be derived from SNeIa. So their combined use with other cosmological probes can bring important and complementary information about the reconstruction of dark energy, and gives us the possibility to detect eventually traces of a dynamical equation of state. In contrast to SNeIa compilation, where high redshift objects can be calibrated using nearby SNeIa, the lack of GRBs at $z < 0.1$ which are cosmology independent, requires that GRBs have to be calibrated for each cosmological model. Thus, the GRB data must be fitted for calibration and to infer cosmological parameters at the same time. This makes the use of GRBs as a cosmological probe somewhat awkward. The calibration of GRB data can be done in several ways, but in [145] an idea of the distance ladder to calibrate GRBs in a completely cosmology-independent way has been proposed. In the same way to the calibration of SNIa by using Cepheid variables which are primary standard candles, one can calibrate GRBs with a large amount of SNIa. And then, the calibrated GRBs can be used to constrain cosmological models without the circularity problem. Many empirical formulas have been given to describe the peak energy-peak luminosity correlation. In [145] the correlation between peak energy of the spectrum, E_p, and the peak luminosity, L_p, is given by the so called *Yonetoku relation* (see[298])

$$L_p \propto E_p^2. \tag{1.107}$$

The GRBs sub-sample at low redshift $z < 1.6$ is calibrated without assuming any cosmological model, using an empirical formula for the luminosity distance estimated from those of SNeIa in the same redshift range.This formula can be applied to GRBs to obtain the calibrated $E_p - L_p$ relation which is then applied to the high redshift GRBs sub-sample giving a final

data set made up of a set of calibrated luminosity distances:

$$d_L(z_i) = 10^2 4cm \sqrt{\frac{1.31}{4\pi f^i_{p,obs}}} \left[E^i_{p,obs}(1+z^i)\right]^{,1.68/2} \tag{1.108}$$

with $f^i_{p,obs}$ the observed flux peak in units erg cm^{-2}s^{-1} and $E^i_{p,obs}$ the measured energy peak in keV.

Once GRBs data are calibrated, they can be used to obtain the parameters of the cosmological model which best fit these data taking into account the contribution to the total chi-square of the GRBs as:

$$\chi^2_{\rm GRB}(\boldsymbol{\theta}) = \sum_{j=1}^{63} \frac{(d_L(z_j;\boldsymbol{\theta}) - d_L^{obs}(z_j))^2}{\sigma^2_{\rm d_L}(z_j)}, \tag{1.109}$$

where the $\sigma^2_{\rm d_L}$ are the measurement variances.

1.6.3 Cosmological Microwave Background

The Cosmological Microwave Background (CMB) was discovered by Penzias and Wilson in 1965 [204]. Given the uniformity of the radiation, they measured the same frequency in every direction. The nature of this radiation was attributed to a blackbody with a temperature near $T \simeq 3.5$K. Since then, there have been many terrestrial antennas that have tried to get further and figure out the nature of the CMB. However, it was in 1992 when the COBE team led by G. Smoot sent a satellite which studied the properties of the CMB in a wide range of frequencies and detected temperature or intensity fluctuations of 10^{-5} from one part of the sky to another [256]. This discovery has become an important highlight in Cosmology because it gives us the chance to learn about the physics of the the first stages of the Universe. With time, the experiments have improved, and the anisotropies first detected by COBE are now being measured with high precision.

In section 1.5.1 we have seen how small inhomogeneities, perturbations in the energy density of the components of the Universe (matter or radiation), can evolve from early times to the present. Matter inhomogeneities which have grown through gravitational instabilities give origin to the structures like galaxies and clusters that we can observe today. The same primordial perturbations generated the observed anisotropies in the CMB. As these perturbations were originated at the time of recombination, the CMB represents a direct window to the physics of early times, inaccessible in other ways.

Photons in the early universe were in thermal equilibrium, but this equilibrium started to disappear near the epoch of recombination producing the first anisotropies. With the decoupling, radiation spread out through an inhomogeneous gravitational field which enlarge these anisotropies. Given the spherical geometry, they are usually expressed in terms of spherical harmonics:

$$\frac{\Delta T}{T}(\mathbf{n}) = \sum_{l=0}^{\infty} \sum_{m=-l}^{l} a_{lm} Y_{lm}(\mathbf{n}), \tag{1.110}$$

where $\mathbf{n}$ is a unit vector which represents the direction of the line of sight; it can also be represented by a pair of angles (θ, ϕ). T is the average temperature, $T = \int d\Omega T(\theta, \phi)$, and $\Delta T(\mathbf{n}) = T(\theta, \phi) - T$ is the deviation given a direction $\mathbf{n}$. The coefficients a_{lm} describe the temperature perturbation and satisfy the following relation:

$$\langle a_{lm} a^{\star}_{l'm'} \rangle = \delta_{ll'} \delta_{mm'} C_l, \tag{1.111}$$

where the brackets indicate an average over a set of realisations and $\delta_{ll'}$ the Kronecker symbol. The quantity C_l defines the angular power spectrum:

$$\langle \left| \frac{\Delta T}{T}(\mathbf{n}) \right|^2 \rangle = \frac{1}{4\pi} \sum_{l=0}^{\infty} (2l+1) C_l, \tag{1.112}$$

$(2l+1)$ being the contribution of the multipole l to the mean square temperature distribution of the CMB. So, given a theoretical model for the early universe one can obtain the corresponding set of C_ls. However, if we want to compare this prediction with observations, we have to take into account that C_ls are obtained as an ensemble average, whereas we only measure the actual value, not its expectation value. This effect is known as *cosmic variance*, and one can estimate the uncertainty of the measured angular power spectrum $\hat{C}_l$ compared to the theoretical prediction C_l [280]:

$$\langle (\hat{C}_l - C_l)^2 \rangle = \frac{2}{2l+1} C_l^2. \tag{1.113}$$

In Eq. (1.110) for the expansion of the anisotropies, the index l can be physically interpreted as the angular scale $\theta \sim \pi/l$. Thus as l gets larger, the spherical harmonics vary on smaller angular scales. The term corresponding to $l = 0$ is the *monopole correction*, which modifies the mean temperature for the particular sky of an observer respect to the global mean over all possible skies. For $l = 1$ we have the *dipole term*, the largest anisotropy of the CMB. It accounts for our motion through space relative to the microwave background due to Doppler Effect. As these two terms do not provide information about the intrinsic properties of CMB they are treated separately, and the maps of the temperature anisotropies provide results with these modes removed. Higher values of l, those with $l \geq 2$ are assigned to intrinsic anisotropy produced by perturbations in density at early universe. These kind of anisotropies are known as *primary anisotropies*. However, additional perturbations are added due to the travel of photons from decoupling to the present driving the so called *secondary anisotropies* which are produced by:

- The thermal **Sunyaev-Zel'dovich effect** which is produced when a galaxy cluster is in the path of photons. The hot gas in the cluster interacts with the photons through Compton scattering.

- **Integrated Sachs-Wolfe effect**. This effect is due to varying gravitational potentials which change the frequency, energy, direction and velocity of the travelling CMB photons. It can be divided into two categories, *early ISW* and *late ISW*. The former is important around recombination when anisotropies start growing. The latter depends

on the background cosmological parameters.

- Lensing.
- Doppler effect caused by the motion of the cluster gas.

The characteristics of the spectrum, i.e. the existence of peaks and troughs, the spacing between them, and also the location of the first peak depend on the initial conditions at time where the CMB was produced and the energy density contents before and after recombination. Thus, the CMB is an exceptional tool to investigate not only the physics of the early universe but also its current energy content. The way the cosmological parameters affect the anisotropies is well understood and explained with the physics of the evolution of linear perturbations within a background FRW cosmology. It is possible to calculate the temperature power spectrum, but it requires a sophisticated numerical computation to include each of the many processes that took place at time of CMB production. For this purpose some codes have been developed such as CAMB[4] [164, 166] or CLASS[5] [163] which do it in an efficient and fast way.

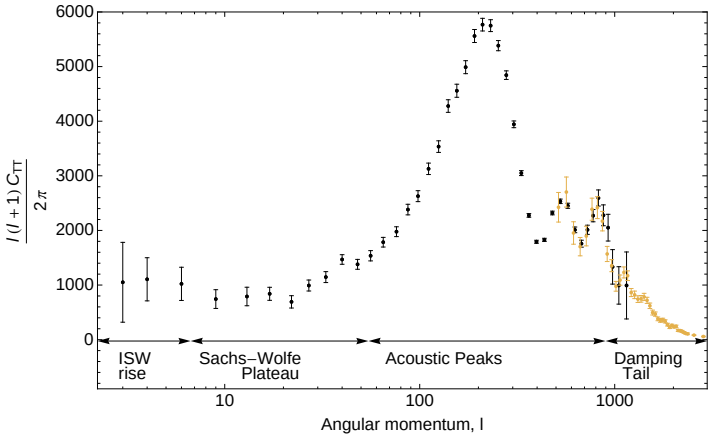

Figure 1.7: *CMB temperature power spectrum given by WMAP7-year (black points) and Atacama Cosmology Telescope (ACT) (yellow points) where the most differentiate features are indicated: Integrated Sachs-Wolf rise, Sachs-Wolf plateau, the region of the acoustic peaks and the damping tail.*

What follows is a summary of the underlying physics that would explain the distinctive features of the power spectrum. From Fig. 1.7 one can see that there are three differentiated regions:

- **The Sachs-Wolfe plateau for $l \leq 100$:** an initial almost flat region at large angular scales. A scale invariant or almost scale invariant adiabatic primordial spectrum for matter density oscillations ($P(k) \propto k^{n_s}$ with an $n_s \simeq 1$) gives a scale invariant power spectrum which corresponds to temperature anisotropies independent of the angle giving a flat power spectrum for temperature. On the other hand, a variation of the

[4] http://camb.info/
[5] http://class-code.net

gravitational potentials raises the C_ls for low values of the multipole momemtum: early ISW effect. It occurs in a universe where $\Omega_m \neq 1$; so dark energy at low redshifts induces a change of CMB photons that enhances the lower C_ls.

- **Acoustic peaks** $100 \leq l \leq 1000$**:** a region of successive peaks and troughs of smaller amplitude called *Doppler* or *Acoustic peaks*. These peaks are induced by acoustic oscillations in the baryon-photon fluid in the early Universe. An overdensity of matter at that epoch does not collapse until it enters its own particle horizon (where every point is in causal contacted with others). Once the perturbation enters, it will keep collapsing until the Jeans length, when radiation pressure counteracts gravity and initiates acoustic oscillations.

- **Damping tail for** $l \geq 1000$**:** we can see that in the region corresponding to small scales, the peaks suffer a damping. These multipole momenta correspond to characteristic scales of previous epochs to the last scattering. The damping is mainly due to the imperfect coupling between the photon-baryon fluid caused by shear viscosity and heat conduction. It drives a spreading between them that makes the amplitude of oscillation decrease. This effect is known as *Silk damping* and dominates at $l > 2000$ [247]. Extra effects for high values of the multipole momentum are given by gravitational lensing originated by structures a low redshift as galaxy clusters.

CMB anisotropies in the temperature reveal us the high dependence of these features with cosmological parameters. Thus, CMB observations are crucial to obtain high precision constraints on the cosmological parameters. The temperature power spectrum is not directly related to dark energy, but it gives us strong restrictions on the matter content and on the geometry which indirectly provides a bound on the dark energy quantities. It can also provide us additional information about the spectral index, n_s, of primordial scalar perturbations, the post-recombination electron-scattering optical depth τ, the Hubble constant, H_0, etc.

The amplitudes of the acoustic peaks are determined by the energy content of the Universe $(\Omega_m h^2, \Omega_r h^2)$ before recombination. An increase of the baryon content of the Universe at that epoch, reduces the pressure at the last scattering surface, which enlarges anisotropies and decreases the sound speed of the baryon-photon fluid. These effects have direct consequences on the C_ls: an enhancement of the amplitude of oscillations pushing acoustic peaks to smaller scales. A rise of $\Omega_b h^2$ inhibits the diffusion, having consequences on the damping tail of the power spectrum. On the other side, if the total matter content of the Universe gets bigger, it anticipates the epoch of equality, shifting the z_{eq} to higher redshifts and minorating the early ISW, which pushes down and narrows the first acoustic peak. The change of the radiation-matter equality, increases the comoving angular diameter distances to recombination, $D_A(z_{\rm rec})$. As a consequence, it varies the acoustic scale

$$\theta_A = \frac{r_s(z_{\rm rec})}{D_A(z_{\rm rec})}, \tag{1.114}$$

and shifts the peaks positions to lower ls, $l_n \sim n\pi/\theta_A$. From this expression we can easily see that the position of the first peak also depends on the geometry of the Universe and on the history of the dark energy density. The impact of the Ω_{DE} on the power spectrum, besides

moving the peaks to larger angular scales, induces the late-time ISW. As the influence of Ω_k and Ω_{DE} is given through D_A, there is a degeneracy with the effect of other parameters, i.e. their variation produces an effect on the CMB similar to that from for example Ω_m or Ω_b. To avoid this degeneracy, CMB data are normally used in combination to other datasets as SNIea, a measure of the Hubble parameter H_0 or Baryon Acoustic Oscillations (BAO) as we will see in the next section.

Now that the influence of the cosmological parameters on the CMB has already been described, it is time to give details about the main procedures to obtain observational constraints on them using the power spectrum of temperature anisotropies. The most direct would be to compare directly the predicted C_ls given by the theoretical model with those given by observational data. The predicted C_ls can be obtained with the public free software CAMB and the corresponding software to compute the likelihood. Modules for this are usually given by each of the teams that have measured and post-processed the CMB data, and can be acquired at the LAMBDA project web-page[6]. However there are cases where the cosmological model is quite complicated and it requires modifications of the CAMB software itself. In these cases it is easier to directly compare a bunch of quantities directly obtained from the analysis of the CMB power spectra with those predicted by the specific theoretical model. A good quantity is the distance to the recombination epoch because, as we have seen, the peaks and troughs of acoustic oscillations are sensitive to it. Therefore, the CMB provides a good measure of the ratio of the angular diameter distance to the recombination epoch divided by the sound horizon size at that time, $D_A(z_{\rm rec})/r_s(r_{\rm rec})$. Under the assumption of a flat universe, instead of $D_A(z)$, one can directly use the comoving distance:

$$D_c(z) = c\int_0^z \frac{dz'}{H(z')}. \tag{1.115}$$

Thus, the ratio, $D_c(z_{\rm rec})/r_s(r_{\rm rec})$, is directly given by the angular scale of the sound horizon at recombination, l_A,

$$l_A(z_{\rm rec}) \equiv \frac{\pi D_c(z_{\rm rec})}{r_s(z_{\rm rec})}. \tag{1.116}$$

The only remaining issue then is to compute $z_{\rm rec}$. For this purpose, following the fitting function can be used [124]:

$$z_{\rm rec} = 1048\left[1 + 0.00124\left(\Omega_b h^2\right)^{-0.738}\right]\left[1 + g_1\left(\Omega_c h^2\right)^{g_2}\right], \tag{1.117}$$

the expressions for the g_1 and g_2 being

$$g_1 = \frac{0.0783\left(\Omega_b h^2\right)^{-0.238}}{1 + 39.5\left(\Omega_b h^2\right)^{0.763}}, \tag{1.118}$$

$$g_2 = \frac{0.560}{1 + 21.1\left(\Omega_b h^2\right)^{1.81}}. \tag{1.119}$$

[6] http://lambda.gsfc.nasa.gov/

Finally, the corresponding comoving sound horizon at recombination is

$$r_s(z_{\rm rec}) = \int_0^{t_{\rm rec}} \frac{c_s dt}{a} = \int_{z_{\rm rec}}^{\infty} \frac{c_s}{H(z)} = c\int_0^{a_{\rm rec}} \frac{da}{\sqrt{3(1+\bar{R}_b a)a^4 H^2(z)}} = \frac{c}{\sqrt{3}}\int_0^{1/(1+z_{\rm rec})} \frac{da}{a^2 H(a)\sqrt{1+\frac{3\Omega_b}{4\Omega_\gamma}a}} \tag{1.120}$$

with $\bar{R}_b = (3\rho_b)/(4\rho_\gamma)$, $\bar{R}_b = 31500\Omega_b h^2 (T_{CMB}/2.7K)^{-4}$, $\Omega_\gamma = 2.469\cdot 10^{-5}h^{-2}$, $c = 2.9979\cdot 10^5 \mathrm{Kms}^{-1}$ (for $T_{CMB} = 2.725K$) and $h = 0.72$ [146]. Alternatively, the sound horizon at recombination can by evaluated using an aproximative expression as it is described in [87]:

$$r_s(a_{\rm rec}) = \frac{4000}{\sqrt{\Omega_b h^2}}\frac{\sqrt{a_{eq}}}{\sqrt{1+\eta_\nu}} \ln\left\{\frac{[1+R(z_{\rm rec})]^{1/2} + [R(z_{\rm rec})+R_{eq}]^{1/2}}{1+\sqrt{R_{eq}}}\right\} \mathrm{Mpc},$$

where $\eta_\nu = 0.6813$ is the ratio of the energy density in neutrinos to the energy in photons, $R(a) = \bar{R}_b a$ and a_{eq}, the scale factor at which radiation and matter have equal densities, $a_{eq}^{-1} = 24185\left(\frac{1.6813}{1+\eta_\nu}\Omega_m h^2\right)$.

From the CMB power spectrum it is also possible to obtain a measure of the *shift parameter* or scaled distance to the last scattering surface, $R(z)$, which is related to D_c [47] through

$$R(z_{\rm rec}) \equiv \sqrt{\Omega_m H_0^2} D_c(z_{\rm rec}). \tag{1.121}$$

In the end, the vector containing all these quantities, $\mathbf{v} = (l_A, R, z_{\rm rec})$, provides a good summary of the CMB data to constrain the dark energy parameters. At this stage, one can directly use the maximum likelihood values of WMAP 7-year [147], $\mathbf{v}^{\rm CMB} = (302.69, 1.726, 1091.36)$ and derive the correspoing χ^2 for the CMB,

$$\chi^2_{\rm CMB} = (v_i - v_i^{\rm CMB})(\mathbf{C}^{-1})_{ij}^{\rm CMB}(v_j - v_j^{\rm CMB})^T \tag{1.122}$$

where $(\mathbf{C^{-1}})^{CMB}$ is the inverse covariance matrix of the data, also provided by [147].

1.6.4 Baryon Acoustic Oscillations

Baryon Acoustic Oscillations (BAO) have recently come out as a promising standard ruler in cosmology. They can provide precise measurements of the dark energy parameters with a minimum of systematic errors [23, 44, 46, 62, 89, 122, 241, 288]. The fight between radiation pressure and gravity forces set up these acoustic oscillations of the density perturbations before recombination. Once photons decoupled and propagated freely, the acoustic wave of baryons got stuck, leaving a signature of the primordial perturbations not only on the CMB temperature distribution but also on the matter power spectrum, and as a consequence, on galaxy correlation, encoded in the function, $\xi(z)$. These oscillations give evidence of a

characteristic scale, the sound horizon at recombination:

$$s \equiv r_s(z_{\rm rec}) = \int_{z_{\rm rec}}^{\infty} \frac{c_s(z)}{H(z)} dz, \tag{1.123}$$

where c_s is the sound speed and $z_{\rm rec}$ the redshift at recombination [23, 206].

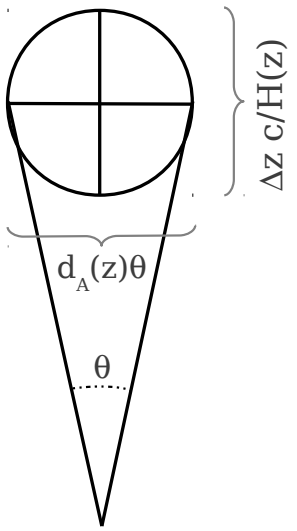

Figure 1.8: *BAO imprint a feature on the clustering of galaxies, providing a measure of the angular diameter distance $D_A(z)$ and Hubble parameter $H(z)$ in units of the sound horizon, s.*

This scale depends on the baryon and matter densities and also on the redshift of equality z_{eq} and recombination $z_{\rm rec}$. As the CMB provides good constraints on these quantities, it becomes a good calibrator of the characteristic scale. Independently, BAO features can be also determined from a galaxy survey, providing a measure of the angular diameter distance $D_A(z)$ and Hubble parameter $H(z)$ in units of the sound horizon, s, over a series of redshift slices, see Fig. 1.8. Measuring the BAO scale from galaxy clustering along the line of sight, $s_\parallel$, will be equivalent to measuring differences of redshift, and it is possible to obtain in that way a measure of the Hubble parameter:

$$s_\parallel H(z) = c\Delta z \tag{1.124}$$

Doing the same but in the tangential direction, $s_\perp$, i.e. a variation of the angular sizes, provides a measurement of the angular diameter distance:

$$\frac{s_\perp}{D_A(z)} = \Delta\theta(1+z), \tag{1.125}$$

which is directly related through $D_A(z) = r(z)/(1+z)$ to the comoving distance at a given

redshift:

$$r(z) = \int_0^z \frac{cdz'}{H(z')}. \tag{1.126}$$

Then, comparing the observed BAO measures with the scale given by CMB we directly have $r(z)$ or D_A, and $H(z)$.

However, it is a challenge to obtain BAO data due to the weak signal at high redshift. As a consequence, a vast volume of the Universe has to be mapped in order to detect BAO features; this is carried out through galaxy redshift surveys as SDSS [90], 2dFGRS [207, 208], WiggleZ [45] or the future EUCLID [32, 218][7] or J-PAS[33]. The data obtained are usually combined with other datasets to give tighter constraints on the dark energy parameters. At low redshift, the combination with SNeIa provides an accurate view of the redshift-distance relation, as BAO gives absolute distance scales while SNeIa provide precise relative distances. At larger redshifts $(z > 0.5)$ BAO becomes a direct access to $H(z)$.

In spite of BAO giving us the possibility of measuring simultaneously $r(z)$ and $H(z)$, it is easier to provide a composite measure of the physical $D_A(z)$ and $H(z)$ as an averaged BAO scale which is represented by a volume averaged distance $D_V(z)$:

$$D_V(z) = \left[(1+z)^2 D_A^2(z) \frac{c\,z}{H(z)}\right]^{1/3}, \tag{1.127}$$

see [45, 90, 208, 209].

In [209] for example, Gaussian values on the distance ratio, $r_s(z_{\rm drag})/D_V(z)$, at redshifts $z = 0.2$ and $z = 0.35$, are given from the measures obtained by combining the spectroscopic Sloan Digital Sky Survey (SDSS) and the Two-Degree Field Galaxy Redshift Survey (2DFGRS) data. This distance ratio represents the comoving sound horizon at the baryon dragging epoch, $z_{\rm drag}$, which reads

$$r_s(z_{\rm drag}) = c \int_{z_{\rm drag}}^{\infty} \frac{c_s(z)}{H(z)} {\rm d}z\ , \tag{1.128}$$

over the effective distance $D_V(z)$.

In order to estimate the dark energy and other cosmological parameters we need a definition of the χ^2 which reflects the difference between the observational data and the values given by our models. For this, one requires an expression for the comoving sound horizon at the baryon dragging epoch [209] (or recombination, depending of the way the observational data are provided). The dragging epoch took place after recombination [124], when the photon pressure was unable to balance the gravitational trend of baryons to collapse. The redshift at which it occurred can be well approximated by the fitting formula proposed in [88]:

$$r_s(z_{\rm drag}) = 153.5 \left(\frac{\Omega_b h^2}{0.02273}\right)^{-0.134} \left(\frac{\Omega_m h^2}{0.1326}\right)^{-0.255}. \tag{1.129}$$

[7] http://sci.esa.int/euclid

In contrast, if the observational data provided are given in terms of the sound horizon at recombination, we will need its expression which is given by Eqs. (1.117)-(1.120).

Now, the only remaining task is to construct the corresponding χ^2. Constructing the corresponding data vector $v_i = \left\{ \frac{r_s(z_{\rm drag},\Omega_m,\Omega_b;\boldsymbol{\theta})}{D_V(z_i,\Omega_m)} \right\}$, containing the Gaussian values at different redshifts, we obtain:

$$\chi^2_{\rm BAO} = (v_i - v_i^{\rm BAO})(\mathbf{C}^{-1})^{\rm BAO}_{ij}(v_j - v_j^{\rm BAO}) \tag{1.130}$$

where $\mathbf{C}^{-1}$ is the inverse of the covariance matrix of the data.

1.7 Statistics and data analysis

The improvement and development of technology have revolutioned observational cosmology. The amount of data and their quality and precision have increased enormously. And this trend is expected to persist in the future. Given this situation, we have to develop the corresponding tools to analyse and extract as much information as possible with the lowest computational effort. Thus, in the context of a given physical model which depends on some parameters, we use these statistical techniques with two targets: fixing the "most likely" values of the parameters that yield the series of available observational data, and on the other hand, measuring the degree of confidence in those data generated by the best fit parameters in an estimated interval.

For this purpose we need to define a quantity that encapsulates the information about the theoretical model and its parameters and those corresponding to the available observational data. Then this quantity has to be maximized or minimized with the corresponding methods to extract the values and the interval of confidence of the parameters that best fit with the observational data.

1.7.1 Parameter estimation

The typical central pillar of data analysis is the likelihood function. The likelihood function, $\mathcal{L}(\mathbf{d}|\boldsymbol{\theta},\mathcal{M})$, is defined up to proportionality, as the probability of measuring the data $\mathbf{d} = \{d_1,\ldots,d_n\}$ given the model $\mathcal{M}$ and its parameters taking the values $\boldsymbol{\theta} = \{\theta_1,\ldots,\theta_\nu\}$ [80, 280].

Despite our aim to keep the discussion in this section as general as possible, when we analyse particular datasets we will assume, as usual, that the measurements are normally distributed around their true value, so the likelihood function takes the form

$$\mathcal{L}(\mathbf{d}|\boldsymbol{\theta},\mathcal{M}) \propto e^{-\chi^2(\boldsymbol{\theta})/2}. \tag{1.131}$$

The probability density function $p(\boldsymbol{\theta}|\mathbf{d},\mathcal{M})$ of the parameters to have values $\boldsymbol{\theta}$ given the data, $\mathbf{d}$, under the assumption that the true model is $\mathcal{M}$, is provided by Bayes' theorem [280]:

$$p(\boldsymbol{\theta}|\mathbf{d},\mathcal{M}) = \frac{\mathcal{L}(\mathbf{d}|\boldsymbol{\theta},\mathcal{M})\pi(\boldsymbol{\theta},\mathcal{M})}{\int \mathcal{L}(\mathbf{d}|\boldsymbol{\theta},\mathcal{M})\pi(\boldsymbol{\theta},\mathcal{M})d\boldsymbol{\theta}}, \tag{1.132}$$

where $p(\boldsymbol{\theta}|\mathbf{d},\mathcal{M})$ and $\pi(\boldsymbol{\theta},\mathcal{M})$ are the posterior and prior probability density functions (pdf) respectively [67, 80, 276, 277, 280]. The prior pdf encodes all previous knowledge about the parameters before the observational data have been collected. It can be regarded as a subjective procedure, but its use is compulsory in the Bayesian framework, which is the approach used in theoretical frameworks where only one particular realization of the measurement is available; the opposite of what happens in a laboratory, where multiple realizations of the same experiment can be done.

Parameter estimation in the Bayesian framework is based on maximizing the posterior pdf $p(\boldsymbol{\theta}|\mathbf{d},\mathcal{M})$, whereas in a "strict" frequentist approach one just maximizes $\mathcal{L}(\mathbf{d}|\boldsymbol{\theta},\mathcal{M})$. When one uses flat priors in the Bayesian approach then the same conclusions are drawn from both approaches, so the difference turns out to be conceptual only [275–277]. If the measured observables are independent from each other and Gaussian distributed around their true value, $\mathbf{d}(\boldsymbol{\theta})$, with a covariance matrix, $\mathbf{C}$, given by the experimental errors, maximizing $\mathcal{L}$ is equivalent to minimizing the chi-square function

$$\chi^2(\boldsymbol{\theta}) \equiv \left(\mathbf{d}^{obs} - \mathbf{d}(\boldsymbol{\theta})\right)\mathbf{C}^{-1}\left(\mathbf{d}^{obs} - \mathbf{d}(\boldsymbol{\theta})\right)^T; \tag{1.133}$$

for uncorrelated data, $\mathbf{C}_{ij} = \delta_{ij}\sigma_i^2$ and

$$\chi^2(\boldsymbol{\theta}) \equiv \sum_{i=1}^{n}\left(\frac{\mathbf{d}^{obs} - \mathbf{d}(\boldsymbol{\theta})}{\boldsymbol{\sigma}_i^{obs}}\right)^2. \tag{1.134}$$

The second step toward constraining parameters satisfactorily is to construct credible intervals [276] which measure the degree of confidence that a certain data was generated by parameters belonging to the estimated interval. This approach is a common practice when reporting the errors on the parameters in a form of a confidence region or contour. In the Bayesian approach, the credible intervals are drawn around the maximum likelihood point, which gives the best fit parameters. After obtaining it by the minimization of the $\chi^2(\boldsymbol{\theta})$, the boundaries of the confidence regions are those of a region containing $100n\%$ of the likelihood determined by the values of the ν parameters for which χ^2 has increased by a certain quantity

$$\chi^2 - \chi^2_{min} = \Delta\chi^2 = \mathcal{R}^n_\nu \tag{1.135}$$

with

$$n = \int_0^{\mathcal{R}^n_\nu} \mathcal{P}_{\chi^2_\nu}(t)dt = \frac{\displaystyle\int_0^{\frac{\mathcal{R}^n_\nu}{2}} \left(\frac{t}{2}\right)^{\frac{\nu}{2}-1} e^{-(t/2)}dt}{2\Gamma\left(\frac{\nu}{2}\right)} = 1 - \frac{\Gamma\left(\dfrac{\nu}{2}, \dfrac{\mathcal{R}^n_\nu}{2}\right)}{\Gamma\left(\dfrac{\nu}{2}\right)} \tag{1.136}$$

where $\Gamma\left(\frac{\nu}{2}, \frac{\Delta_{\nu,k}}{2}\right)$ is the incomplete Γ function [155], [213]. Table 1.2 shows the values of $\mathcal{R}^n_\nu$ up to 2 parameters and different likelihood content.

n		$0.683(1\sigma)$	$0.954(2\sigma)$	$0.997(3\sigma)$
ν	1	1.00	4.00	9.00
	2	2.30	6.17	11.80

Table 1.2: *Values of $\mathcal{R}^n_\nu$ (deviation of the χ^2 from the minimum) for $\nu = 1, 2$ parameters and different likelihood content, $n = 0.683, 0.954, 0.997$ which respectively corresponds to 1σ, 2σ and 3σ.*

The 1σ and 2σ errors of the parameter θ_i are given by the 68.30% and 95.45% credible interval contours, respectively. If one reads the errors from the contours, the upper limit error is the maximum value of the contour and the lower one the minimum one.

1.7.2 Bayesian evidence

In Bayes' approach the evidence is employed as a tool which informs about how well the parameters of the model fit the data, after doing an averaging over all the parameter values that were theoretically plausible before the measurement ever took place [170].

Then Bayes' evidence is calculated as the average likelihood of the model over its prior parameter space:

$$\mathcal{E}(\mathcal{M}) = \int \pi(\boldsymbol{\theta}, \mathcal{M}) \mathcal{L}(\mathbf{d}|\boldsymbol{\theta}, \mathcal{M}) d\boldsymbol{\theta}, \tag{1.137}$$

where $\pi(\boldsymbol{\theta}, \mathcal{M})$ is the model's prior on the set of parameters normalized to unity:

$$\int \pi(\boldsymbol{\theta}, \mathcal{M}) d\boldsymbol{\theta} = 1.$$

The most common choice is the top hat prior, $\pi(\boldsymbol{\theta}, \mathcal{M}) = 1/V$ with $V = \prod_{\alpha=1}^{\nu} (\boldsymbol{\theta}_{\alpha,max} - \boldsymbol{\theta}_{\alpha,min})$. In that case one rewrites Bayes evidence as

$$\mathcal{E}(\mathcal{M}) = \frac{1}{V} \int_V \mathcal{L}(\boldsymbol{\theta}) \, d\boldsymbol{\theta}. \tag{1.138}$$

One important and unavoidable inconvenient of the use of the evidence is its dependence on the prior ranges chosen for the parameters, so one has to take this into account when the evidence is evaluated or computed for different prior ranges to find the most suitable one for the model.

Once we have arrived at this point, a remark is required. The usual situation in Cosmology is that one has more than one set of statistically independent observational data, $\{\mathbf{d}^{(1)}\}, \ldots \{\mathbf{d}^{(m)}\}$, to constrain the parameters $\boldsymbol{\theta}$; in that case, one can resort to the joint probability density function,

$$p(\boldsymbol{\theta}|\mathbf{d}^{(1)} \cap \cdots \cap \mathbf{d}^{(m)}, \mathcal{M}) = p(\boldsymbol{\theta}|\mathbf{d}^{(1)}, \mathcal{M}) \times \cdots \times p(\boldsymbol{\theta}|\mathbf{d}^{(m)}, \mathcal{M}). \tag{1.139}$$

With this definition the whole discussion above can be conveniently generalized for a situation with more than one dataset.

1.7.3 Error propagation in derived quantities

It is common that the parameters do not have symmetric errors, i.e. that the posterior distribution of the parameters is not completely Gaussian and symmetric. Then, the standard error propagation formula cannot be used, and a modification has to be performed in order to account for these non-gaussianities, [154]. Consider that the constraints on the parameters are given in the form $\theta_{i-\delta\theta_{i,l}}^{+\delta\theta_{i,u}}$, where $\delta\theta_{i,u}$ and $\delta\theta_{i,l}$ are positive quantities which account for the upper and lower error.

Following [154], the estimated error in a quantity depending on them, $f(\boldsymbol{\theta})$, will be given by an upper limit

$$\Delta f_u = \sqrt{\sum_{i=1}^{n} \left(\max\left(\Delta f_{iu}, -\Delta f_{il}\right)\right)^2}, \tag{1.140}$$

and a lower one

$$\Delta f_l = \sqrt{\sum_{i=1}^{n} \left(\min\left(\Delta f_{iu}, -\Delta f_{il}\right)\right)^2}, \tag{1.141}$$

where

$$\Delta f_{iu} = f(\dots\theta_{(i-1)}, \theta_i + \Delta\theta_{iu}, \theta_{(i+1)}, \dots) - f(\boldsymbol{\theta}), \tag{1.142}$$

$$\Delta f_{il} = f(\dots\theta_{(i-1)}, \theta_i - \Delta\theta_{il}, \theta_{(i+1)}, \dots) - f(\boldsymbol{\theta}). \tag{1.143}$$

This error estimation is based on finite differences, however it can be refined if the errors are small enough, i.e. $\Delta\theta_{i,u} = \delta\theta_{i,u}$ and $\Delta\theta_{i,l} = \delta\theta_{i,l}$. In that case one can write

$$\Delta f_u \simeq \delta f_u = \sqrt{\sum_{i=1}^{n} \left(\max\left(\frac{\partial f}{\partial\theta_i}\delta\theta_{iu}, -\frac{\partial f}{\partial\theta_i}\delta\theta_{il}\right)\right)^2} \tag{1.144}$$

and

$$\Delta f_l \simeq \delta f_l = \sqrt{\sum_{i=1}^{n} \left(\min\left(\frac{\partial f}{\partial\theta_i}\delta\theta_{iu}, -\frac{\partial f}{\partial\theta_i}\delta\theta_{il}\right)\right)^2}. \tag{1.145}$$

In Gaussian situations, where $\Delta\theta_{i,u} = \Delta\theta_{i,l} = \Delta\theta_i$, one recovers the standard error propagation formula and $\Delta f_u = \Delta f_l$.

1.7.4 Grid Method for minimization and the Levenberg-Marquadt algorithm

Given the appropriate $\chi^2(\boldsymbol{\theta})$ function, the next step is to find the values of the model parameters which minimize it. A common practice, when the number of parameters is reasonable, is to construct a grid: one divides the physical range of each parameter to be explored into several points to obtain a complex mesh which defines the points where the χ^2 has to be evaluated. After that it is possible to detect the point in the parameters space which gives the χ^2_{min}. Thus, combining some intuitive guesses to define the ranges of the parameters to be explored with the knowledge provided by literature on the topic, it is well

recommended to work with two grids, one for an initial guess and a second one, finer and narrower, around the first minimum. With this procedure one will typically find a suitable initial point to feed the **Levenberg-Marquadt algorithm**, which will provide us with a more refined minimum of the χ^2 function, together with the estimated covariance matrix $\mathbf{C}(\theta_1, \theta_2, ..., \theta_n)$ for the model parameters.

Levenberg-Marquadt algorithm

This method, based on the inverse-Hessian method, is commonly used to provide a numerical minimum of a non-linear function [213]. The main idea is to find the gradient of the function χ^2 with respect to the set of parameters $\boldsymbol{\theta}$, which will be equal to zero for χ^2_{min}. Thus, we have to be able to compute the corresponding numerical partial derivatives of the function to minimize and define these two quantities:

$$\beta_i = -\frac{1}{2}\frac{\partial \chi^2}{\partial \theta_i} \qquad \text{and} \qquad \alpha_{ij} = \frac{1}{2}\frac{\partial^2 \chi^2}{\partial \theta_i \partial \theta_j}. \tag{1.146}$$

The increment, $\delta\boldsymbol{\theta}$, that has to be added to the initial guess of parameters to give the next estimate, is defined in terms of the gradient

$$\alpha_{ij}\delta\theta_j = \beta_i. \tag{1.147}$$

The Levenberg-Marquadt algorithm then gives the recipe for iteratively moving around the parameter space to estimate in the finest way the minimum of the function. It can be summarized in 4 steps:

1. First compute the value of $\chi^2(\boldsymbol{\theta})$ for the picked set of parameters. If this is the first iteration, these values must have been obtained previously from the grid.

2. Select a value for the constant λ (see below). In the first attempt it is usually initialized as $\lambda = 0.001$.

3. Solve a modification of Eq. (1.147) to obtain $\delta\boldsymbol{\theta}$

   $$\alpha'_{ij}\delta\theta_j = \beta_i, \tag{1.148}$$

   which is written in terms of

   $$\begin{aligned} \alpha'_{ii} &= \alpha_{ii}(\lambda + 1), \\ \alpha'_{ij} &= \alpha_{ij}. \end{aligned} \tag{1.149}$$

   Obtain the value of the new $\chi^2(\boldsymbol{\theta} + \delta\boldsymbol{\theta})$.

4. Compare $\chi^2(\boldsymbol{\theta} + \delta\boldsymbol{\theta})$ with the previous value $\chi^2(\boldsymbol{\theta})$:

   - If $\chi^2(\boldsymbol{\theta} + \delta\boldsymbol{\theta}) \geq \chi^2(\boldsymbol{\theta})$: Increase by a factor of 10 the previous value of λ and start again from step 3.

- If $\chi^2(\boldsymbol{\theta}+\delta\boldsymbol{\theta}) \leq \chi^2(\boldsymbol{\theta})$: reduce in a factor of 10 the previous value of λ and start again from step 3, having now as a new solution, the value $\boldsymbol{\theta}+\delta\boldsymbol{\theta}$.

  The iteration process has to be stopped when a certain convergence is achieved. The usual control to opperate this stop is to see that χ^2 has decreased less than 0.01 in 2 successive steps.

Once the convergence has been reached, setting $\lambda = 0$, the inverse of $\boldsymbol{\alpha}$ defines the covariance matrix of the parameters: $\mathbf{C} = \boldsymbol{\alpha}^{-1}$.

1.7.5 Monte Carlo Markov Chain algorithm and convergence test

When a large amount of parameters are taken into account, methods as the grid one are not efficient to minimize the χ^2 any more, as they require a huge amount of computational effort. In these case the probability distributions of the problem are explored with Markov Chain Monte Carlo (MCMC) methods. These methods (fully described in [36], [183], [193] and references therein) extract samples, known as Markov chains, sequentially using a probabilistic algorithm. The most used algorithm in Cosmology for the MCMC is the Metropolis-Hastings [114, 191] based on the Bayesian statistical approach. The Metropolis-Hastings algorithm works as follows: starting from an initial point of the parameter space $\boldsymbol{\theta}$, another trial point, $\boldsymbol{\theta}'$, is picked using a *proposal density function* $q(\boldsymbol{\theta}', \boldsymbol{\theta})$, which represents the conditional probability to have $\boldsymbol{\theta}'$ given $\boldsymbol{\theta}$. The transition kernel, $T(\boldsymbol{\theta}, \boldsymbol{\theta}')$, which gives the conditional probability to move form one point $\boldsymbol{\theta}$ to another $\boldsymbol{\theta}'$, has to satisfy the "balance equation" to ensure that the Markov chain will recover the posterior distribution $P(\boldsymbol{\theta}|\mathbf{d})$:

$$P(\boldsymbol{\theta}'|\mathbf{d})T(\boldsymbol{\theta}', \boldsymbol{\theta}) = P(\boldsymbol{\theta}|\mathbf{d})T(\boldsymbol{\theta}, \boldsymbol{\theta}'). \tag{1.150}$$

This condition is achieved if the new point is accepted with probability,

$$\alpha(\boldsymbol{\theta}, \boldsymbol{\theta}') = \min\left\{1, \frac{P(\boldsymbol{\theta}'|\mathbf{d})q(\boldsymbol{\theta}', \boldsymbol{\theta})}{P(\boldsymbol{\theta}|\mathbf{d})q(\boldsymbol{\theta}, \boldsymbol{\theta}')}\right\}, \tag{1.151}$$

and the transition kernel being defined as $T(\boldsymbol{\theta}, \boldsymbol{\theta}') = \alpha(\boldsymbol{\theta}, \boldsymbol{\theta}')q(\boldsymbol{\theta}, \boldsymbol{\theta}')$. Here $P(\boldsymbol{\theta}|\mathbf{d})$ is the conditional probability to have the parameter set $\boldsymbol{\theta}$ given the observational data $\mathbf{d}$.

As from Bayes' theorem it follows that the posterior probability is $P(\boldsymbol{\theta}|\mathbf{d}) \propto L(\mathbf{d}|\boldsymbol{\theta})\pi(\boldsymbol{\theta})$ and q($\boldsymbol{\theta}$,$\boldsymbol{\theta}$') is chosen to be symmetric to ensure Eq. (1.150), if the trial point improves the likelihood, it will be accepted with a probability equal to 1, otherwise it will be accepted with a certain probability given by $L(\mathbf{d}|\boldsymbol{\theta}')\pi(\boldsymbol{\theta}')/L(\mathbf{d}|\boldsymbol{\theta})\pi(\boldsymbol{\theta})$. Then, if the chain moves to the new set $\boldsymbol{\theta}'$, one says that it has been accepted, and if not, then the point has been rejected.

The prior is usually chosen to depend on the physical requirements a given parameter has. The proposal density is typically a multivariate Gaussian of zero mean and standard deviation described by a certain covariance matrix, $\mathbf{C}_0$. The trial point can be obtained from a vector made of a set of random numbers which follow a Gaussian distribution of unit variance and zero mean, $\mathbf{x}$: $\boldsymbol{\theta}' = \boldsymbol{\theta} + \mathbf{C}_0^{-1/2}\mathbf{x}$. As a first attempt, as we usually do not have information about the correlation of the parameters, $\mathbf{C}_0$ is chosen as a diagonal matrix with the values of the expected uncertainties of the parameters.

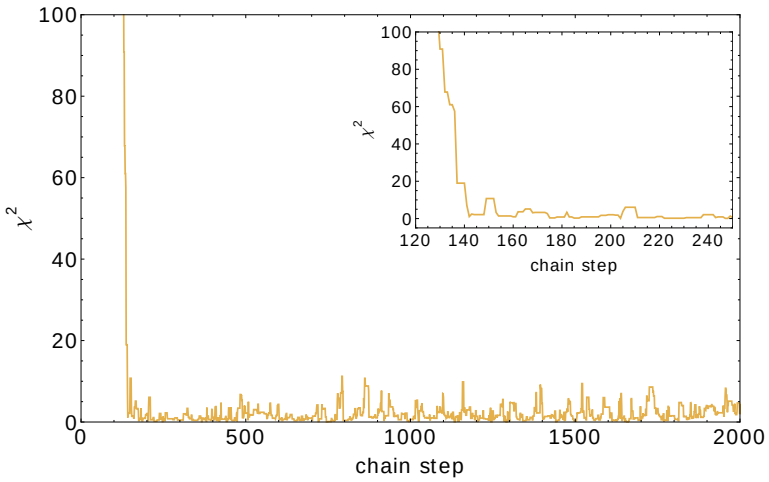

Figure 1.9: *χ^2 for each step of the MCMC chain. As it can be seen, there is a initial "burn-in" region, with high values of χ^2, before the chain reaches the relaxation distribution.*

Initial samples usually have to be discarded because there is an initial "burn-in" region where chain has not reached the relaxation distribution (see Fig.1.9). This happens when the chain has been initiated with a point lying far away of the region of high probability. For that reason, it is recommended to run a first chain, to not only figure out the best region to start the definitive chain, but also to measure the possible correlation between the parameters and obtain a representative covariance matrix that will account for it, $\mathbf{C}_T$. This will help us to avoid the "burn-in" phase in the next chain and to optimize the procedure with the new proposal density function $\boldsymbol{\theta}' = \boldsymbol{\theta} + 2.4\frac{\mathbf{C}_T^{-1/2}}{\sqrt{D}}\mathbf{x}$. This routine is proposed in [82], where it is shown that with this modification the number of accepted points increases and the computational time required to obtain a representative chain get reduced.

Convergence Test

The main problem when running a Markov chain concerns how to avoid biased inferences or underestimations on errors of the theoretical parameters. The *problem of the convergence* is the main one among the problems of that sort, and it can be formulated as follows: how can one be sure that the properties of a sample from the MCMC algorithm are a good representation of the unknown distribution to be explored? One can say that a chain has reached convergence when the statistical properties of the extracted samples can describe the statistical properties of the unknown probability distribution with *good accuracy*. Probability theory says that Markov processes will reach the exact final distribution in an asymptotic way, which means a sample's length will become infinite in an infinite computation time. Of course, as one is forced to operate with finite length samples, the question arises of how this truncation can bias the final statistical results, and if there are any parameters that can be able to give information about the goodness of the process. In the literature, the most

used parameter for this task is the *convergence ratio* (see [82]), defined as

$$r = \frac{\sigma^2_{\overline{x}}}{\sigma^2_0}. \tag{1.152}$$

This is the ratio between the variance of the mean of the samples and the variance of the underlying unknown distribution (we will operate with standard distributions so that $\sigma^2_0 = 1$). Then r is required to be below a cut-off limit value, typically 0.01, to have a guaranteed convergence of the chain. This parameter is used in other convergence tests, such as the Gelmann-Rubin test (see [104]), which runs many parallel multiple chains and estimates r at any step at the expense of high amounts of time and hardware.

An alternative solution to this problem is the spectral analysis approach proposed by [82]. It is clear that all the steps in the MCMC are correlated; this correlation is somewhat intrinsic to the code, at least before having reached convergence, but it depends also on the value of σ_T. But what is even more important is the behaviour of the correlation when the convergence has been reached: in this case the MCMC will sample from the underlying distribution and it will work like a random sampler, so that there will be no correlations in this regime.

This is the key idea of the test by [82]: if we take the *power spectra* of the MCMC samples, we will have a large correlation on small scales, but the spectrum will become flat (like a white noise spectrum) when convergence has been reached. Then, checking the spectrum of just one chain (instead of many parallel chains as in Gelmann-Rubin's test) will be sufficient to assess that convergence has indeed been reached. We will give just a short account of the steps to be followed to implement the test, but for a more detailed reference see [82].

In brief, we calculate the discrete power spectrum of the chains,

$$P_j = |a^j_N|^2, \tag{1.153}$$

with

$$a^j_N = \frac{1}{\sqrt{N}} \sum_{n=0}^{N-1} x_n \exp\left[i \frac{2\pi j}{N} n\right], \tag{1.154}$$

where N and x_n are respectively the length and a given element of the sample from the MCMC, $j = 1, \ldots, N/2 - 1$, and the wave number k_j of the spectrum is related to the index j by the relation $k_j = 2\pi j/N$. Then we fit it to an analytical template:

$$P(k) = P_0 \frac{(k^*/k)^\alpha}{1 + (k^*/k)^\alpha}, \tag{1.155}$$

or in equivalent logarithmic form:

$$\ln P_j = \ln P_0 + \ln\left[\frac{(k^*/k_j)^\alpha}{1 + (k^*/k_j)^\alpha}\right] - \gamma + r_j, \tag{1.156}$$

where $\gamma = 0.57216$ is the Euler-Mascheroni number and r_j are random measurement errors

with $< r_j >= 0$ and $< r_i r_j >= \delta_{ij}\pi^2/6$. The fit provides estimates of three parameters, but only two of them are fundamental to our analysis. The first one is P_0, which is the value of the power spectrum extrapolated for $k \to 0$; this is an important parameter because from it we can derive the convergence ratio using $r \approx P_0/N$, which has to be lower than 0.01. The second important parameter is j^* (the index corresponding to k^*), which is related to the turnover point from a power to a flat spectrum; the estimated value of j^* has to be $\gtrsim 20$, so one can be sure that the number of points in the sample coming from the convergence region is larger than the number of noisy points. If these two conditions are met for all the parameters, then the chain has reached convergence, and the statistics from the MCMC procedure describes well the underlying probability distribution. In [82] the authors propose to perform the fit over the range $1 \leq j \leq j_{max}$, with $j_{max} \sim 10j^*$, with a first estimation of j^* from a fit with $j_{max} = 1000$, and then perform a second (or even a third) iteration to have a better estimation of it. If after this the convergence criteria have been met, we can consider that the chain is convergent, otherwise more points will have to be added to achieve it.

1.7.6 Model selection tests

After having estimated the value of the set of parameters using the MCMC approach, we need a tool for comparing, selecting and testing the statistical goodness of our results. The related literature is too extensive, so we will only refer in some detail to those tools most used in cosmological model selection [170].

Since the MCMC technique is based on a Bayesian approach, the best way for comparing models is arguably the Bayesian Evidence, see Eq. (1.7.2). It is clear from its definition that the evidence of a model is the average likelihood of the model with respect to the prior: models which fit the data well and make narrow predictions are likely to fit well over much of their available parameter space, giving a high evidence. So using the evidence for comparing models is a very appropriate task. Model comparison requires defining then **Bayes factor**,

$$B_{ij} = \frac{E(M_i)}{E(M_j)}, \tag{1.157}$$

which is the ratio between the evidence values of two models, M_i and M_j. If $B_{ij} > 1$ then the model M_i is preferred with respect to the model M_j. By convention, Bayes' factor is judged on Jeffreys' scale [131]:

- for $1 < \ln B_{ij} < 2.5$ there is a "substantial" evidence in favour of the model with the greatest Bayesian evidence.
- for $2.5 < \ln B_{ij} < 5.0$ the evidence is "strong".
- for $\ln B_{ij} > 5$ the evidence is "decisive".

Moreover, in favour of the Bayesian evidence it has to be underlined that it is a full implementation of Bayesian inference, and can be directly interpreted in terms of model probabilities. Unfortunately, it being a highly-peaked multi-dimensional integral, its estimation typically requires a hard and challenging numerical effort. Even if some algorithms

have been found which simplify this operation, it is always preferable to have easier tools for estimating it and comparing models.

The easiest and most used tools are different versions of the *Information Criteria*. Generally, the introduction of a higher number of parameters improves the fit to the chosen dataset, regardless of whether or not these new parameters are really relevant. As a consequence, the simple comparison of the maximum likelihood value of different models will tend to favour the model with the highest number of parameters. The information criteria work just in this direction: they compensate this behaviour by penalising models which have more parameters. In what follows we detail the most used information criteria.

Akaike Information Criterion (AIC)

The Akaike Information Criterion (AIC) is defined as

$$\mathrm{AIC} = -2\ln\mathcal{L} + 2k \tag{1.158}$$

where $\mathcal{L}$ is the maximum likelihood value and k is the number of parameters of the model [5]. The AIC is derived by an approximation of the Kullback-Leibler information entropy, which measures the difference between the true data distribution and the model one [50, 271]. The best model is the one which minimises the AIC, and no requirement for the models is asked for.

There also exists an AIC version for small sample sizes, the corrected AIC, AIC_c [50] given by

$$\mathrm{AIC}_c = \mathrm{AIC} + \frac{2k(k+1)}{N-k-1}, \tag{1.159}$$

where N is the number of points in the dataset. Since the correction term disappears for large sample sizes, $N >> k$, it is convenient to use this corrected definition for comparing models as pointed out in [171].

Residual Information Criterion (RIC)

From the same principles of AIC, the minimisation of the Kullback-Leibler information entropy, another comparison tool can be derived, the Residual Information Criterion (RIC). However, as it seems that the motivation for the RIC criterion is not correct, the corrected version proposed in [162] is comonly used, where the RIC_c is defined as

$$\mathrm{RIC}_c = -2\ln\mathcal{L} + (k-1) + \frac{4k}{N-k-1}\,. \tag{1.160}$$

When $N >> k$, RIC_c has a smaller penalty than AIC_c.

Generally, when $\Delta\mathrm{AIC}_c \gtrsim 1$ (or $\Delta\mathrm{RIC}_c \gtrsim 1$), it follows that the two models are significantly different, and the one with the lowest value of AIC (or RIC) is the preferred one. Finally, we have to keep in mind that $\mathrm{AIC}_c/\mathrm{RIC}_c$ tends to favour models with a high number of parameters, and it is "dimensionally inconsistent", namely, that even if the dataset size tends to infinity, the probability of the $\mathrm{AIC}_c/\mathrm{RIC}_c$ incorrectly picking an overparametrized model does not tend to zero [170].

Bayesian Information criterion (BIC)

The Bayesian Information criterion (BIC) was introduced in [237] and is defined as

$$\text{BIC} = -2\ln\mathcal{L} + k\ln N\ . \tag{1.161}$$

Again, in this case the best model has the lowest BIC, and it is clear from this expression that models with a high number of parameters are more penalized by BIC than by AIC. Since the BIC is a good approximation for twice the log of the Bayes factor, it can be compared with Jeffreys' scale, so that $\Delta\text{BIC} > 5$ means a "strong" evidence in favour of the model with lowest BIC values, while for $\Delta\text{BIC} > 10$ this evidence is "decisive".

Deviance information criterion (DIC)

The Deviance information criterion (DIC) [263] mixes elements from both Bayesian and information theory. It is easily computable from posterior samples such as those coming from MCMC runs. It relies on the definition of the effective number of parameters, p_D, also known as the Bayesian complexity, which is defined as

$$p_D = \overline{D(\theta)} - D(\overline{\theta}), \tag{1.162}$$

where

$$D(\theta) = -2\ln\mathcal{L}(\theta) + C \tag{1.163}$$

with C a constant which vanishes from any derived quantity, and the chi-square defined as usual, that is, $\chi^2 = -2\ln\mathcal{L}$. This definition shows that p_D can be considered as the mean deviance minus the deviance of the means, and this is the key quantity for estimating the degrees of freedom of a test. Finally the DIC is defined by

$$\text{DIC} = D(\overline{\theta}) + 2p_D = \overline{D(\theta)} + p_D, \tag{1.164}$$

where one can recognise a similar-to-AIC formulation in the first expression, while a Bayesian definition and measure of model adequacy, penalised by an additional term related to the model dimensionality is implicit in the second one. The DIC is also useful for another reason: it overcomes the difficulties AIC and BIC have to discount parameters which are unconstrained by data, BIC is of even more suspicious validity when there is any parameter degeneracy. Finally, DIC (like BIC) is not dimensionally inconsistent, so it is able to detect wrong high dimensionality parametrizations.

1.7.7 Dark Energy Experiments comparison tool

Despite so many efforts, we are a stage at which current observational data cannot provide rigorous constraints on the dark energy parameters. This allows a wide range of possibilities ranging from a time evolving equation of state to ΛCDM. For this reason all the hope lies

in future experiments as EUCLID [32, 218][8], J-PAS [33][9], Dark Energy Survey (DES)[10], BigBoss [235, 236], Large Synoptic Survey Telescope (LSST)[11], Square Kilometer Array (SKA) [12] which are very ambitious as they expect to improve present-day constraints with high accuracy extended datasets. In these circumstances we need a useful tool to compare the capability on constraining dark energy of these upcoming experiments.

A good quantity for this purpose is the Figure-of-Merit (FoM), which has been defined in several slightly different but related ways in the literature [6, 251]. Perhaps the most popular version of the FoM was the one proposed by the "Dark Energy Task Force" (see [8] for a recent revision of the topic) which is defined as the inverse of the area of the confidence region ellipse defined by the plane $w_0 - w_a$ and it simply reads

$$\text{FoM}_{\text{DETF}} = \frac{1}{\sqrt{\det \mathbf{C}(w_0, w_a)}}, \tag{1.165}$$

where $\mathbf{C}(w_0, w_a)$ is the covariance matrix between the two dark energy parameters for the CPL parametrization, see Eq. (1.53). Even though this definition of the FoM is widely used, it presents some drawbacks, as it fails to capture success of other variations of the equation of state w with the redshift. In that direction, in [286] a generalization of the FoM was presented for any parametrization of the dark energy equation of state concerning several parameters:

$$\text{FoM}_{\text{Wang}} = \frac{1}{\sqrt{\det \mathbf{C}(c_1, c_2, c_3, ...)}}, \tag{1.166}$$

where $\mathbf{C}(c_1, c_2, c_3, ...)$ is the covariance matrix of the corresponding c_i dark energy parameters one is concerned with. As explained in [286], this specific definition has two advantages: firstly, it is easy to calculate for either real or simulated data, and secondly, it has an easy physical interpretation. The FoM penalizes experiments that yield very correlated estimates for the dark energy parameters. Hence the FoM is larger when the dark energy parameters c_i are chosen such that they are minimally correlated with each other. But obviously, if the model considered does not have a low degree of correlation *per se*, one will be giving a poor estimation of the performance of the observational tests.

The main difference between FoM_{Wang} and FoM_{Wang} is that in the latter the two relevant parameters are w_0 and w_a, and not any others. However, w_a is a parameter informing about early time asymptotics, which is a region with extremely hard observational access and physical interpretation, and thus, the debate persists of whether a FoM using that parameter may not be giving artificially large results.

[8] http://sci.esa.int/euclid
[9] http://j-pas.org/
[10] http://www.darkenergysurvey.org/
[11] http://www.lsst.org/lsst/
[12] http://www.skatelescope.org/

Equivalence between FoM_{DETF} and FoM_{Wang}

As it is presented in [240], following [59] it is easy to show the relation between the covariance matrix corresponding to two different sets of parameters $\{p_i\}$ and $\{p'_i\}$:

$$\mathbf{C'^{-1}} = \mathbf{M}^T\mathbf{C^{-1}}\mathbf{M}, \tag{1.167}$$

where

$$\mathbf{C} = \begin{pmatrix} \sigma_1^2 & \sigma_{12} \\ \sigma_{12} & \sigma_2^2 \end{pmatrix}, \tag{1.168}$$

and $M_{ij} = \partial p_i/\partial p'_j$ is the Jacobian of the parameter transformation. For a parametrization in terms of w_0 and $w_{0.5} = w(z = 0.5)$ as Eq. (1.62), $\{p_1, p_2\} = \{w_0, w_{0.5}\}$ and $\{p'_1, p'_2\} = \{w_0, w_a\}$, and specifically $w_{0.5} = m_1 + m_2 w_0 + m_3 w_a$ with m_1, m_2, m_3 coefficients different in the different parametrizations considered other than the CPL one, thus

$$\mathbf{M} = \begin{pmatrix} 1 & 0 \\ m_2 & m_3 \end{pmatrix}. \tag{1.169}$$

It is a simple matter of algebra to see that

$$\mathbf{C'} = \begin{pmatrix} \sigma_1^2 & \dfrac{\sigma_{12} - m_2\sigma_1^2}{m_3} \\ \dfrac{\sigma_{12} - m_2\sigma_1^2}{m_3} & \dfrac{m_2^2\sigma_1^2 - 2m_2\sigma_{12} + \sigma_2^2}{m_3} \end{pmatrix} \tag{1.170}$$

and $\sqrt{\det C'} = \sqrt{\det C}/m_3$. Therefore we get the simple relationship between the two definitions of FoM

$$\text{FoM}_{\text{DETF}} = m_3 \text{FoM}_{\text{Wang}}. \tag{1.171}$$

CHAPTER 2

DIRAC-BORN-INFELD MODELS FOR THE UNIFICATION OF DARK MATTER AND DARK ENERGY

Current observations reveal that the Universe is mainly filled with Dark Energy ($\sim 72\%$) and Dark Matter ($\sim 23\%$) with only a ($\sim 4.6\%$) of baryonic matter and ($\sim 0.4\%$) of radiation, see Fig. 1.4 and 1.5. Therefore, in this context, unified models of the two main components of the Universe, dark energy and dark matter, represent an interesting option for explaining the substantial evidence of the current acceleration of the Universe. On the one hand, as it has been pointed in the previous Chapter, no observational direct evidence of either of them is available, so it might well be the case that they do simply not exist and there is a bolder explanation for the effects we attribute to them; perhaps extra dimensions are the answer. On the other hand, if one believes these two entities really fill our universe in a huge joint proportion as compared to the other components, it remains to discover what their nature is. In a way, finding out that they happen to be manifestations of the same fluid would at least simplify the problem in the sense one should have to care about the fundamentals of a single fluid. Only at worst, if investigations along these lines were able to refute this idea that the two components are just one, we would at least be able to face the future in the confidence that dark energy and dark matter can be treated separately.

Following the tradition of trying to find an interconnection between the world of Particle Physics and Cosmology, it is customary to try and view unified dark energy models as scalar field scenarios [13–15, 34, 138, 200] . One possibility is to explore the evolutions contained in a given scalar field model, this is actually the approach of this work. We consider a scalar field setup, and by fixing some of its degrees of freedom, we obtain an expansionary cosmology which mimics a dark matter dominated background at early times and a dark energy dominated one at the late stages of its history, see Fig. 1.1(a). On the other hand, a popular procedure to find a motivation based on scalar fields for a given evolution is to

start from a given equation of state and then "reconstruct" the corresponding Lagrangian by specifying its kinetic term and potential. This widely followed approach has its caveats, however, as in general the scalar field model one ends up with is in fact a richer scenario, and contains other evolutions that the original seed. Leaving aside these remarks, the route of scalar fields toward unified dark energy scenarios may offer interesting possibilities, and our efforts in this work go in this direction.

It has been suggested that acceleration might be the manifestation of non-perturbative features of some string theory versions [214]. This idea has gathered quite a lot of attention as it could provide an explanation to early time acceleration, that is, inflation; see [9, 29, 31, 48, 53, 54, 57, 84, 106, 116, 125, 136, 137, 140, 149, 160, 172, 248, 258–260] and references therein for regular papers and [203] for a review. According to this description, the inflaton could be a mode accounting for the position of a D-brane with three spatial dimensions rambling radially in a ten-dimensional space-time with a warped metric. This interpretation seems to have the virtue, among others, that it would allow inflation to proceed with much steeper potentials than in the standard weakly coupled slow roll inflation model.

So, a somewhat natural question to ask is this one: could a Dirac-Born-Infeld (DBI) model be responsible for the acceleration we observe at present? Moreover, given the similarity of the DBI Lagrangian to that of the most popular unified dark energy model, the Chaplygin gas, could it also offer a satisfactory and perhaps even more suitable alternative for the unification of dark matter and dark energy? The investigations we report below show that is indeed the case. We construct a purely kinetic DBI model for the joint description of the two main components of the Universe, with the bonus that the effective dark energy component displays a late-time phantom behavior even though the model does not include at all a scalar field with the wrong sign in the kinetic energy.

Any conclusions about the capability of our model to represent a solid alternative to other dark energy scenarios must ideally be reached from both the theoretical and the observational perspectives. To that end, first we carry out the computation and interpretation of the linear gauge invariant perturbations of the model. After that, we perform a thorough analysis of this novel unified dark sector scenario using geometric means: specifically we use the SNIa, the BAO, and the CMB shift test. These combination of tests allows to take into account the early, mid and late time behavior of our model, which is expected to have its own features as compared to models in which dark energy and dark matter are different components. Our analysis is performed in the Bayesian spirit and it allows us to identify the best fit and errors, and to complete the information obtained with a computation of the evidences on different ranges of the parameters and constraints on kinematical quantities of interest.

2.1 The model

Our scenario is that of a four-dimensional spatially flat FRW spacetime, see Eq. (1.6), filled with a non-canonical scalar field of DBI type described with the action

$$\mathcal{S} = -\int d^4x\, a(t)^3 \left(f(\phi)^{-1} \left(\sqrt{1 - f(\phi)\dot{\phi}} - 1 \right) + V(\phi) \right), \tag{2.1}$$

where, in principle, $f(\phi)$ and $V(\phi)$ are arbitrary functions. In general, as we shown in Sec. 1.4.3, a scalar field can be described with an action of the following form:

$$\mathcal{S} = -\int d^4x\, \sqrt{-g}\mathcal{L}\left(\phi, X\right), \tag{2.2}$$

where the kinetic term X is defined as $X = -\frac{1}{2}g^{\mu\nu}\partial_\mu\phi\partial_\nu\phi$ and $\mathcal{L}$ is an arbitrary function of ϕ and X. The corresponding energy-momentum tensor can be obtained varying the action with respect to $g_{\mu\nu}$:

$$T_{\mu\nu} = \frac{-2}{\sqrt{-g}}\frac{\delta\mathcal{S}}{\delta g^{\mu\nu}} = \frac{\partial\mathcal{L}}{\partial X}\partial_\mu\phi\partial_\nu\phi + \mathcal{L}g_{\mu\nu}. \tag{2.3}$$

Comparing this expresion with the corresponding one for a perfect fluid, see Eq. (1.9), we set

$$\rho = \frac{\gamma - 1}{f} + V(\phi), \tag{2.4}$$

$$p = \frac{\gamma - 1}{\gamma f} - V(\phi), \tag{2.5}$$

with

$$\gamma = \frac{1}{\sqrt{1 - f(\phi)\dot{\phi}^2}}. \tag{2.6}$$

The usage of the symbol γ was originally motivated by its analogy to the Lorentz factor of Special Relativity, given that $\sqrt{f(\phi)}\dot{\phi}$ is interpreted as the proper velocity of the brane [248].

Assuming for the above fluid a barotropic equation of state of the form $p = (\Gamma - 1)\rho$, we get

$$\Gamma = -\frac{2\dot{H}}{3H^2} = \frac{\gamma\dot{\phi}^2}{\rho}, \tag{2.7}$$

and the conservation equation (1.13) reads

$$\dot{\rho} + 3H\Gamma\rho = 0. \tag{2.8}$$

In this work we explore the case in which both $f(\phi) = f_0$ are $V(\phi) = V_0$ constants. The goal is to obtain a purely kinetic model as in other unified dark sector models [35, 41, 56, 138, 234], so that the field ϕ depends solely on the scale factor; and, as a consequence, the

same holds for the effective pressure and energy density. To that end we insert

$$\rho = \frac{\gamma - 1}{f_0} + V_0, \tag{2.9}$$

into the conservation equation (5.4) and obtain

$$\dot{\gamma} + 3f_0 H \gamma \dot{\phi}^2 = 0. \tag{2.10}$$

Upon replacement of the derivative γ,

$$\dot{\gamma} = f_0 \gamma^3 \dot{\phi} \ddot{\phi}. \tag{2.11}$$

and using the Eqs. (2.6), (2.10) we arrive at

$$\frac{\ddot{\phi}}{\dot{\phi}} + 3H + \frac{\dot{\gamma}}{\gamma} = 0, \tag{2.12}$$

which has the following first integral:

$$\dot{\phi} = \frac{c}{\gamma} \left(\frac{a_0}{a}\right)^3. \tag{2.13}$$

Thus, it is possible to write

$$\gamma^2 = 1 + c^2 f_0 \left(\frac{a_0}{a}\right)^6. \tag{2.14}$$

with c an arbitrary integration constant and a_0 the value of the scale factor today, which we fix as $a_0 = 1$.

On the one hand, we have accomplished our goal of obtaining a DBI model which is purely kinetic throughout the evolution. On the other hand, the behavior of the model obtained is quite appealing. Using (2.14) it can be seen that at very late times $\gamma \simeq 1$, i.e. in the regime $a \gg a_0$, one has $\rho \sim V_0$, whereas at early epochs, i.e. for $a \ll a_0$, one has $\gamma \simeq a^{-3}$ instead, which in turn gives $\rho \sim 1/a^3$, see Fig. 2.1. Thus, synthetizing, the solution found interpolates between a dust and a de Sitter model, with the V_0 piece acting as a cosmological constant and the absence of any trace of the genuinely DBI degree of freedom f_0. Of course, for a positive $f_0 V_0$ it is easy to see from Eqs. (5.4) and (2.9) that $H > 0$, so the evolution is indeed expansionary.

This new model represents an alternative description for the unification of dark matter and dark energy, and as popular models of this sort, it can be linked to a non-canonical scalar field model obtained from the following Lagrangian [258]:

$$\mathcal{L}(X) = -\frac{1}{f_0}\left(\sqrt{1 - f_0 X} - 1\right) - V_0, \tag{2.15}$$

with $X = \dot{\phi}^2$.

The background evolution of our unified model happens to mimic that induced by the joint contribution of a conventional Chaplygin gas (Cg) and a cosmological constant (Λ).

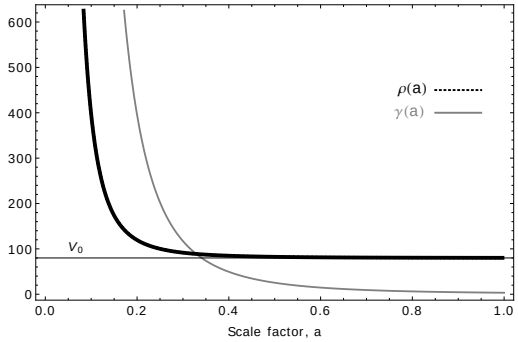

Figure 2.1: *Evolution of the energy density, ρ and the factor γ with the scale factor, a, for $f_0 = 10$ and $V_0 = 80$.*

This would require a cosmological constant of the form $V_0 - 1/f_0$ which seems to mix in a too fine tuned way the parameters V_0 and f_0. Let us stress that one of the key points here is that such background behaviour is realized with a single fluid, and therefore represents a novelty by itself, which is enabled precisely because of the non-canonicality of the DBI framework. The equation of state of this unified fluid is

$$p = \frac{1}{f_0}\left(1 - \frac{1}{\rho f_0 - V_0 f_0 + 1}\right) - V_0, \tag{2.16}$$

and we will make use of this expression in the next section.

However, if one wants to stick to a reinterpretation of the model in a two components fashion by separating the cosmological constant term (V_0) plus a fluid with an energy density ρ_x, it turns out that the equation of state of the extra component is

$$p_x = \frac{\rho_x}{1 + f_0 \rho_x}. \tag{2.17}$$

Thus, the natural splitting hinted by the asymptotic behavior does not leave us with a Cg plus a Λ, but rather with a different picture in which the parameters V_0 and f_0 do not appear simultaneously in the equations of the state of the two fluids.

Nevertheless, one must keep in mind the possibility out of the scope of this work that the Universe is made of two fluids, the DBI one plus cosmic dust, which ultimately should be confronted with the model we present here. This possibility has been recently explored from an asymptotic behaviour perspective in [187].

2.2 Linear perturbations

As we have already seen in Section 1.5.1, in the "Synchronous Gauge" the line element is given by Eq. (1.80) where the comoving coordinates are related to the proper time t and position $\boldsymbol{r}$ by $d\tau = dt/a$, $d\boldsymbol{x} = d\boldsymbol{r}/a$, and h_{ij} is the metric perturbation. We choose not to use the longitudinal gauge, which was used in [102] for Lagrangians of this sort, because it is only applicable to the analysis of scalar perturbations; whereas the synchronous gauge,

which is the one we work with, allows for a more general treatment. The scalar mode of h_{ij} is described by the two fields $h(\boldsymbol{k},\tau)$ and $\eta(\boldsymbol{k},\tau)$ in the Fourier space:

$$h_{ij}(\boldsymbol{x},\tau) = \int d^3k e^{i\boldsymbol{k}\cdot\boldsymbol{x}} \left[\hat{\boldsymbol{k}}_i\hat{\boldsymbol{k}}_j h + (\hat{\boldsymbol{k}}_i\hat{\boldsymbol{k}}_j - \frac{1}{3}\delta_{ij})6\eta\right], \tag{2.18}$$

with $\boldsymbol{k} = k\hat{\boldsymbol{k}}$. The Einstein equations to linear order [1] in k-space, expressed in terms of h and η, are given by the following four equations [180]:

$$k^2\eta - \frac{1}{2}\frac{a'}{a}h' = 4\pi G a^2 \delta T^0_0, \tag{2.19}$$

$$k^2\eta' = 4\pi G a^2(\rho + p)\theta, \tag{2.20}$$

$$h'' + 2\frac{a'}{a}h' - 2k^2\eta = -8\pi G a^2 \delta T^i_i, \tag{2.21}$$

$$h'' + 6\eta'' + 2\frac{a'}{a}(h' + 6\eta') - 2k^2\eta = \\ -24\pi G a^2(\rho + p)\sigma. \tag{2.22}$$

Here, the quantities θ, Σ^i_j and σ were previously introduced in Section 1.5.1 and denote the divergence of the fluid's velocity, the traceless component of the tensor T^i_j and the shear stress respectively, see Eqs. (1.86) and (1.92).

Let us consider a fluid moving with a small coordinate velocity $v^i = dx^i/d\tau$, then, v^i can be treated as a perturbation of the same order as the energy density, pressure and metric perturbations. Hence, as we have seen in Section 1.5.1, considering the perturbations to linear order of the energy-momentum tensor, with vanishing anisotropic shear perturbation Σ^i_j, Eqs. (1.83)-(1.85), the perturbed part of energy-momentum conservation equations $T^{\mu\nu}_{\ \ ;\mu} = 0$ in the k-space leads to the equations

$$\delta' = -(1+w)\left(\theta + \frac{h'}{2}\right) - 3\mathcal{H}\left(\frac{\delta p}{\delta\rho} - w\right)\delta, \tag{2.23}$$

$$\theta' = -\mathcal{H}(1-3w)\theta - \frac{w'}{1+w}\theta + \frac{\delta p/\delta\rho}{1+w}k^2\delta, \tag{2.24}$$

where $\mathcal{H} = a'/a = aH = \dot{a}$. Assuming strictly adiabatic contributions to the perturbations, the speed of sound for the fluid is

$$c_s^2 = \frac{\delta p}{\delta\rho} = \frac{\dot{p}}{\dot{\rho}} = \frac{1}{\gamma^2} = \frac{a^6}{c^2 f_0 + a^6}, \tag{2.25}$$

and the time variation of w is

$$w' = -3\mathcal{H}(1+w)(c_s^2 - w). \tag{2.26}$$

[1] It has been pointed out that linear perturbations may not be sufficient to treat unified dark sector models, and a method to do so has been proposed in [42].

Hence, inserting these last two equations in (2.23) and (2.24), they become

$$\delta' = -(1+w)\left(\theta + \frac{h'}{2}\right) - 3\mathcal{H}(c_s^2 - w)\delta, \tag{2.27}$$

$$\theta' = -\mathcal{H}(1-3c_s^2)\theta + \frac{c_s^2}{1+w}k^2\delta. \tag{2.28}$$

Besides, using equations (2.19), (2.21), (1.83) and (1.85) we arrive at

$$h'' + \mathcal{H}h' + 3\mathcal{H}^2(1+3c_s^2)\delta = 0. \tag{2.29}$$

At early times, when the overall fluid has $w \approx 0$, the effective fluid perturbations evolve similarly to those of ordinary dust, with $\dot{\theta} = \theta = 0$, $a \sim t^{2/3}$, and from Eqs. (2.23) and (2.29) we obtain

$$\delta'' + \mathcal{H}\dot{\delta} - \frac{3}{2}\mathcal{H}^2\delta = 0 \tag{2.30}$$

and $\delta = c_1 t^{-1} + c_2 t^{2/3}$, where c_1 and c_2 are arbitrary integration constants. In this dust dominated era the perturbation grows as $\delta \approx a$, showing an initial unstable phase compatible with the observation that the primordial universe would have tiny perturbations which seeded the formation of structures in the universe. Conclusions about the clustering capabilities of other cosmic settings with DBI fluids have been studied in [37].

At late times, we are interested in finding the evolution of the linear scalar perturbations for any mode k. To this end we write the second order differential equation for the density perturbation δ, see [30]:

$$\delta'' + [1+6(c_s^2-w)]\mathcal{H}\delta' + \Big[9(c_s^2-w)^2\mathcal{H}^2 + 3(c_s^{2\prime} - w')\mathcal{H} + 3(c_s^2-w)(\mathcal{H}' + \mathcal{H}^2) + c_s^2k^2 - \frac{3}{2}(1+3c_s^2)(1+w)\mathcal{H}^2\Big]\delta = -3c_s^2(1+w)\mathcal{H}\theta. \tag{2.31}$$

Taking into account that in the late time regime the scale factor behaves as $a \propto e^{\sqrt{\frac{V_0}{3}}t}$ we can calculate $\mathcal{H}$

$$\mathcal{H} = a'/a = \dot{a} \propto a. \tag{2.32}$$

Considering the expression of γ given by Eq. (2.14), one obtains the late-time expansion in terms of $1/a$ for ρ, p, w, c_s^2, w' and $\mathcal{H}$. In this way, replacing these expansions in Eqs. (2.28) and (2.31) and keeping only the most significant terms one gets

$$\delta'' + 13\mathcal{H}\delta' + \left[9(c_s^2-w)^2\mathcal{H}^2 + 2(c_s^2-w)\mathcal{H}^2 + c_s^2k^2\right]\delta = -3c_s^2(1+w)\mathcal{H}\theta \tag{2.33}$$

$$\theta' = 2\mathcal{H}\theta + \frac{V_0k^2a^6}{c^2}\delta. \tag{2.34}$$

From Eqs. (2.33) and (2.34) the evolution of the perturbation becomes mode dependent with the $k^2/\mathcal{H}^2$ term, and for low energy modes their solutions can be obtained assuming a

power law dependence of the perturbations with the scale factor, $\delta \propto a^n$ and $\theta \propto a^s$. In this case the approximate solutions are given by

$$\theta \approx \theta_0 a^2, \tag{2.35}$$

$$\delta \approx \frac{\delta_1}{a^4} + \frac{\delta_2}{a^{10}} + \frac{\theta_1}{a^5}, \tag{2.36}$$

where θ_0, δ_1 and δ_2 are integration constants while θ_1 is a function of θ_0, c and V_0. This shows that the coupling to θ in Eq. (2.31) can be neglected for all scales we are interested on. We also find that the energy density perturbation decreases for large cosmological times for modes satisfying the condition $k^2/\mathcal{H}^2 \ll 1$. For high energy modes, $k^2/\mathcal{H}^2 \gg 1$, Eq. (2.33) is like the equation of motion of a dissipative mechanical system. This resemblance emerges using the analogy with the classical potential problem

$$\frac{d}{d\tau}\left[\frac{\delta'^2}{2} + \mathcal{V}(\delta)\right] = -13\mathcal{H}\delta'^2, \tag{2.37}$$

where

$$\mathcal{V}(\delta) = \frac{k^2\delta^2}{2}, \tag{2.38}$$

As for any mode k the potential $\mathcal{V}$ has a minimum at $\delta = 0$, the function inside the square bracket in Eq. (2.37) is a Liapunov function and the perturbation decreases asymptotically reaching $\delta = 0$ in the limit $t \to \infty$.

2.3 Observational constraints

Once the behaviour of the model has been well studied, it is time to set constraints on its parameters from a Bayesian perspective, see Section 1.7.1 for details. Our analysis will use geometrical tests: the SN Type Ia luminosity test, the CMB shift test with WMAP5-year data [146, 287], and the BAO test [208] as it has been detailed in Sections 1.6.1, 1.6.3 and 1.6.4. As these two last tests involve early universe quantities (the sound horizon at decoupling and dragging epochs), one must consider a slightly more general setup and include radiation, which must be conserved independently from the DBI fluid. This way, the Friedmann equation (1.29) for a flat universe turns out to be

$$3H^2 = f_0^{-1}\left(\sqrt{1 + c^2 f_0 \left(\frac{a_0}{a}\right)^6} - 1\right) + V_0 + \rho_{r0}\left(\frac{a_0}{a}\right)^4. \tag{2.39}$$

In terms of the fractional energy densities and the redshift we have

$$\frac{H^2}{H_0^2} = \sqrt{\Omega_f^2 + \Omega_c^2(1+z)^6} + \Omega_\Lambda + \Omega_r(1+z)^4,$$

where

$$\Omega_f = \frac{1}{3H_0^2 f_0}, \tag{2.40}$$

$$\Omega_\Lambda = \frac{f_0 V_0 - 1}{3H_0^2 f_0}, \tag{2.41}$$

$$\Omega_r = \frac{\rho_{r0}}{3H_0^2} \quad \text{and} \tag{2.42}$$

$$\Omega_c = \frac{c^2 f_0}{3H_0^2}. \tag{2.43}$$

The latter are subject to the normalization condition

$$\sqrt{\Omega_f^2 + \Omega_c^2} + \Omega_\Lambda + \Omega_r = 1. \tag{2.44}$$

In addition, the CMB and BAO tests require that we identify a combination of parameters which behaves effectively as Ω_m in the high energy regime. In our case this mimicry is played by Ω_c.

As a approach to this model, we are setting constraints only on Ω_c and Ω_f. In contrast, we fix a prior for Ω_b, taking the WMAP 5-year best fit, $\Omega_b = 0.0432$ [146]. Using the tests mentioned before in the framework of Bayesian statistics, one should minimize the corresponding χ^2 function in order to obtain Ω_c and Ω_f, see Section 1.7.

We have used two different compilations for SNIa data: ESSENCE [77, 150], which combines the first results of the survey [292] with the results of Riess et al. detected by the HST [222] and UNION [148], a vast sample which brings together 414 SN from 13 independent datasets: recent samples (SLS, ESSENCE), old datasets and distant supernovae from the HST. In the case of the UNION sample, the best values obtained are $\Omega_c = 0.256^{+0.012}_{-0.010}$, $\Omega_f = 0.160^{+0.171}_{-0.160}$ and for the ESSENCE sample $\Omega_c = 0.257^{+0.013}_{-0.011}$ and $\Omega_f = 0.202^{+0.177}_{-0.202}$ with the corresponding 68.30% uncertainties. The lines in the upper regions of the plots in Fig. 2.2 represent the locations on the parameter space which correspond to Chaplygin gas cases and the points in each of the lines indicate the case with the lowest χ^2 value. From visual inspection one can infer that the Chaplygin gas is rejected by our model. In contrast, ΛCDM (the $\Omega_f = 0$ locations) is not significantly excluded, as for a certain range of Ω_m, ΛCDM cases lie in the 68.30% likelihood credible interval. All in all, our model provides better fits.

With the aim of compensating for the arbitrariness in the choice of priors when one computes the evidence, Eq. (1.7.2), we explore different priors on Ω_c and Ω_f. In the case of Ω_c we have the guidance of all the literature of constraints on dark energy, which more or less suggests preferred regions. To take advantage of this, we explore four priors of different lengths, all centered at the value $\Omega_c = 0.25$. In contrast, to illustrate the effect of changing the prior on Ω_f, which is a new parameter on which we have no previous clues, we divide the physically allowed region $\Omega_f \in [0.00, 1.0]$ into four equal intervals. From Fig. 2.3 and Tab. 2.1 one can conclude that among the priors considered, the region $\Omega_f \in [0.00, 0.25]$, $\Omega_c \in [0.24, 0.26]$ gives the best constraints for the parameters.

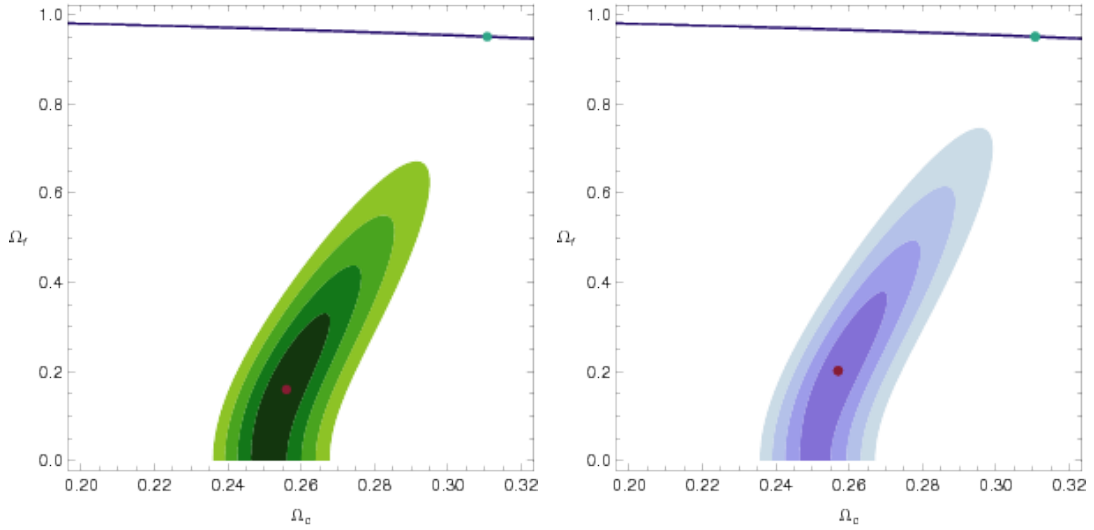

(a) UNION (b) ESSENCE

Figure 2.2: *Credible intervals from the combination of SN+CMB+BAO constraints for two different SN compilation samples.*

2.4 Model kinematics

As this is a new model, it is worth examining it from different perspectives, the kinematic one being specially relevant. We investigate the redshift dependence of the effective equation of state parameter, $w(z)$, and derived quantities such as the acceleration parameter, $q(z)$, or the redshift at which the transition from a decelerated to an accelerated universe transition occurs, z_t. In order to obtain the behavior of $w(z)$, we use the expression that relates it with the Friedman equation [194, 231]

$$w(z) = \frac{\frac{2}{3}\frac{d\ln H}{dz}(1+z) - 1}{1 - \left(\frac{H_0}{H}\right)^2 \Omega_c (1+z)^3}. \tag{2.45}$$

In our model it takes the form

$$w(z) = \frac{\left(\Omega_r(1+z)^4 - 3\Omega_\Lambda\right)\sqrt{{\Omega_c}^2(1+z)^6 + {\Omega_f}^2} - 3{\Omega_f}^2}{3\sqrt{{\Omega_c}^2(1+z)^6 + {\Omega_f}^2}\left(\Omega_r(1+z)^4 - \Omega_c(1+z)^3 + \Omega_\Lambda + \sqrt{{\Omega_c}^2(1+z)^6 + {\Omega_f}^2}\right)}. \tag{2.46}$$

Analyzing the redshift dependence of the equation of state parameter we can see that the current observational data in the context of our model restrict it to be smaller than -1, $w(z) \leq -1$ with $dw/dz|_{z=0} > 0$ for the current time. More precisely, we obtain $w(z=0) = -1.052^{+0.052}_{-0.081}$, $dw/dz|_{z=0} = 0.081^{+0.081}_{-0.140}$ with the UNION sample and $w(z=0) = -1.074^{+0.074}_{-0.078}, dw/dz|_{z=0} = 0.074^{+0.074}_{-0.199}$ with the ESSENCE sample, with the uncertainties

(a) UNION

	$\Omega_c \in [0.24, 0.26]$	$\Omega_c \in [0.23, 0.27]$	$\Omega_c \in [0.26, 0.28]$	$\Omega_c \in [0.25, 0.29]$
$\Omega_f \in [0.00, 0.25]$	$4.534 \cdot 10^{-71}$	$2.655 \cdot 10^{-71}$	$7.797 \cdot 10^{-72}$	$2.258 \cdot 10^{-71}$
$\Omega_f \in [0.25, 0.50]$	$2.060 \cdot 10^{-72}$	$5.970 \cdot 10^{-72}$	$1.242 \cdot 10^{-71}$	$7.289 \cdot 10^{-72}$
$\Omega_f \in [0.50, 0.75]$	$4.312 \cdot 10^{-81}$	$1.667 \cdot 10^{-76}$	$3.760 \cdot 10^{-74}$	$4.681 \cdot 10^{-74}$
$\Omega_f \in [0.75, 1.00]$	$5.250 \cdot 10^{-100}$	$6.557 \cdot 10^{-90}$	$8.821 \cdot 10^{-83}$	$2.975 \cdot 10^{-79}$

(b) ESSENCE

	$\Omega_c \in [0.24, 0.26]$	$\Omega_c \in [0.23, 0.27]$	$\Omega_c \in [0.26, 0.28]$	$\Omega_c \in [0.25, 0.29]$
$\Omega_f \in [0.00, 0.25]$	$2.052 \cdot 10^{-45}$	$1.194 \cdot 10^{-45}$	$3.359 \cdot 10^{-46}$	$1.003 \cdot 10^{-45}$
$\Omega_f \in [0.25, 0.50]$	$1.750 \cdot 10^{-46}$	$4.628 \cdot 10^{-46}$	$9.751 \cdot 10^{-46}$	$5.798 \cdot 10^{-46}$
$\Omega_f \in [0.50, 0.75]$	$3.435 \cdot 10^{-54}$	$6.867 \cdot 10^{-50}$	$9.742 \cdot 10^{-48}$	$1.058 \cdot 10^{-47}$
$\Omega_f \in [0.75, 1.00]$	$8.433 \cdot 10^{-72}$	$4.257 \cdot 10^{-62}$	$2.501 \cdot 10^{-55}$	$4.115 \cdot 10^{-52}$

Table 2.1: *Bayesian evidences for our unified dark energy DBI model from the combination of SN+CMB+BAO observations for two different SN compilation samples.*

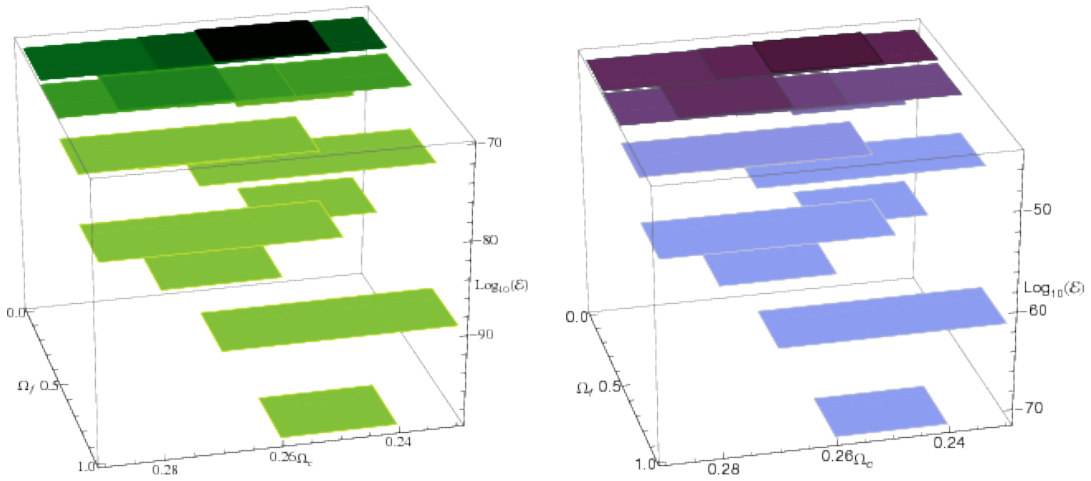

(a) UNION (b) ESSENCE

Figure 2.3: *3D representation of Bayesian evidences for our unified dark energy DBI model from the combination of SN+CMB+BAO observations for two different SN compilation samples.*

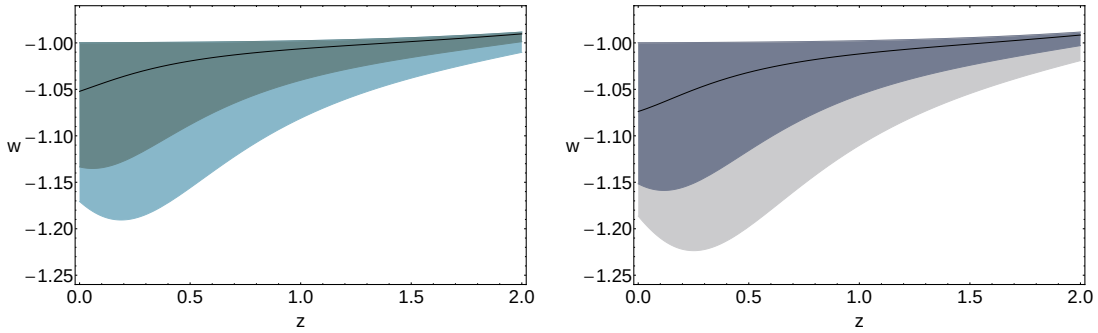

(a) UNION (b) ESSENCE

Figure 2.4: *Variation of the equation of state parameter with the redshift for two different SN compilations.*

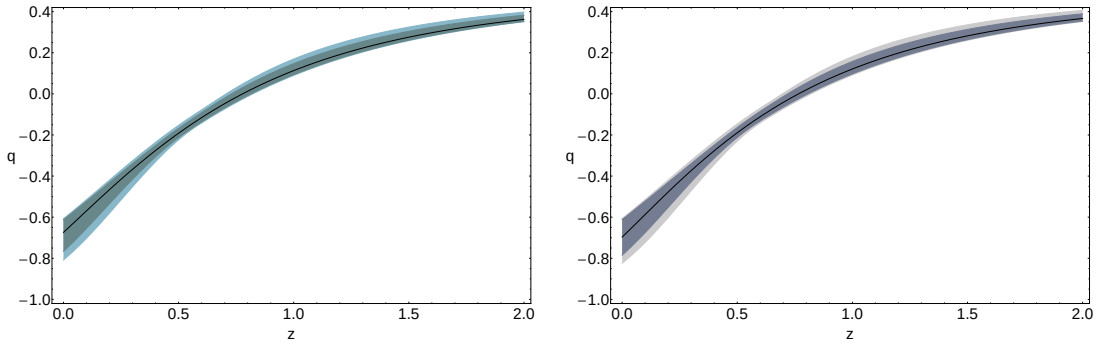

(a) UNION (b) ESSENCE

Figure 2.5: *Variation of the acceleration parameter with the redshift for two different SN compilations.*

corresponding to the 68.30% interval of confidence.

In addition, we study the acceleration parameter, $q(z)$, which for instance can be expressed as

$$q(z) = \frac{3}{2}\left(1 - \frac{\Omega_c\,(1+z)^3}{H^2}\right) w(z) + \frac{1}{2}. \tag{2.47}$$

Figs. 2.4 and 2.5 depict the shape of the equation of state and acceleration parameters with their corresponding 68.30% and 95.45% error bands. From the analysis of the acceleration parameter we gather that there is a strong evidence of the transition from a deceleration to an acceleration stage. For a better insight on this matter, we have inferred in different ways the redshift at which the transition happens.

Since we have an expression for $q(z)$,

$$q(z) = \frac{(1+z)\left(4\Omega_r(1+z)^3 + \dfrac{3\Omega_r^2(1+z)^5}{\sqrt{\Omega_f^2+\Omega_r^2(1+z)^6}}\right)}{2\left(1-\sqrt{\Omega_c^2+\Omega_f^2}-\Omega_r+\Omega_r(1+z)^4+\sqrt{\Omega_f^2+\Omega_c^2(1+z)^6}\right)} - 1, \tag{2.48}$$

we can directly compute the redshift at which the acceleration parameter vanishes, $q(z_t) = 0$, to obtain the transition redshift, z_t. For the ESSENCE compilation of SNIa we have $z_t = 0.766^{+0.041}_{-0.047}$, and for the UNION sample $z_t = 0.778^{+0.036}_{-0.048}$.

In [221] another approach was proposed. It requires an expansion of the acceleration parameter, $q(z)$, into two terms:

$$q(z) = q_0 + z\left.\frac{dq}{dz}\right|_{z=0}. \tag{2.49}$$

Under this definition, we get $z_t = 0.649^{+0.096}_{-0.079}$ with the UNION sample and $z_t = 0.650^{+0.139}_{-0.078}$ with the ESSENCE sample. These results are in good agreement with the results obtained in [109, 221, 285].

Yet another parametrization was considered in [70, 297]:

$$q(z) = q_0 + q_1\frac{z}{1+z}, \tag{2.50}$$

where $q_0 = q(z=0)$ is the value of the deceleration parameter at present and q_1 is the parameter that contains the correction in the distant past ($\lim_{z\to\infty} q(z) = q_0 + q_1$ for $z \gg 0$). With this parametrization we get that the value of the transition redshift is $z_t = 0.674^{+0.092}_{-0.062}$ for ESSENCE and $z_t = 0.697^{+0.088}_{-0.085}$ for UNION.

As the value of z_t obtained directly by the explicit equation (2.48) is bigger that the approximate one, we infer that the approximations are not good enough for accounting accurately for the tendency of our DBI fluid to induce a phantom stage. The result obtained by our procedure tells us that the acceleration-deceleration transition happens before than the other definitions allow to estimate.

2.5 Conclusions

Here we have proposed a new alternative to the popular models which attempt at a unification of dark matter and dark energy components of the Universe. This new model stems from a purely kinetic DBI action, and therefore suggest that these non-canonical actions, which have been resorted to as a way to model the early acceleration in the Universe, can also serve the same purpose for the late time acceleration. The transition from an $H^2 \sim a^{-3}$ regime to a de Sitter phase is realized with a single fluid, so this is a novel scenario and demands a perturbative analysis of its own. We can summarize the results as follows. At early times, the divergence of the velocity perturbation is negligible, whereas the energy density perturbation is a growing one, thus signaling the initial unstable phase required for the onset of structures. At late times, the velocity and energy density perturbations decouple, and the latter becomes negligible as the Universe becomes dominated by vacuum energy.

The observational analysis suggests that our model presents some attractive features which extend its value beyond the theoretical perspective. To begin with, current constraints show our model is by far better suited to the observations that the most popular unified dark sector model: the Chaplygin gas [35, 138]. Our results also indicate a modest preference of our model as compared to the ΛCDM one. Perhaps the most remarkable outcome of this observational analysis is that the best fit corresponds to a phantom behaviour, i.e. the effective equation of state parameter $w_{\rm eff}$ lies at present below the -1 line. It must be remembered that this behaviour is achieved without actually having to resort to a genuine phantom component, so we do not have to be concerned with the associated instabilities.

This study, which has been carried out from different relevant angles and the results achieved, convinces us that our model represents a worthy model for the unification of the dark sector, reinforces the theoretical interests of DBI models by extending the range of interest to the late Universe, and suggests the interest of exploring generalizations of this model, probably by relaxing the assumption of a purely kinetic Lagrangian, as perhaps further degrees of freedom would allow an even better suitability to astronomical observations.

CHAPTER 3

OSCILLATIONS IN THE DARK ENERGY EQUATION OF STATE: NEW MCMC LESSONS

We have nowadays a great amount of independent data sets available for studying the present dynamical state of the Universe. High quality data coming from the Hubble diagram of Type Ia Supernovae [16, 58, 221]; the measurements of cluster properties as the mass, the correlation function and the evolution with redshift of their abundance [17, 18, 91, 283]; the optical surveys of large scale structure [60, 90, 212]; the anisotropies of the cosmic microwave background [78, 261]; the cosmic shear measured from weak lensing surveys [216, 282] and the Lyman-α forest absorption [68, 189] are evidences toward an *apparently clear* picture of our universe at present which is characterised by: I. spatial flatness, II. a subcritical matter content, III. and accelerated expansion.

But the *clarity* of this sketch poses a more interesting and deeper question: how can we interpret all these features in the framework of a self-consistent theoretical cosmological model? This is the main task of modern cosmology, and no unique answers have been given so far.

The ΛCDM model is, from a statistical point of view, the simplest and the most accepted; it is called *concordance model* just for this reason. In this scenario, acceleration is driven by the famous cosmological constant, Λ, as was detailed in Sec. 1.4.1, this component represents the major contribution to the energy/matter content of the Universe. At the same time, it requires the presence of a large amount of *cold dark matter* which does not interact with electromagnetic radiation, but it is detectable only by its gravitational interaction with ordinary baryonic matter. This model provides a good fit to most of the data [233, 239, 274], giving a reliable snapshot of the current Universe; but it is also affected by serious theoretical shortcomings that have motivated the search for alternative candidates generically referred to as *dark energy* or *quintessence*. Such models range from conventional scalar fields rolling down self-interaction potentials, to non-canonical scalar field models

(phantom, k-essence,etc.); from phenomenological unified models of dark energy and dark matter to alternative gravity theories [64, 199, 202].

Unfortunately, so many data are not yet able to give us a definitive answer about the origin and nature of the acceleration of the Universe; and neither able to to solve the *coincidence problem* nor to state what the right EoS of dark energy is.

Regarding the EoS, using current data one typically will only be able to infer that the dark energy effective EoS parameter w is close to -1 at present. But any small deviation from this value could give a different theoretical scenario: if it is *exactly equal* to -1, when of course referring to observational errors, we have a cosmological constant; if it is larger than -1, we have a quintessence model; while if it is smaller than -1 we have the so called phantom dark energy as was detailed. In addition, the data seem to indicate that the fractional energy densities of the two main components of the Universe, i.e. dark matter and dark energy, are very similar at present, and the label "coincidence problem" has been coined to refer to this striking similarity.

In Sec. 1.4.2 we have already seen that one of the most interesting solutions proposed to try and throw some light on these questions is *oscillating dark energy* ([81, 98, 229]). Such a model can easily solve the coincidence problem in a very natural way due to periods of acceleration, and can be also used as a good candidate for the unification of the late time acceleration (the one observed at present) with inflation (an early time acceleration period). In this context we have to underline the difference between assessing a periodic or non-monotonic potential and an oscillating dark energy EoS. In many cases such potentials do not give rise to a periodic w; one example can be found in [101], where the proposed field is clearly periodic, but the derived w can be well described by the CPL parametrization for dark energy introduced in [55] and [174] and given by Eq. (1.53).

In this chapter we are going to follow the method from [175], by examining some directly proposed phenomenological periodic equations of state for the dark energy using different cosmological observations. Specifically, we are going to set constraints on the location of the centre of the range about which w oscillates. We will also constraint the amplitude of the oscillations and the fractional energy density of matter.

Actually, in the models to be considered there is another important parameter, the frequency of the oscillation. Relevant though it is, leaving this parameter completely free leads to a high-dimensionality statistical problem, but given the precision of the data available at present, it seems that problems of that sort cannot be tackled satisfactorily. As it has been already pointed out, there is not enough quality in the present data to constrain more than two dark energy parameters [177, 269]. In the literature on oscillating dark energy, the usual practice has been choosing a specific single value of this oscillation frequency and stick with it. In order to fix it one may resort to an argument by [175], which suggests the lowest bound on this frequency to be able to discriminate an oscillating behaviour from a monotonic one for the data in use. We wish to carry out here a more thorough study of oscillating dark energy than previous works, and to this end we choose a discrete set of values of the frequency (above and below that bound), and then obtain constraints on the rest of parameters. Relaxing assumptions on the frequency, as compared to previous works, will allow us to draw stronger conclusions; yet this is not the only novelty of our analysis, as will be shown in what follows.

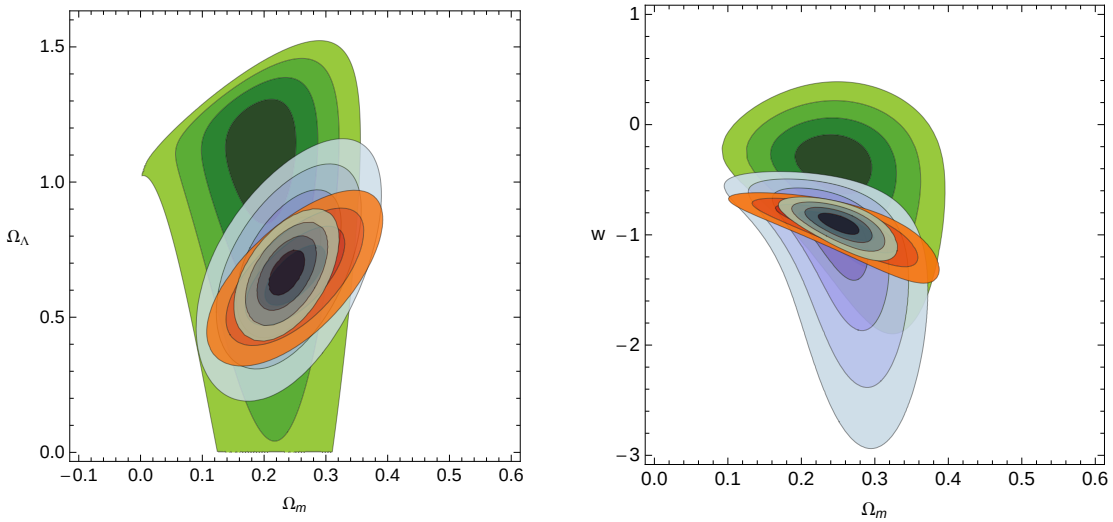

(a) ΛCDM (b) Constant EoS

Figure 3.1: *Credible intervals of the different observational data sets: green ones correspond to GRBs, purple to Hubble parameter data, orange to SNeIa and blue to the combination of all observational data. To construct these contour plots we have considered a prior on Ω_m and w_0 from WMAP-5years.*

In this exploration of possible oscillating patterns in the expansion of the Universe induced scenarios which display a similar start off to the popular oscillating model by Linder [175], but then depart from it as their amplitude gets smaller as z grows and the distance between nodes tends to converge to a specific value. In this direction, we propose a pair of models in which dark energy oscillations are modelled via special functions. Comparison between models of that sort and the usual trigonometric parametrization provides hints about which features in the oscillations are favoured or disfavoured.

Moreover, the present work innovates in another direction: we choose a combination of datasets with interesting characteristics: we combine the statistically most powerful dataset available, the luminosity measurements of SNeIa, with other datasets: the luminosity measurements of Gamma Ray Bursts and direct measures of the Hubble parameter. GRBs are particularly useful for the study of oscillating models, as they typically inform us of higher redshifts than supernovae data, so they improve the capability for detecting oscillating features, at lower frequencies, if they exist. In addition, the inclusion of the direct Hubble data can, in principle, enhance the sensitivity of our tests to the presence of oscillations, as the use of these data does not involve an averaging of the inverse of the Hubble factor, and then a possible smoothing of the oscillations is partially compensated for. Another point in favour of the usage of this particular combination of three datasets is the rather good concordance among them (see Fig. 3.1), which applies at least for the case of a constant w quintessence, and therefore seems a priori a property that will be shared by models with a dynamical EoS parameter.

3.1 Oscillating dark energy

3.1.1 Our parametrizations

We have just presented motivations for studying oscillating dark energy. In general, in order to infer conclusions about the dynamical behaviour of dark energy and its consequences in the expansion of the Universe, one has to make some concessions to try and make the best out of a collection of noisy scattered data. It has been pointed out that one of the most popular is to propose a parametric reconstruction obeying some basic requirements. Our proposal fits precisely in this kind of approach, and in order to examine the adequacy of oscillating patterns in the dark energy EoS we consider a simple and periodic phenomenological parametrization for the EoS, as proposed and studied in [175]:

$$w(a) = w_c - A\sin(B\ln a - \Theta). \tag{3.1}$$

Equation (3.1) describes evolutionary dark energy with

- Θ being the phase of the oscillation, which for simplicity is assumed to be zero.
- w_c being the centre of the range about which $w(a)$ oscillates. In the $\Theta = 0$ case the parameter w_c is equal to the present value of the dark energy EoS, $w(a = 1) = w_c = w_0$.
- A being the amplitude of the oscillations, which obviously must be non zero for a dynamical w. If this EoS is the effective realisation of a canonical scalar field, A should fulfil the constrain $w_0 - A \geq -1$; but we leave it completely free and let the observational data speak out its value.
- B being the frequency of the oscillations; and there are some key remarks to be made about it. In order to notice distinctly the presence of an oscillatory behaviour B should fulfil the condition

  $$|B\ln a_{min}| > 2\pi, \tag{3.2}$$

  where a_{min} is given by the highest redshift in the dataset. For our observational data this value is associated with a GRB at $z = 5.6$, for which we infer the constraint $B > 3.3$. Nevertheless, as SNeIa represent by far the dataset with the largest statistical power in our analysis and they span a smaller redshift range, it seems reasonable that an oscillating pattern will be only detectable for larger values of B.

Previous works have attempted to set constraints in these parameters, but they have not been able to distinguish an oscillatory model from one with a constant EoS. This is partly due to the data sets employed, but also because of excessive restrictions on the parameters.

In this new attempt at exploring oscillating dark energy we use a new combination of data sets so as to obtain more reliable constraints, but we also make a few other key changes: specifically we carry out an analysis for a discrete set of fixed B values to try and avoid the arbitrariness in the choice of this parameter present in works by other authors.

In addition, and given the lack of grounds for very strong restrictions on phenomenological parametrizations of dark energy we have analysed two more models which represent a slight departure from the perhaps excessively nicely shaped trigonometric parametrization by Linder. Our first proposal in this direction is

$$w(a) = w_c - A\ J_1(B\ln a - \Theta), \tag{3.3}$$

where again we have set the phase $\Theta = 0$ so that $w_c = w_0$, and J_n is the Bessel function of the first kind with $n = 1$. The Bessel function $J_1(x)$ shows oscillations which are damped with growing x, as opposed to the constant amplitude of the trigonometric case. So, in this case, the EoS parameter w would have an oscillating trend modulated by a damping effect which makes the amplitude smaller and smaller as we go back in time (in the redshift space).

As we have to set observational constraints on parameters, we have to compute the Hubble factor, which in the flat case takes the form

$$H^2(a) = \Omega_m a^{-3} + (1-\Omega_m)a^{-3(1+\overline{w}(a))}. \tag{3.4}$$

In this case, it only depends on the present value of the fractional matter density Ω_m, and on the averaged equation of state parameter

$$\overline{w}(a) = \frac{\int_0^{\ln(a)} w(a) d\ln(a)}{\ln(a)}. \tag{3.5}$$

So, we will work at some points with this expression of the EoS parameter instead of the usual one. It can be noticed that for the two parametrizations presented above the averaged forms follow a common pattern; for example, the parametrization given by the Eq. (3.1) takes the form

$$\overline{w}(a) = w_0 + \frac{A}{B}\frac{\cos(B\ln a) - 1}{\ln(a)}, \tag{3.6}$$

whereas the parametrization given by Eq. (3.3) reads

$$\overline{w}(a) = w_0 + \frac{A}{B}\frac{J_0(B\ln a) - 1}{\ln(a)}. \tag{3.7}$$

With Eq. (3.7) and Eq. (3.6) as a reference, we propose another parametrization with a damped oscillating behaviour:

$$\overline{w}(a) = w_0 + \frac{A}{B}\frac{(\pi/2)H_{-1}(B\ln a) - 1}{\ln(a)}, \tag{3.8}$$

where w_0 is the value of the EoS at present, and H_{-1} is the Struve function, H_α, of order $\alpha = -1$. The Struve function lies between the trigonometric case, with constant amplitude, and the Bessel function, being less acutely damped than the Bessel function. It can be checked that the $w(a)$ function for this new proposal is an oscillating one as well, so this new model fits is the aim of the discussion.

Anyway, we have to underline that our three w models depend on $\ln a$ (i.e. $\ln(1+z)$), so these effects are quite smoothed and not so evident when depicted on even a large redshift interval such as the one limited by the re-ionisation one ($z = 1089$). However, such parametrizations, as first shown by [175], allow for analytical expressions of $H(z)$ (see Eq. (3.5)) and thus result convenient for evaluation purposes.

Interestingly, as we will discuss later, the main consequences of an oscillating equation of state are more evident on the deceleration $q(z)$ function than on the Hubble function or the dark energy fractional density Ω_X.

3.1.2 Earlier Works

In [222] an interesting observational clue of a possible oscillating behaviour in the EoS was found. Indications that such oscillations might be really present were found fitting a quartic polynomial of $w(z)$ to SNeIa observations. Even though the redshift range where these oscillations seem to be present is actually rather small; these results motivated a plethora of works trying to analyse this possibility deeper.

In [294] the formulation

$$w(z) = w_0 + w_1 \sin(z), \tag{3.9}$$

was used to model a quintom scenario phenomenologically. The analysis was conducted using luminosity distances of SNeIa, the CMB shift parameter and the linear growth rate from large scale structure. The best fit values found combining all these data sets were $w_0 = -1.33$, $w_1 = 1.47$. Such oscillating model differs very little from the linear one ($w(z) = w_0 + w_1 z$) when considering constraints from SNeIa only, and the oscillating case is only mildly preferred. This was somehow to be expected, as for low redshifts the two parametrizations are very similar. Note that, as in this study the oscillation frequency was fixed to a specific value, we meet again the difficulties to make general inferences.

An extension of the latter was done in [295], where

$$w(a) = w_0 + w_1 \sin\left(w_2 \ln a + w_3\right), \tag{3.10}$$

was proposed, therefore now including also a period and a phase. One further degree of sophistication was introduced in the analysis as it was carried out using a modified version of CosmoMC so as to take into account dark energy perturbations. The results indicate that w_0 is acceptably well constrained, while w_1 is poorly constrained, and w_2 and w_3 can be regarded as completely unconstrained. This is not surprising, though, as highly dimensional parametrizations of dark energy seem to suffer this problem typically, given the precision of observational data at present.

In [296] constraints on the cosmological parameters of some oscillating models were analysed using simulated data from future Planck measurements. Two different parametrizations of the dark energy EoS were used, the CPL one, Eq. (1.53), but in terms of the scale factor:

$$w(a) = w_0 + w_1 (1 - a), \tag{3.11}$$

and a reformulation of the [175] oscillating one,

$$w(a) = w_0 + w_1 \sin(w_2 \ln(a)), \tag{3.12}$$

having fixed the phase parameter to zero. In addition, one further choice was made: for simplicity and for focusing the analysis on low redshifts, the period parameter was fixed as $w_2 = 3\pi/2$ (because it corresponds to a period in the redshift range $0 < z < 2$ where data from supernovae are more robust). Then the authors used present data from WMAP3-year [262], ESSENCE SNeIa [77], SDSS [90] to derive best fit values for the EoS parameters which are assumed as the fiducial values for deriving constraints from Planck mission details. The following results were obtained for the CPL EoS:

$$w_0 = -1.03^{+0.15+0.36}_{-0.15-0.26}, \quad w_1 = -1.03^{+0.562+0.781}_{-0.587-1.570}, \tag{3.13}$$

whereas these were the results for the oscillating model:

$$w_0 = -0.981^{+0.320+0.534}_{-0.340-0.748}, \quad w_1 = -0.068^{+0.561+1.037}_{-0.591-1.245}. \tag{3.14}$$

Assuming the CPL EoS they were able to conclude that a Quintom scenario with a $w(z)$ which crosses the phantom divide is favoured against the ΛCDM scenario (it is mildly favoured with present data while future surveys would provide narrower constrains). Assuming the oscillating EoS the same conclusion can be derived, even if the constraints are weaker, and the low value for the amplitude of oscillation makes the constant $w(z)$ (i.e. ΛCDM model) equally possible.

For what concerns the oscillating model, these results are backed up in [178], where the following 68% CL values were obtained:

$$w_0 = -0.958 \pm 0.098, \quad w_{amp} = 0.030^{+0.124}_{-0.130}. \tag{3.15}$$

From these results one can conclude that the EoS fit with current data provides as good as ΛCDM, and that the oscillation amplitude is limited: $|w_{amp}| < 0.232$ at 95%CL.

An oscillating model different from the one proposed by Linder is analysed in [129] (inspired by a previous idea in [98]). The authors used SNeIa, the CMB shift parameter and the measurement of the BAO peak from SDSS [90] in order to constrain the sine version of the oscillating EoS written in the form

$$w(a) = w_0 - A \sin(B \ln a), \tag{3.16}$$

and the alternative

$$w(a) = -\cos(b \ln a). \tag{3.17}$$

The frequency parameter b in the second model drives the accelerating/decelerating epochs, and in the small b limit one has $w(a) \sim -1$.

Final results show that $b = 0.06 \pm 0.01$ at 1σ level, a value which is consistent with limits required by the CMB and a correct power spectrum, and which represents a *clear* evidence for an oscillating behaviour with a very long period (i.e. small but clear deviation from a

cosmological constant).

Another interesting work is [151], where many different EoS were compared with a Bayesian approach. They worked with the so called linear EoS, i.e. CPL model; with pure oscillating models, the cosine one, $w(z) = w_0 \cos(w_c \ln(1+z))$, and the sine one, $w(z) = -1 + w_0 \sin(w_s \ln(1+z))$; with a damped version of previous oscillating models, $w(z) = w_0(1+z)^3 \cos(w_c \ln(1+z))$ or $w(z) = -1 + w_0(1+z)^3 \sin(w_s \ln(1+z))$; and with a more complicated version of the dark energy EoS directly derived from the dynamics of the phantom scalar field (see reference for details). Analysing the values of the Bayesian evidences obtained fitting data (SNeIa, CMB, BAO) for each particular model, and comparing them with the Jeffreys' scale [131], they concluded that there is a substantial evidence for preferring the pure oscillating model (sine) and the one derived from phantom field dynamics over the linear one, while damped versions are completely excluded. In addition, they found no strong evidence to favour ΛCDM over the oscillating models.

As it has been stated previously, completely different approaches are possible as well; for example, in [227] the starting point was an oscillating model for $H(z)$ instead of $w(z)$. Finally, it is possible to consider oscillating fields, which do not necessarily produce an oscillating EoS [101].

3.2 Observational data

We have tested the possible periodicity of the Hubble function, Eq. (3.4), by using three different observational data sets, i.e.:

- the reconstructed Hubble data given in [266];
- the *Constitution* Supernovae data set described in [117];
- the Gamma Ray Bursts luminosity distances measured and analysed in [145].

3.2.1 Hubble parameter: Stern et al. 2009 data set

Recently, in [266] an update of the Hubble function $H(z)$ data extracted from differential ages of passively evolving galaxies previously published in [249] was presented. Constraining the background evolution of the Universe using these data is interesting for several reasons. Firstly, they can be used together with other cosmological tests in order to get useful consistency checks or tighter constraints on models. Secondly, and more importantly, in contrast to standard candle luminosity distances or standard ruler angular diameter distances, the Hubble function is not integrated over. This is a key point because if a periodic behaviour is present in $w(a)$ it should be directly detectable in $H(a)$ while it could be lost in luminosity or angular diameter distances because of integration stages.

The Hubble parameter dependence on the differential age of the Universe in terms of redshift is given by

$$H(z) = -\frac{1}{1+z}\frac{dz}{dt}. \tag{3.18}$$

Thus, $H(z)$ can be determined from measurements of dt/dz. As reported in [133], [134], [249] and [266], values of dt/dz can be computed using absolute ages of passively evolving galaxies.

The galaxy spectral data used by [266] come from observations of bright cluster galaxies done with the Keck/LRIS instrument (see [267] for a detailed description of the observations, reductions and the catalogue of all the measured redshifts). The purposely planned Keck-survey observations have been extended with other datasets: SDSS improvements in calibration available in the Public Data Release 6 (DR6) have been applied to data in [134]; the SPICES infrared-selected galaxies sample in [265]; and the VVDIS survey by the VLT/ESO telescope in [156].

The authors of these references bin together galaxies with a redshift separation which is small enough so that the galaxies in the bin have roughly the same age; then, they calculate age differences between bins which have a small age difference which is at the same time larger than the error in the age itself [266]. The outcome of this process is a set of 11 values of the Hubble parameter versus redshift. A particularly nice feature of this test is that the sensitivity of differential ages to systematic error is lower than in the case of absolute ages [135].

Observed values of $H(z)$ can be used to estimate DE parameters by minimising the quantity

$$\chi^2_{\rm H}(H_0, \{\theta_i\}) = \sum_{j=1}^{9} \frac{(H(z_j; \{\theta_i\}) - H_{obs}(z_j))^2}{\sigma^2_{\rm H}(z_j)}, \tag{3.19}$$

where $H_0 \doteq 100\,h$ will be fixed as $h = 0.742$ ([223]), while the vector of model parameters, θ_i, will be $\theta_i = (\Omega_m, w_0, A, B)$ here in this case.

3.2.2 Supernovae: Hicken et al. 2009 data set

We use one of the most recent SNeIa samples, the *Constitution* sample described in [117], which is a data set obtained by combining the Union data set by [148] with new 90 nearby objects from the CfA3 release described in [117].

The Union SNeIa compilation is a data set of low-redshift nearby-Hubble-flow SNeIa, and is built with new analysis procedures for working with several heterogeneous SNeIa compilations. It includes 13 independent sets with SNeIa from the SCP, High-z Supernovae Search (HZSNS) team, Supernovae Legacy Survey and ESSENCE Survey, the older data sets, as well as the recently extended data set of distant supernovae observed with HST. After various selection cuts were applied in order to create a homogeneous and high-signal-to-noise data set, a final collection of 307 SNeIa events distributed over the redshift interval $0.15 \leq z \leq 1.55$ was obtained.

The CfA3 data set was originally made of 185 multi-band optical SNeIa light curves obtained at the F.L. Whipple Observatory of the Harvard-Smithsonian Center for Astrophysics (CfA); 90 of the original 185 objects passed the quality cuts of [148] and were added to the Union data set to form the Constitution one.

The statistical analysis of the Constitution SNeIa sample rests on the definition of the distance modulus, $\mu(z)$, which is directly related to the Hubble free luminosity distance,

$D(z)$, as it is detailed in Sec. 1.6.1. The best fits to be presented will be obtained by minimising the quantity $\chi^2_{\rm SN}(\mu_0, \{\theta_i\})$. However it will have to be marginalised over μ_0, which encodes the Hubble parameter and the absolute magnitude M. Thus, giving the heterogeneous origin of the Constitution data set, and the procedures described in [148] and [117] for reducing data, we have worked with an alternative version, Eq. (1.106), which is already minimised with respect to μ_0.

3.2.3 GRBs: Kodama et al. 2008 data set

The GRBs sample, described in [145], is made of 33 GRBs within the redshift interval $z < 1.62$, and 30 GRBs in the redshift interval $1.8 < z < 5.6$. It is well known that GRBs are not standard candles as SNeIa; at the same time they contain a lot of important information about high redshift properties of the Universe which cannot be derived from SNeIa. So their combined use can bring important and complementary information about the reconstruction of dark energy and gives us the possibility to detect eventually traces of an oscillatory behaviour on a larger redshift range. The calibration of GRB data can be done in several ways, but here we follow the prescriptions given in Sec. 1.6.2 using the peak energy-peak luminosity correlation described by the *Yonetoku relation* [298]. Thus, the chi-square function of GRBs data will be that given by Eq. (1.109).

3.3 Constraints and assumptions

We will explore the posterior probability distributions of our problem with the Markov Chain Monte Carlo (MCMC) method, described previously in Sec. 1.7.5 with the corresponding convergence test to check the validity of our chains, i.e. if our MCMC chain is large enough to obtain a good estimation of the parameters.

With the aim to improve results, we have implemented a few priors for running our MCMC chains. The main one has been to set the control $0 < \Omega_m < 1$, which is a minimum physical requirement. We have also set mild Gaussian priors on Ω_m and w_0 with the 3σ error bar from WMAP5-year [146] as a reference.

As we stated in the previous sections it would be possible to set physical limits on the parameters of the oscillating model, such as A and B. The amplitude A should have a value which depends on the theoretical scenario chosen to be the fiducial one. In the case of ΛCDM, one could require that the minimum value for the EoS was $w_0 - A \geq -1$. But it is clear that with this case will exclude the possibility of a phantom behaviour, which is a scenario present data do not rule out, and in some cases seem to be the preferred one. For that reason we regard leaving A free as the best option.

At the same time, the frequency (period) parameter B should be subject to $|B \ln a_{min}| > 2\pi$. The highest redshift of our observational data corresponds to a GRB observation at $z = 5.6$. For that choice, B should be $B > 3.3$. As we have no strong clues *a priori* about the validity of a periodic oscillating EoS, there is scarce guidance regarding a suitable lower bound on B. We could have oscillations with a period bound given by the highest redshift in the supernovae data, so in this case we would have $B > 5.7$; or we could have no detectable oscillations at all in our redshift range, so that a really small value of B could turn out to

be the best fit. In addition, rigorously the bound on B we are commenting about proposed in [175] makes only sense for the sine oscillating model, which has a valid definition for the *oscillation period*, and not for the other two models. However, also in these cases the B parameter can be related to periodic properties of the dark EoS parameter, so we treated it on the same footing in the analysis of the three models.

There is also another problem concerning the number of free parameters one introduces in a model. In our case we would have a dark energy EoS with three free parameters, namely w_0, A and B, which become four parameters because of the presence of Ω_m in the expression for the Hubble function and luminosity distance. This poses a well known problem in reconstructing or modeling the EoS with parametric relations: how many parameters can we inquire about? Following the Occam's razor prescription one could be tempted to choose the minimalistic option: models with few parameters are the best ones. But sometimes this could be a *physically* not good choice: complex systems could require complex analytical formulas and a large number of parameters could describe a more suitable behaviour of dark energy. It is also possible that not all the parameters introduced are really free, and there is a correlation/dependence between some of them; but this cannot be known a priori when proposing a new model.

The only solution is to decide depending on the physical problem one has to face with. In preliminary runs we left all the parameters free, but it soon emerged that there is a strong degeneracy between some of them, mainly between A and B. While Ω_m and w_0 were well constrained, the two main parameters of our oscillating models showed a degeneracy which made them eventually unconstrained, and yielded no satisfactory information about our proposed EoS.

So we turned to another way to proceed: we fixed the value of B to a set of discrete values scanning entirely the range of values which could potentially lead to detectable oscillations of our observable functions given the criteria discussed above.

3.4 Results

Tables 3.1, 3.2 and 3.3 summarize our results. As ours is a more exhaustive analysis than previous ones in the literature, it is clear that we can draw stronger conclusions. The main one is that current data do not seem to give as strong constraints on A as on the other parameters Ω_m and w_0, but a clear trend in A can be guessed, which becomes quite evident in Fig. 3.3(a). A fit of A as a function of B using a linear relation turns out to be the best one for the sine model; whereas, for the Bessel and Struve function a quadratic relation is preferred.

If we pay attention to the behaviour of w_0, which is the present value of the EoS, we see that it is very well constrained. There is a slight difference between the sine and the Bessel or Struve cases, but in all cases we can exclude phantom like behaviour at 1σ level; the prior does not in principle hinder it as it is rather weak. In Fig. 3.3(b), we can see that the behaviour for w_0 as a function of B agrees with the tendency of the amplitude A: as B grows the value of A becomes more negative so w_0 moves to less negative values, see Eq. (3.3) and Eq. (3.1). If we explore by means of fits how w and B are related, we find the same pattern as for A, the linear fit is preferred for the EoS with a sine form, and the

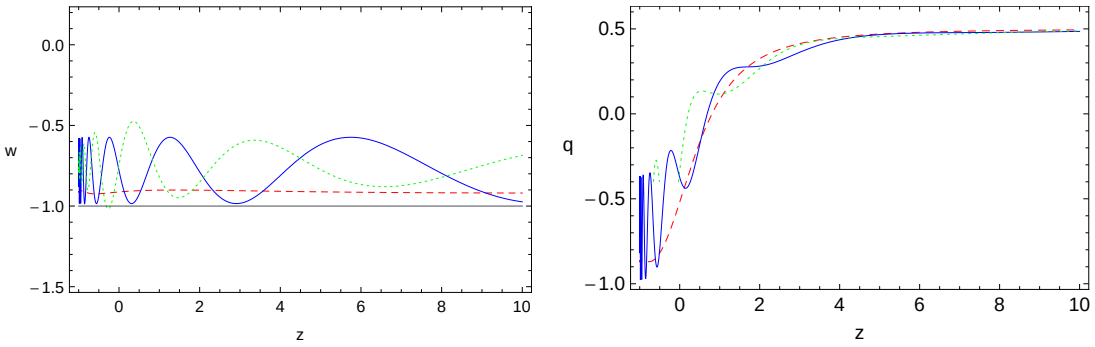

(a) Variation of EoS with the redshift, $w(z)$.

(b) Variation acceleration parameter with the redshift, $q(z)$.

Figure 3.2: *In these figures we plot the redshift-variation of the EoS and the acceleration for the best values of the parametrizations. The colors have the same meaning of Figs. 3.3.*

B	χ^2_{red}	z_{min}	Ω_m	A	w_0
$\frac{\pi}{2}$	1.0787	53.59	$0.25^{+0.02}_{-0.02}$	$0.23^{+0.37}_{-0.53}$	$-0.95^{+0.13}_{-0.12}$
$\frac{2\pi}{3}$	1.0797	19.09	$0.25^{+0.02}_{-0.02}$	$0.04^{+0.38}_{-0.37}$	$-0.91^{+0.12}_{-0.13}$
$\frac{5\pi}{6}$	1.0796	10.02	$0.25^{+0.02}_{-0.02}$	$0.10^{+0.30}_{-0.35}$	$-0.93^{+0.13}_{-0.14}$
π	1.0799	6.39	$0.25^{+0.02}_{-0.02}$	$0.07^{+0.34}_{-0.38}$	$-0.93^{+0.17}_{-0.17}$
$\frac{7\pi}{6}$	1.0803	4.55	$0.26^{+0.02}_{-0.02}$	$-0.08^{+0.34}_{-0.41}$	$-0.86^{+0.21}_{-0.16}$
$\frac{4\pi}{3}$	1.0802	3.48	$0.25^{+0.02}_{-0.02}$	$-0.14^{+0.36}_{-0.35}$	$-0.84^{+0.22}_{-0.19}$
$\frac{3\pi}{2}$	1.0794	2.79	$0.25^{+0.02}_{-0.02}$	$-0.18^{+0.30}_{-0.34}$	$-0.80^{+0.21}_{-0.17}$
$\frac{5\pi}{3}$	1.0788	2.32	$0.25^{+0.02}_{-0.02}$	$-0.21^{+0.30}_{-0.27}$	$-0.78^{+0.17}_{-0.20}$
$\frac{11\pi}{6}$	1.0783	1.98	$0.25^{+0.02}_{-0.02}$	$-0.21^{+0.26}_{-0.22}$	$-0.78^{+0.14}_{-0.19}$

Table 3.1: *Averaged EoS:* $\overline{w}(a) = w_0 + \frac{A}{B}\frac{\cos(B\ln a)-1}{\ln(a)}$.

B	χ^2_{red}	z_{min}	Ω_m	A	w_0
$\frac{\pi}{2}$	1.0806	53.39	$0.25^{+0.02}_{-0.02}$	$-0.11^{+1.00}_{-.93}$	$-0.89^{+0.13}_{-0.14}$
$\frac{2\pi}{3}$	1.0801	19.09	$0.25^{+0.02}_{-0.02}$	$-0.02^{+0.82}_{-0.81}$	$-0.91^{+0.14}_{-0.13}$
$\frac{5\pi}{6}$	1.0801	10.02	$0.26^{+0.02}_{-0.02}$	$-0.00^{+0.60}_{-0.60}$	$-0.90^{+0.12}_{-0.13}$
π	1.0818	6.39	$0.26^{+0.02}_{-0.02}$	$-0.20^{+0.63}_{-0.65}$	$-0.86^{+0.15}_{-0.14}$
$\frac{7\pi}{6}$	1.0809	4.55	$0.25^{+0.02}_{-0.02}$	$-0.19^{+0.67}_{-0.55}$	$-0.86^{+0.15}_{-0.17}$
$\frac{4\pi}{3}$	1.0807	3.48	$0.26^{+0.02}_{-0.02}$	$-0.20^{+0.59}_{-0.67}$	$-0.85^{+0.18}_{-0.17}$
$\frac{3\pi}{2}$	1.0816	2.79	$0.26^{+0.02}_{-0.02}$	$-0.55^{+0.70}_{-0.66}$	$-0.73^{+0.21}_{-0.22}$
$\frac{5\pi}{3}$	1.0808	2.32	$0.26^{+0.02}_{-0.02}$	$-0.58^{+0.66}_{-0.62}$	$-0.71^{+0.20}_{-0.23}$
$\frac{11\pi}{6}$	1.0807	1.98	$0.25^{+0.02}_{-0.02}$	$-0.75^{+0.63}_{-0.56}$	$-0.65^{+0.19}_{-0.23}$

Table 3.2: *Averaged EoS:* $\overline{w}(a) = w_0 + \frac{A}{B}\frac{J_0(B\ln a)-1}{\ln(a)}$.

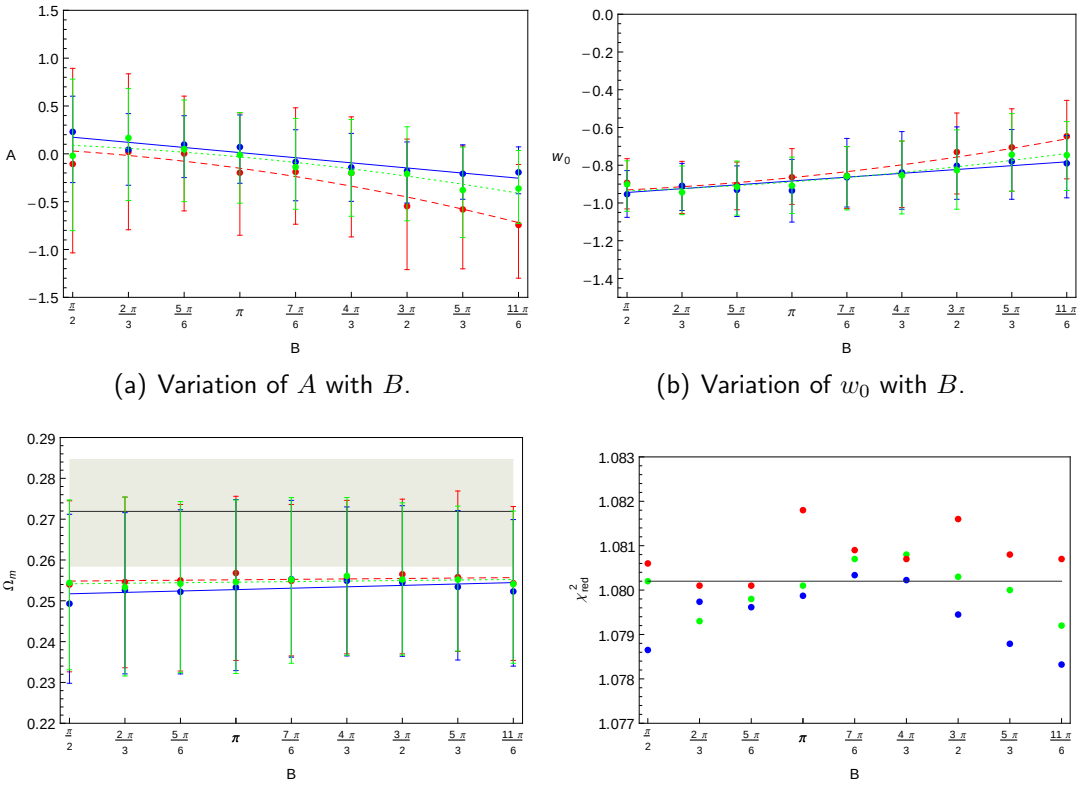

(a) Variation of A with B.

(b) Variation of w_0 with B.

(c) Variation of Ω_m with B.

(d) Variation of χ_{best} with B.

Figure 3.3: *In these figures we plot the free parameters Ω_m, A, w_0 and the reduced χ^2 value versus the fixed B value for the different models. The blue points refer to the sine model Eq. (3.1); the red ones to the Bessel model Eq. (3.3), and the green ones to the Struve model Eq.(3.8). The gray line in Fig. 3.3(c) and Fig. 3.3(d) corresponds to ΛCDM values. In Fig. 3.3(c) the gray region indicates the values of Ω_m within 1σ error that describe ΛCDM.*

B	$\chi^2_{\rm red}$	$z_{\rm min}$	$\Omega_{\rm m}$	A	w_0
$\frac{\pi}{2}$	1.0802	53.39	$0.25^{+0.02}_{-0.02}$	$-0.02^{+0.80}_{-0.78}$	$-0.90^{+0.12}_{-0.14}$
$\frac{2\pi}{3}$	1.0793	19.09	$0.25^{+0.02}_{-0.02}$	$0.17^{+0.52}_{-0.65}$	$-0.94^{+0.14}_{-0.12}$
$\frac{5\pi}{6}$	1.0798	10.02	$0.25^{+0.02}_{-0.02}$	$0.05^{+0.51}_{-0.55}$	$-0.91^{+0.14}_{-0.15}$
π	1.0801	6.39	$0.25^{+0.02}_{-0.02}$	$0.01^{+0.44}_{-0.50}$	$-0.91^{+0.15}_{-0.15}$
$\frac{7\pi}{6}$	1.0807	4.55	$0.26^{+0.02}_{-0.02}$	$-0.14^{+0.51}_{-0.44}$	$-0.86^{+0.16}_{-0.18}$
$\frac{4\pi}{3}$	1.0808	3.48	$0.26^{+0.02}_{-0.02}$	$-0.20^{+0.56}_{-0.45}$	$-0.84^{+0.18}_{-0.20}$
$\frac{3\pi}{2}$	1.0803	2.79	$0.26^{+0.02}_{-0.02}$	$-0.21^{+0.49}_{-0.49}$	$-0.83^{+0.21}_{-0.21}$
$\frac{5\pi}{3}$	1.0800	2.32	$0.26^{+0.02}_{-0.02}$	$-0.38^{+0.45}_{-0.50}$	$-0.74^{+0.22}_{-0.19}$
$\frac{11\pi}{6}$	1.0792	1.98	$0.25^{+0.02}_{-0.02}$	$-0.36^{+0.39}_{-0.36}$	$-0.75^{+0.18}_{-0.19}$

Table 3.3: *Averaged EoS:* $\overline{w}(a) = w_0 + \frac{A}{B}\frac{(\pi/2)H_{-1}(B\ln a)-1}{\ln(a)}$.

quadratic one for the EoS with the Bessel or Struve function.

The remaining parameter, Ω_m, is very well constrained and fully agrees with the expected values in the literature, being $\Omega_m \simeq 0.25$ and this value changes negligibly with B, see Fig. 3.3(c).

So, with the current data it seems that B cannot be really constrained, that is, all B values seem to be of similar statistical validity. We have a very slight preference for values which are different from those chosen by other authors. Generally, the chosen value is $B = 3\pi/2$ as corresponds to the typical supernovae redshift range. In our analysis the lowest value of for χ^2 does not correspond to that value of B; for the sine and Struve models the minimum is for $B = 11\pi/6$ which means that we can detect oscillations within a redshift $z \sim 1.98$, comprised by our data. For the Bessel oscillating model we have a χ^2 minimum value at $B = 2\pi/3$ which will need a redshift $z \sim 19.09$, which is outside of our observational data range. Fig. 3.2 reflects clearly these behaviours: the best values, from the statistical point of view, for the sine and Struve models allow us to detect a complete oscillation in the range of our observational data.

Nevertheless, focusing our attention on Fig. 3.3(d), we can see that for almost all the values of the frequency, B, the values of χ^2 of the sine parametrization are smaller than those of others parametrizations. If we take this into account together with the fact that the best value of this parametrization corresponds to a $B = 11\pi/6$, we could say that observational data show a preference for a periodic EoS with a small period.

At the same time, if we look at the variation of the acceleration parameter Fig. 3.2(b) in the recent past we can observe that it has recently peaked and is slowing down at present as have been pointed in [244].

Moving to the statistical side of the analysis, we have to argue if the proposed models are reasonably good or not, and above all if they can compete with the the concordance ΛCDM model. From our results we conclude an oscillating pattern in dark energy is an admissible *possibility*, as there is so far no concluding evidence against it; and from some statistical perspectives they even represent a better option that its main competitor, ΛCDM. Tables 3.4 summarizes our findings on the statistical side.

If we take a look at the reduced chi-square values, we can see that all the models have lower values than the ΛCDM one, even if the differences are really small. In particular, the

Model	$\boldsymbol{\chi^2}$	$\boldsymbol{\chi^2_{red}}$	ΔAIC$_c$	ΔBIC	ΔRIC$_c$	ΔDIC$_c$
ΛCDM	507.7003	1.0802	0	0	0	0
Sine	504.6550	1.0783	0.9975	9.2687	−1.0282	1.9145
Bessel	505.4669	1.0801	1.8094	10.0806	−0.2163	2.0344
Struve	505.0848	1.0792	1.4273	9.6985	−0.5984	2.0023

Table 3.4: *Statistical criteria*

sine model seems the best one. If we take a look to the AIC$_c$ values, we see that the sine model is just in a border line position if we consider the limit we discussed in Section 1.7.6, i.e. $\Delta\text{AIC} \gtrsim 1$. On the contrary, we should absolutely reject the Bessel and Struve models. But the situation changes when considering RIC$_c$: we know that it has a small penalty than AIC$_c$ when $N >> k$ as it is in our case, where we have $N = 472$ and $k = 3$. And we see that its values favour the oscillating models with respect of ΛCDM; they are even negative, meaning that the RIC$_c$ of oscillating parametrizations are better.

The situation reverses again when moving to BIC; if we compare the values obtained with the Jeffreys' scale, we should conclude that there is an *almost decisive* evidence against oscillating patterns. But we have to remember that BIC has some problem when facing degeneracies between parameters, like the behaviours of the amplitude and of w_0 seem to reflect.

These degeneracies would well be the reason of the "bad results" offered by BIC, which is also challenged by another criterion, DIC, which looks more favourable with oscillating dark energy. Since DIC relies also on the Bayesian approach, we can apply Jeffreys' scale to it in the same fashion as above, and from this we conclude there is not a significant evidence against oscillations.

3.5 Conclusions

In this work we have performed a quite detailed analysis towards the detection of oscillating patterns in the dark energy EoS. We have considered different phenomenological models, starting from the original sine models and then introducing two new ones, based on the special functions. Those new models differ from the sine one mainly because they show a damped amplitude in the oscillations when moving into the past.

Compared to prior works devoted to oscillating dark energy we can highlight that fact that instead of fixing the frequency parameter to a particular value, we have explored a discrete set of frequency values.

We have also introduced some novelty with respect to the datasets used, as we take direct measurements of the Hubble factor and GRB luminosity data, which are arguably two directions of improvement, as the sensitivity to oscillating patterns gets increased and a wider redshift range comes into play. Our theoretical setup has been complemented with a detailed statistical analysis using different model selection tools.

Numerical results show that while parameters like the matter content, Ω_m, and the present value of dark energy EoS, w_0, can be constrained very well, this is not true for the amplitude

and the frequency. In particular, between the amplitude A and w_0 a degeneracy that cannot be solved seems to be working. About the frequency, we can say that χ^2 values are not really in favour of a particular value, being all in a very narrow range. But the best values favour values of the frequency which mean detectable oscillations inside the present redshift range of SNeIa.

The statistical analysis does not seem to provide such a conclusive answer as desirable, though we think that oscillations can be considered as a possible alternative to a ΛCDM model for addressing the well know problems it suffers from. All but one (BIC) of the statistical criteria used considered here are keen to the possible detection of oscillations in the EoS, there is even one of them (RIC) which seems to favour an oscillating pattern against a cosmological constant.

CHAPTER 4

SNEIA AND BAO CONSTRAINTS ON (NEW) POLYNOMIAL DARK ENERGY PARAMETRIZATIONS: CURRENT RESULTS AND FORECASTS

More than a decade ago it was discovered that the Universe is expanding with increasing velocity, and this fact was brought to light by SNeIa observations [16, 210, 220, 221]. We have seen that this accelerated expansion, which today is confirmed by many other independent observations, can be explained postulating the existence of a "new" component in the Universe, the so called "dark energy", which represents the major fraction of the energy/masa content of the Universe, and would counteract the effects of the gravitational attraction produced by ordinary contents. In this context, although the simplest model, ΛCDM, agrees rather well with observational data, there are still some points it cannot describe. Thus, this situation has motivated the appearance of other models with a slightly time-variable dark energy as the agent producing the cosmic acceleration. Many of them have emerged along theoretical approaches as quintessence, Chaplygin gas, etc. However, as we have seen in the previous chapter, another natural way to address this situation is to study an effective parametrization of the dark energy equation of state. In Chapter 3, we have proposed an oscillating equation of state, but we have seen this kind of parametrizations are not strongly favoured by observational data to became a firm alternative to a ΛCDM model. This allows considering alternatives, here we propose two new polynomial parametrizations of dark energy and we will argue their interest later. As before, we will perform cosmological tests to compare them to the most popular dark energy parametrization in the literature, both in its classical fashion and a new, improved reformulation. But in this case we resort to several criteria to perform our comparison: in addition to the χ^2 value, we also pay attention to the correlation of the coefficients, figure of merit, fractional errors on the free dark energy parameters and the deviance information

criterion (DIC). The reason for an analysis from several perspectives is that we find χ^2 to be an insufficiently informative tool, as it does not offer any reward upon some important improvements like tighter constraints or lower correlation.

Our tests make use of SNeIa and BAO, which are so far the best representatives in the categories of standard candles and standard rulers. Such probes provide us with distance measures related to the Hubble factor $H(z)$, and as they are low redshift datasets, their suitability for constraining dark energy is strong, as this component of the cosmic soup has began to govern the evolution of the Universe just recently, according to most evidences. This combination has additional advantages: SNeIa measurements come in the form of luminosity distances and therefore give a smeared out information on $H(z)$ (two integrations are required) but still remain extremely useful because of the large number of measurements and their considerably good quality. On the other hand, BAO measurements, though currently scarce, involve $1/H(z)$ directly, so they are expected to favour sensitivity considerably, besides being of even better quality than SNeIa data. In principle, one could also consider including CMB data, but typically they do not improve constraints on dark energy parameters significantly (WMAP7-year data alone constrain w in quiessence models with about a 40% error [147]), and the dark matter density Ω_m is generally the only parameter on which those data exert a strong impact. A good compromise between simplicity and advantages offered by CMB as regards Ω_m is the use of priors, and that is the approach we use.

Interestingly, we will not only use the latest observational data to obtain the constraints on the parameters of the models, but we will also consider mock data simulating a forthcoming survey. We present mock datasets for the two main measurable quantities expected from a line-of-sight, high-resolution spectroscopic baryon acoustic oscillations survey [32, 205, 218][1].

We combine these data with synthetic pre-WFIRST (Wide-Field Infrared Survey Telescope) supernovae data to throw further light on the constraining power and suitability of the parametrizations proposed, so we are allowed to strengthen our conclusions.

4.1 Dark energy parametrizations

The Friedman equations (1.12) and (1.11) explain how an homogeneous and isotropic universe expands in the context of General Relativity (or generalizations). It is well proved that at present, the two main fluids which fill the Universe are dark matter and dark energy, the last being the governor. Dark energy can enter our picture in an effective way represented by a phenomenological equation of state (EoS), $w(z) = \rho_{de}/p_{de}$, which determines the Hubble parameter $H(z)$, given by Eq. (1.51) which is written in terms of the dark energy density function as described by Eq. (1.52), which is the exponential of an averaged EoS.

Considering the huge number of contributions to the topic, and the knowledge so far gathered, it might seem hard to make improvements, but we believe some avenues opened by Y. Wang in [286] are worth exploring and allow for modest, yet valuable, advances towards parametrizations that make the best out of the data available. Questions like the most convenient choice of the two dark energy parameters or the most suitable model comparison criterion are worth being looked at once and again, particularly to build a more

[1] http://sci.esa.int/euclid

solid background to make the most out of future data and their expected far better statistical value.

The quest to delineate the expansion history of the Universe is expected to make big ambitious moves in the future. As a result it is expected that many more and better observational data will be available. Obviously it is worth getting prepared to making the best profit out of this avalanche of data to come, and this can be done by learning as much as possible from the data we already have. With the aim of obtaining from observational data the most exact information about dark energy, we do not only have to be able to recognize witch model fits better with reality, but also to provide the most accurate interpretation of the results. In that direction, it is extremely important to choose previously a dark energy parametrization with clear rewards: model parameters with a clear physical meaning and low correlation between them, which at the same time have to show their capability to be tightly constrained. Suitability criteria for parameters along those grounds can be sketched with the help of comparison tools rewarding for those nice features. The (frequentist) FoM favours low correlation, whereas the (Bayesian) DIC does not only favour that feature, but it also rewards for tight constraints also, so both these criteria (FoM and DIC) do poorly when high correlation is present in the dark energy parametrization one considers. In this respect, one must make a fair use of those statistical tools. For instance, if one performs a reparametrization of a certain scenario, the FoM and DIC as calculated for both cases will typically be direct indicators of improvements (or worsenings) in terms of correlation, but changes in the value of those quantities should not be held in the same grounds as the changes occurring when constraining the same single parametrization with two different datasets.

Although the CPL parametrization, Eq. (1.53) is widely used, its parameters $\{w_0, w_a\}$ suffer from quite a significant correlation, besides the fact that constraints on w_a are typically large in percentual terms. However, as it presents nice features, a convenient redefinition as concerns those two issues was put forward to yield an improved situation, although the encoded information remains exactly the same. As mentioned, this was done in [286], where a new dark energy description was given in terms of its value at present, w_0, and at redshift $z = 0.5$, $w_{0.5}$. Explicitly, Eq. (1.62) was proposed, and it represents a rearrangement of the classic CPL parametrization with a lower correlation between the parameters. Thus, it allows us to obtain tight constrains on parameters with a clear interpretation, just in the spirit of making an optimal use of observational data from future surveys.

The results of this work reinforce the view that Eq. (1.62) is a preferred way of exploiting the CPL parametrization, and on the other hand we suggest, with the help of two new parametrizations, that the $w_0, w_{0.5}$ couple is indeed a very good choice despite the specifics of the dark energy evolution, provided it is smooth enough and with bounded early asymptotic behaviour.

4.1.1 Polynomial parametrizations

The two proposals we are making are somewhat inspired on the one hand by the CPL parametrization, and on the other hand by an a proposal consisting in a expansion in powers of the quantity $(1 + z)$ which emerged naturally from the relationship between the redshift

and the scale factor and showed computationally convenience. This second inspiring setup we are referring to was proposed for the first time in [289] in the form

$$w(z) = -1 + c_1(1+z) + c_2(1+z)^2. \tag{4.1}$$

However, this sort of parametrization poses problems at high redshifts, as $|w(z)|$ grows unboundedly with z, and one will either end up with a superphantom model or a superluminal one. This motivates considering generalizations which are devoid of this pathology and may match or event surpass the nicety of CPL or its reformulation (recall Eq. (1.62)).

Two possible routes that retain some similarity with the previous case but also bring some improvements arise from

$$w(z) = -1 + c_1(1+f(z)) + c_2(1+f(z))^2, \tag{4.2}$$

with $f(z)$ a smooth and at the same time simple function, or from

$$w(z) = -1 + c_1\, g_1(1+f(z)) + c_2\, g_2(1+f(z)), \tag{4.3}$$

where g_1 and g_2 are some smooth and simple functions as well.

Conventional polynomial

In the spirit of the first scheme above we propose

$$f(z) = \frac{z}{1+z} \tag{4.4}$$

so we avoid high-redshift unboundedness by the same via as in CPL. Therefore we have

$$w(z) = -1 + c_1\left(1+\frac{z}{1+z}\right) + c_2\left(1+\frac{z}{1+z}\right)^2, \tag{4.5}$$

which we dub conventional polynomial parametrization. If more compactness is desired one can also write the latter as

$$w(z) = -1 + c_1\left(\frac{1+2z}{1+z}\right) + c_2\left(\frac{1+2z}{1+z}\right)^2. \tag{4.6}$$

It is convenient to leave out the constant term of value -1 from the computational point of view because as one does not expect a large departure from a ΛCDM setting, it is reasonable to confine (at least initially) the parameter search region to $|c_1| < 1$ and to $|c_2| < 1$.

However, as we have discussed already, it is desirable to fit parameters which are more or less physically transparent and which in addition are just lightly correlated. At a first stage we wish to compare our conventional polynomial parametrization with Wang's, so the best way to do so is to consider exactly the same two dark energy parameters. Then, at a later stage, we will check whether the good behaviour as correlation is concerned is shared by our parametrization. With those arguments in mind we reformulate the proposal made in

Eq. (4.6) by letting

$$c_1 = \frac{1}{4}(16w_0 - 9w_{0.5} + 7), \tag{4.7}$$

$$c_2 = -3w_0 + \frac{9w_{0.5} - 3}{4}. \tag{4.8}$$

This way, we move on to a scenario in which w_0 and $w_{0.5}$ are the parameters subject to estimation, which can be explicitly reconstructed using Eq. (1.52):

$$X(z) = (1+z)^{\frac{3}{2}(-8w_0+9w_{0.5}+1)} e^{\left(\frac{3z(w_0(52z+40)-9w_{0.5}(5z+4)+7z+4)}{8(1+z)^2}\right)}, \tag{4.9}$$

which consistently comes down to the ΛCDM case for $w_0 = w_{0.5} = -1$.

For completeness and purposes related to model selection, it is convenient to compute and effective w_a parameter for this model. By analogy with the CPL case we define

$$w_a = \lim_{z\to\infty} w(z) - w_0, \tag{4.10}$$

so in this case

$$w_a = -5w_0 + \frac{9}{2}w_{0.5} - \frac{1}{2} \tag{4.11}$$

is the result we get.

Chebychev polynomial parametrization

Now we want to make a further generalisation in the fashion of our general proposal above, by considering a bit more involved functions. In this case we make use of Chebychev polynomials of the first kind, which have a significant role in most areas of numerical analysis, as well as in other areas of Mathematics (polynomial approximation, numerical integration, and pseudo spectral methods for partial differential equation, etc.)

Once again we have to take into account that we cannot constrain accurately more than two dark energy parameters [177], thus we have cut the expansion at the second order. Specifically we propose

$$w(z) = -1 + c_1 T_1(1 + f(z)) + c_2 T_2(1 + f(z)), \tag{4.12}$$

with T_n being the first kind Chebyshev polynomial of degree n and $f(z) = z/(1+z)$ as before. A convenient presentation of that parametrization is

$$w(z) = -1 + c_1\left(\frac{1+2z}{1+z}\right) + c_2\left[2\left(\frac{1+2z}{1+z}\right)^2 - 1\right]. \tag{4.13}$$

In this case too we switch to more amenable parameters and then let

$$c_1 = \frac{1}{11}(23w_0 - 9w_{0.5} + 14) \tag{4.14}$$

$$c_2 = -\frac{3}{11}(4w_0 - 3w_{0.5} + 1). \tag{4.15}$$

Then, one should simply resort to Eq. (1.52) to produce the whole scenario:

$$X(z) = (1+z)^{-\frac{3}{4}(52w_0 - 45w_{0.5} + 7)} e^{\left(\frac{3z(w_0(68z+56) - 9w_{0.5}(6z+5) + 14z + 11)}{4(1+z)^2}\right)}. \tag{4.16}$$

For this first attempt at depicting a dark energy dominated universe in terms of Chebyshev polynomials we choose w_0 and $w_{0.5}$ as our parameters, but it would be not surprising than one could do better if some extra work was done in the direction of making parameter correlation smaller. For the time being we just pursue to compare directly our polynomial proposal with a preferred presentation of the CPL parametrization on the one hand and with our conventional polynomial proposal on the other hand.

In that direction, and as it has been done before, we compute an effective w_a parameter which in this case takes the form

$$w_a = \frac{1}{11}(-49w_0 + 45w_{0.5} - 4). \tag{4.17}$$

Some additional remarks

In the first place, these two new routes can be viewed as perturbations of ΛCDM, particularly, at low redshifts, which is the region most accurately described by the current data. If one wants to perturb ΛCDM in either the CPL or the Wang scenarios w_0 has to be anchored at -1, and then there is only one free parameter to play with. In contrast, our two new models may model two-parametric departures from ΛCDM, and thus have more flexibility in principle.

Note that it would be possible to consider the two new parametrizations along with CPL (Wang) if one let the parameter space have one more dimension. Indeed, if we let our parametrization be of the form

$$w(z) = b_1 + b_2\left(\frac{1+2z}{1+z}\right) + b_3\left(\frac{1+2z}{1+z}\right)^2, \tag{4.18}$$

then our conventional polynomial case would be obtained for $b_1 = -1$, $b_2 = c1$, and $b_3 = c_2$; the Chebyshev case would follow from the choice $b_2 = c_1$, $b_3 = 2c_2$ and $b_1 = -(1 + c_2)$; and finally the CPL case would be obtained from $b_1 = w_0 - w_a$, $b_2 = w_a$ and $b_3 = 0$.

4.2 Pivot computation

Provided $w_{0.5} = w|_{z=0.5}$ for our new parametrizations, let us try to find the value of w_c, the parameter least correlated with w_0. Following the ideas discussed in Sec. 1.4.5 of Chapter

1, we will obtain the values of w_c in terms of w_0 and $w_{0.5}$ for the models proposed.

4.2.1 Chebyshev polynomial

For our Chebyshev polynomial parametrization we have

$$w_c = \frac{1}{11}\left(-6a_c^2(4w_0 - 3w_{0.5} + 1) + a_c(73w_0 - 63w_{0.5} + 10) - 38w_0 + 45w_{0.5} - 4\right). \tag{4.19}$$

Following the same straightforward calculation as for Wang's case we conclude there will be minimal correlation for

$$a_c = \frac{\sqrt{729\sigma(w_0, w_{0.5})^2 - 2142\sigma(w_0, w_{0.5})\sigma(w_0)^2 + 1681\sigma(w_0)^4} + 63\sigma(w_0, w_{0.5}) - 73\sigma(w_0)^2}{12(3\sigma(w_0, w_{0.5}) - 4\sigma(w_0)^2)}, \tag{4.20}$$

which corresponds to $z_c = 0.17, 0.28$ respectively for real and synthetic data. Sticking to our notation here $\sigma(w_0, w_{0.5})$ denotes the non-diagonal element of the covariance matrix of w_0 and $w_{0.5}$. But one can just want to meet the less restrictive requirement $\sigma_{0c} < \sigma_{12}$, which follows provided

$$(3a_c - 2)(6a_c - 17)\sigma_{12} < \left(24a_c^2 - 73a_c + 38\right)\sigma_0^2. \tag{4.21}$$

4.2.2 Conventional polynomial

Finally, following the same steps as before, but this time considering the conventional polynomial parametrization we have

$$w_c = \frac{1}{4}(4(2 - 3a_c)(a_c - 2)w_0 + 9(a_c - 2)(a_c - 1)w_{0.5} + (2 - 3a_c)a_c + 3a_c - 2). \tag{4.22}$$

The same route as for the two previous cases drives us to the conclusion that the minimal correlation situation is achieved for

$$a_c = \frac{9\sigma(w_0, w_{0.5})}{-8\sigma(w_0)^2}9\sigma(w_0, w_{0.5}) - 12\sigma(w_0)^2, \tag{4.23}$$

which corresponds to $z_c = 0.18, 0.29$ respectively for real and synthetic data. Here the meaning of σ_{12} is exactly the same as in the case before. Finally, one can deduce the condition for the less restrictive requirement $\sigma_{0c} < \sigma_{12}$ to happen is simply

$$\frac{1}{4}(7 - 3a_c)(2 - 3a_c)\sigma_{12} < (2 - 3a_c)(2 - a_c)\sigma_0^2. \tag{4.24}$$

4.3 Observational data

As dark energy is expected to have started to dominate at recent times, low redshift datasets are the obvious choice to put the tightest constraints on each dynamics, whereas high

redshift ones may be viewed as complementary. Thus, the combination of SNeIa and BAO datasets, given their quality in both cases, and the considerable number of data points in the case of the SNeIa, is an excellent choice given the state of the art. Besides, new avenues on BAO [23] are to be open soon which will allow to exploit the tremendous potential of this new astronomical tool towards constraining the main evolutionary features of dark energy. As we have already mentioned, one of our objectives is to introduce new promising parametrizations as alternatives to one of the commonest, but one of the other objectives is to forecast how the old parametrizations and our challengers will cope with new data.

The literature provides a large number of papers where simulated supernovae data are used in the way we have just mentioned, but to our knowledge synthetic baryon acoustic oscillations data have only been presented and exploited in [96]. This builds on considerable theoretical efforts in different forecast aspects [46], which have crystallized in the package Initiative for Cosmology (iCosmo)[2] [217] and its BAO modules, which have allowed us to produce these mock data. We have modified and extended this general purpose software to produce mock data from a line of sight, high-precision BAO spectroscopic survey as the one described in [205][3] and pre-WFIRST supernovae data.

4.3.1 Baryon Acoustic Oscillations

Measurements of the cosmic distance-redshift relation have always constituted one of the most important quantities to probe cosmology of the Universe. In that direction, and as it has been detailed in Sec. 1.6.4, some years ago another way to map the distance-redshift relation appeared. It was based on the measurement of BAOs in the large-scale clustering pattern of galaxies and it is a promising a cosmological standard ruler. One of its characteristics is that it enables precise measurements of the dark energy parameters.

In this work we will make us of two different data sets: one with the latest real data given by [209] and as a first time, a mock sample with represents the forecast of the future BAO survey, EUCLID. In what follows we will give details about these samples.

Percival et al.

In [209] Gaussian values on the distance ratio, $r_s(z_{\rm drag})/D_V(z)$, at redshifts $z = 0.2$ and $z = 0.35$, are given from the measurements obtained by combining the spectroscopic Sloan Digital Sky Survey (SDSS) and the Two-Degree Field Galaxy Redshift Survey (2DFGRS) data. This distance ratio represents the comoving sound horizon at the baryon dragging epoch, $z_{\rm drag}$, over the effective distance $D_V(z)$, see Eqs. (1.128) and (1.127).

In order to estimate the dark energy parameters in the context of Bayesian statistics, as detailed in Section 1.7, we need a definition of the χ^2 which reflects the difference between the observational data and the values given by our models. In our case, this requires giving an expression for the comoving sound horizon at the baryon dragging epoch, and we have used the fitting formula proposed in [88], Eq. (1.129).

[2] http://www.icosmo.org/
[3] http://sci.esa.int/euclid

$\mathbf{z}$	$\mathbf{y}$	$\mathbf{y'}$
0.6	15.005 ± 0.117	21.401 ± 0.291
0.8	19.221 ± 0.109	18.953 ± 0.186
1.0	22.708 ± 0.102	17.012 ± 0.137
1.2	25.762 ± 0.098	15.098 ± 0.101
1.4	28.635 ± 0.096	13.421 ± 0.079
1.6	31.126 ± 0.101	12.213 ± 0.069
1.8	33.540 ± 0.107	10.987 ± 0.061
2.0	35.357 ± 0.112	10.094 ± 0.055

Table 4.1: *Mock BAO data from EUCLID*

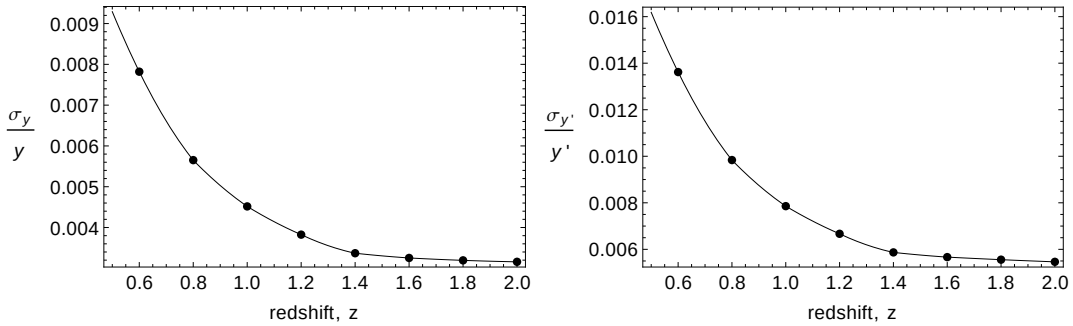

Figure 4.1: *Fractional errors on synthetic BAO data for y (a) and y' (b).*

Now, taking into account the Gaussian values at $z = 0.2$ and 0.35 from the BAO data in [209], we can calculate

$$\chi^2_{\rm BAO} = (v_i - v_i^{\rm BAO})(\mathbf{C}^{-1})_{ij}^{\rm BAO}(v_j - v_j^{\rm BAO}) \tag{4.25}$$

where

$$\mathbf{v} = \left\{ \frac{r_s(z_{\rm drag}, \Omega_m, \Omega_b; \boldsymbol{\theta})}{D_V(0.2, \Omega_m; \boldsymbol{\theta})}, \frac{r_s(z_{\rm drag}, \Omega_m, \Omega_b; \boldsymbol{\theta})}{D_V(0.35, \Omega_m; \boldsymbol{\theta})} \right\}, \tag{4.26}$$

$$\mathbf{v}^{\rm BAO} = (0.1905, 0.1097) \tag{4.27}$$

and

$$\mathbf{C}^{-1} = \begin{pmatrix} 30124 & -17227 \\ -17227 & 86977 \end{pmatrix}, \tag{4.28}$$

being the inverse of the covariance matrix.

High precision spectroscopic redshift surveys

Future BAO surveys are expected to represent a real breakthrough in our knowledge of dark energy. In [205] is proposed a survey to measure spectroscopic redshifts for 6.1×10^7 luminous galaxies and clusters of galaxies out to redshift $z = 2$ over 20000 deg^2, reaching a $dz/(1+z) < 0.001$, enough to resolve the BAO feature along the line of sight, and achieving much better dark energy constraints than their predecessors.

We have used the Initiative for Cosmology (iCosmo) software package to generate the BAO mock data. In this case we are concerned with the following two signatures of the BAO peak:

$$y(z) = \frac{r(z)}{r_s(z_{\rm rec})}, \tag{4.29}$$

$$y'(z) = \frac{r'(z)}{r_s(z_{\rm rec})} = \frac{c/H(z)}{r_s(z_{\rm rec})}. \tag{4.30}$$

The publicly available code has built-in routines based on the universal BAO fitting formulae for the diagonal errors on y and y' presented in [46]. Once we have made the proper modifications of the code to replace the defaults (Peacock and Dodds [201] power spectrum and Smail et al. [252] galaxy distribution) with the survey properties (those quoted above and besides $z_{med} \sim 0.46$, redshift range $0.1 < z < 0.9$), we have written extra codes to generate a large number of normal random realizations around a fiducial model which is specifically the wcdm+sz+lens case from WMAP7-year [147], which has $\Omega_m = 0.26 \pm 0.099$ and is phantom-like with $w = -1.12 \pm 0.43$., Then, after some reduction, the synthetic BAO data presented in Table 4.1 have been obtained. In addition, in the corresponding χ^2 we have introduced priors based on the values of the matter and baryon density presented in [49] as a forecast analysis of Planck: using the result $\Omega_m h^2 = 0.1308 \pm 0.0008$ we construct a weak Gaussian prior, whereas with $\Omega_b h^2 = 0.0223$ we construct a fixed prior. In both cases we use $h = 0.742$ as is given by [223]. See as well Fig. 4.1 for a graphical account of the features of our BAO simulated data.

In this case we need an expression for the sound horizon at recombination to constrain the dark energy parameters:

$$r_s(a_r) = \frac{c}{\sqrt{3} H_0 \Omega_m^{1/2}} \int_0^{a_r} \frac{{\rm d}a}{(a + a_{eq})^{1/2}} \frac{1}{(1+R)^{1/2}}\ , \tag{4.31}$$

which can be evaluated as described by Eq. (1.121). The redshift of recombination $z_{\rm rec}$ is given by [124] in the following fitting formula given by Eq. (1.117). Thus, the χ^2 function for BAO mock data is now defined as

$$\chi^2_{\rm BAO}(\boldsymbol{\theta}) = \frac{1}{1-\rho^2_{y,y'}} \left[\sum_{j=1}^{N_{mock}} \frac{(y(z_j,\Omega_m,\Omega_b;\boldsymbol{\theta}) - y_{mock}(z_j))^2}{\sigma^2_{y,j}} + \sum_{j=1}^{N_{mock}} \frac{(y'(z_j,\Omega_m,\Omega_b;\boldsymbol{\theta}) - y'_{mock}(z_j))^2}{\sigma^2_{y',j}} \right.$$
$$\left. - 2\,\rho_{y,y'} \sum_{j=1}^{N_{mock}} \frac{(y(z_j,\Omega_m,\Omega_b;\boldsymbol{\theta}) - y_{mock}(z_j))(y'(z_j,\Omega_m,\Omega_b;\boldsymbol{\theta}) - y'_{mock}(z_j))}{\sigma_{y,j}\sigma_{y',j}} \right], \tag{4.32}$$

where N_{mock} is the number of mock data, in this case 4, and $\boldsymbol{\theta} = \theta_1, \theta_2, ...$ are the dark energy model parameters. Here we have conveniently accounted for the slight degree of correlation existing between y and y', and as suggested in [242], we will fix for our calculations $\rho_{y,y'} = 0.4$.

4.3.2 Type Ia Supernovae

Type Ia supernovae are the explosions that take place at late stages of the stellar evolution. They have been recognized as a powerful probe of cosmological dynamics, as they give a good measure of the cosmological expansion rate. Supernovae provided the first probe for the cosmological expansion [210, 220] and are considered standard candles [159].

The statistical analysis of such SNeIa samples has been carefully detailed in Section 1.6.1, please refer to this section to see the complete procedure we have followed.

Union2

Union2 [10] is one of the largest Type Ia Supernovae samples up to date, and it consists of 557 SNeIa and covers a redshift range from 0 to 1.4. This sample has increased the number of well-measured Type Ia supernovae of the previous Union [148] at high redshifts by the combination of different data sets. The Union Sample has been extended with six Type Ia supernovae presented in [10], the SNeIa from [11], the low-z and intermediate-z data from [117] and [121] respectively.

This sample has been obtained after some improvements in the Union analysis chain: all light curves have been fitted using a single light curve fitter (SALT2) to eliminate differences and systematic errors have been directly computed using the effect they have on the distance modulus.

Mock data for a pre-WFIRST stage

To create SNeIa mock samples we have reproduced the pre-WFIRST observational situation as reported in [8], which has two population peaks, one at $z < 0.1$ and the other at $0.6 < z < 0.7$; along with a very scarce population at $z > 1.6$. Specifically, the redshift distribution suggested in [8] is reproduced here in Table 4.2.

The formulae for errors on SNeIa magnitudes that we use follows from a prescription used in the binning approach [128, 144, 278], in which they are calculated as follows:

$$\sigma_m^{eff} = \sqrt{\sigma_{int}^2 + \sigma_{pec}^2 + \sigma_{syst}^2}\,, \tag{4.33}$$

where:

- $\sigma_{int} = 0.15$ is the intrinsic dispersion in magnitude per SNeIa, assumed to be constant and independent of redshift for all well-designed surveys;
- $\sigma_{pec} = 5\sigma_v/(\ln(10)cz)$ is the error due to the uncertainty in the SNeIa peculiar velocity, with $\sigma_v = 500$ km/s, c is the velocity of light and z is the redshift for any SNeIa;

redshift bin	# of SNeIa
< 0.1	500
$0.1 - 0.2$	200
$0.2 - 0.3$	320
$0.3 - 0.4$	445
$0.4 - 0.5$	580
$0.5 - 0.6$	660
$0.6 - 0.7$	700
$0.7 - 0.8$	670
$0.8 - 0.9$	110
$0.9 - 1.0$	80
$1.0 - 1.1$	25
$1.1 - 1.2$	16
$1.2 - 1.3$	16
$1.3 - 1.4$	4
$1.4 - 1.5$	4
$1.5 - 1.6$	4
> 1.6	4

Table 4.2: *Redshift distribution of pre-Wfirst SNeIa samples*

- $\sigma_{syst} = 0.02(z/z_{max})$ is the floor uncertainty related to all the irreducible systematic errors with cannot be reduced statistically by increasing the number of observations. The value 0.02 is conservative from the perspective of what space-based missions could achieve. Those are precisely the resources expected to provide high-redshift SNeIa, which are in turn the ones in which the systematic error term is expected to contribute. Note as well that z_{max} is the maximum observable redshift in the considered mission and this linear term in redshift is used to account for the dependence with redshift of many of the possible systematic error sources (for example the Malmquist bias or gravitational lensing effects).

We have included some extra, though very slight, noise, and then we have checked that our mock data are compliant with the main features of the Union2 sample. The fiducial model used is again the wcdm+sz+lens case from WMAP7-year as quoted above, which has $\Omega_m = 0.26 \pm 0.099$ and is phantom-like with $w = -1.12 \pm 0.43$. The χ^2 function for the SNeIa mock data has been constructed as described in Sec. (1.6.1). Then we have let *iCosmo* generate the d_L values for the redshifts in the table a large number of universes drawn randomly and normally distributed around the fiducial one, and finally we have performed a reduction to give our mock sample.

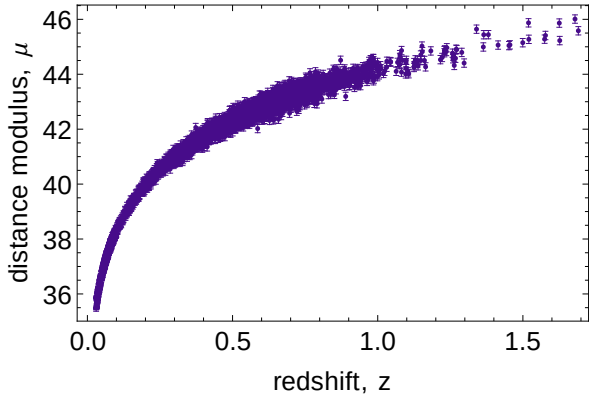

Figure 4.2: *Mock data obtained with iCosmo for the pre-WFIRST specifications.*

4.4 Results

Following Bayesian Statistics, we have inferred the values Ω_m and the dark energy parameters for the models considered using the Grid Method and the Levenberg-Marquadt algorithm for the minimization of the total χ^2. For further details see Sec. 1.7.4. We report our findings in two main ways: on the one hand we present our best fits, errors and derived quantities in Tables 4.3, 4.4; on the other hand we present credible contours obtained after a numerical marginalization over Ω_m, where we have approximated the likelihood as a Gaussian and then have marginalized analytically,

$$\widehat{\chi^2} = -2\log\left(\int_0^1 \exp(-\chi^2/2)d\Omega_m\right), \tag{4.34}$$

see [273] and references therein. The limits in the integral are dictated by the physical range of Ω_m. As mentioned, we have considered the combination of real and mock SNeIa and BAO data as discussed above, and in addition we have introduced in all cases a Gaussian prior on Ω_m and Ω_b deduced in [49] as a forecast analysis of Planck: $\Omega_m h^2 = 0.1308 \pm 0.0008$, $\Omega_b = 0.0223$ with $h = 0.742$ as is given by [223].

The presence of the prior leads to uniformity in the best fit value of Ω_m thus minorating its influence in the dark energy constraints. This trick, together with the marginalization, allows to focus the discussion on the dark energy parameters, thus offering a clearer picture of what each parametrization can offer.

Let us now examine our results using different criteria. First of all, uncertainties in percentage terms on the dark energy parameters can be considered. The conventional polynomial turns out to give the lowest percentage error on w_0 for both current and recent data, and the second best is the Chebyshev setting, although we only get a marginal difference with respect to the conventional polynomial and Wang's model. The situation gets reversed, though, for the percentage error on $w_{0.5}$, and Wang's parametrization is the best performer, but again differences are small when compared to our parametrizations (CPL gets excluded from this discussion item, as the parameter $w_{0.5}$ is not considered).

Model	χ^2_{min}	Ω_m	Dark energy parameters	$\mathrm{FoM}_{\mathrm{Wang}}$ $(\mathrm{FoM}_{\mathrm{DETF}})$	$\rho_{1,2}$	DIC
CPL	544.91	0.315 ± 0.033	$w_0 = -1.033 \pm 0.180$ $w_a = -0.742 \pm 1.520$	14.16 (14.16)	-0.930	10.30
Wang	544.91	0.315 ± 0.033	$w_0 = -1.033 \pm 0.180$ $w_{0.5} = -1.281 \pm 0.361$	42.47 (14.16)	-0.792	8.11
Chebychev P.	544.96	0.314 ± 0.032	$w_0 = -1.049 \pm 0.163$ $w_{0.5} = -1.268 \pm 0.373$	43.63 (11.67)	-0.785	8.02
Conventional P.	544.98	0.314 ± 0.032	$w_0 = -1.055 \pm 0.157$ $w_{0.5} = -1.263 \pm 0.377$	44.11 (9.80)	-0.780	7.98

Table 4.3: *Constraints on dark energy parameters and derived quantities from current data.*

Model	χ^2_{min}	Ω_m	Dark energy parameters	$\mathrm{FoM}_{\mathrm{Wang}}$ $(\mathrm{FoM}_{\mathrm{DETF}})$	$\rho_{1,2}$	DIC
CPL	5320.38	0.269 ± 0.005	$w_0 = -1.151 \pm 0.041$ $w_a = 0.244 \pm 0.207$	616.25 (616.25)	-0.946	21.44
Wang	5320.38	0.269 ± 0.005	$w_0 = -1.151 \pm 0.041$ $w_{0.5} = -1.069 \pm 0.031$	1848.70 (616.25)	-0.712	11.69
Chebychev P.	5320.43	0.269 ± 0.005	$w_0 = -1.140 \pm 0.035$ $w_{0.5} = -1.073 \pm 0.029$	2065.28 (504.85)	-0.666	11.38
Conventional P.	5320.45	0.269 ± 0.005	$w_0 = -1.137 \pm 0.033$ $w_{0.5} = -1.075 \pm 0.028$	2147.57 (477.24)	-0.648	11.29

Table 4.4: *Constraints on dark energy parameters and derived quantities from simulated data.*

Note the substantial reduction on percentual errors when one moves from current to mock data, typically they become almost three times smaller. Up to some degree this may be a consequence of the use of a fiducial model in the simulated data, probably real future data will be significantly better than current ones but perhaps not as remarkably as our synthetic data.

Summarizing this section of the analysis, we see that, in general, choosing w_0 and $w_{0.5}$ as the parameters to constrain is worthy as percentual errors are low. In our two new parametrizations they are indeed valuable from this particular perspective, but are they as valuable when one considers other criteria?

Another interesting point of view to interpret our results is Pearson's correlation coefficient (for dark energy), defined as

$$\rho_{1,2} = \frac{\sigma_{12}^2}{\sigma_1 \sigma_2}, \tag{4.35}$$

which can be used to study the lineal correlation between either two dark energy parameters. Here σ_{12} stands generically for the non-diagonal element of the covariance matrix for the parameters 1 and 2. A value of $\rho_{1,2}$ close to zero will tell us there is no correlation between them, and lowering correlation typically improves constraints, so if a given parametrization achieves that goal naturally then it will most likely provide an overall worthy scenario.

A related magnitude is the (frequentist) Figure-of-Merit (FoM), which has been defined in two slightly different but related ways in the literature; one was introduced by the DETF for the CPL parametrization, $\mathrm{FoM}_{\mathrm{DETF}}$; and the other one, proposed in [286] represents an extension for a wider range of dark energy EoS parametrizations, $\mathrm{FoM}_{\mathrm{Wang}}$. In Section 1.7.7 we present both and discuss their specific features. Here we will report their values for the benefit of the readers keener to one version or the other. According to Section 1.7.7, the two FoMs are linearly related:

$$\mathrm{FoM}_{\mathrm{DETF}} = m_3 \mathrm{FoM}_{\mathrm{Wang}} \tag{4.36}$$

with $m_3 = 1/3, 2/9, 11/45$ for Wang, Chebychev polynomial and Conventional polynomial models respectively.

Our results on the FoM get summarized very simply: the conventional polynomial has the largest value of the $\mathrm{FoM}_{\mathrm{Wang}}$, whereas the results get complete reversed for the $\mathrm{FoM}_{\mathrm{DETF}}$. In addition, the ratios between the different FoMs are very similar for real and synthetic data. However, as follows from our discussion before, the price paid to get a larger FoM (by a redefinition) is to waive the importance of correlation, and further investigations and reflections would be needed to provide a definite solution to this debate, which is, on the other hand, out of the scope of this thesis.

For both sorts of data the conventional polynomial parametrization is naturally less correlated than all three others. The second best is the Chebyshev one, and all three are considerably less correlated than CPL. Nevertheless, even though Wang's second parameter $w_c \equiv w_{0.5}$ is chosen for the low degree of correlation with w_0, a better choice for that purpose would be the dark energy EOS parameter evaluated at a lower redshift (say $z \sim 0.25$). This was already pointed out in [286] and confirmed in [96]. In agreement with our discussion, the degree of correlation at a certain low redshift in our two new parametrizations immediately

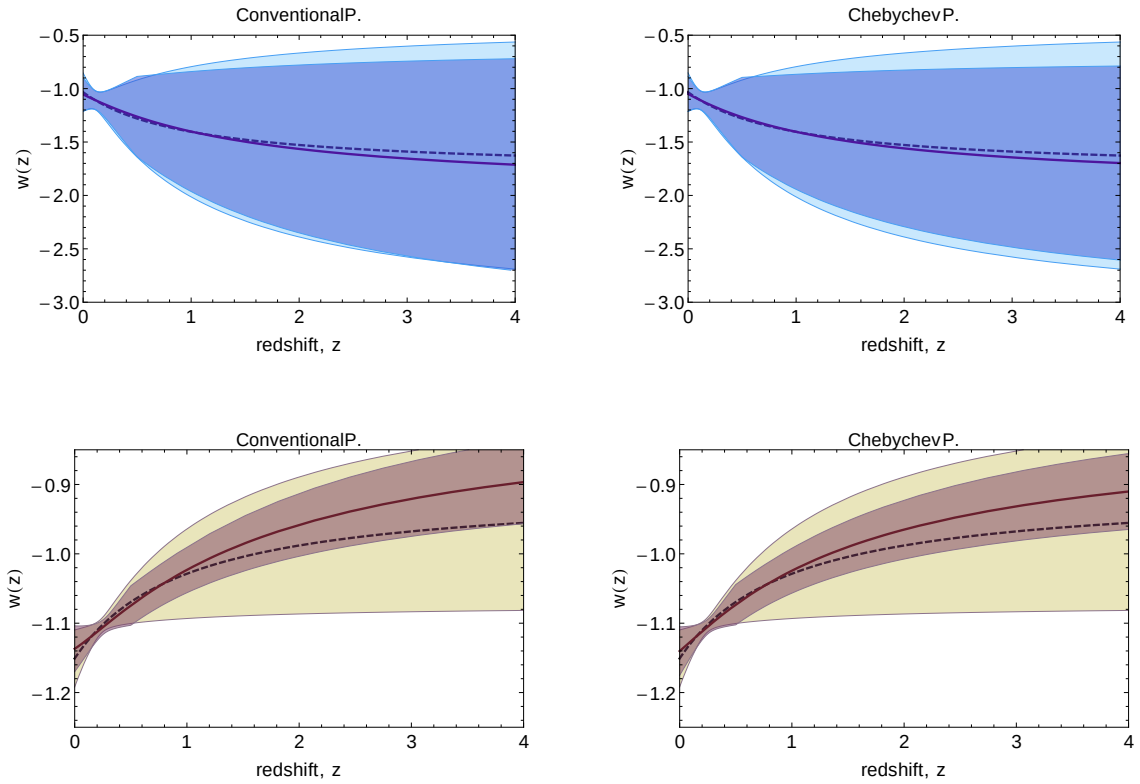

Figure 4.3: *Total 1σ error bands for w corresponding our best fits for real (a) and mock data (b) compared with the results for the CPL parametrization (dashed lines and light contours).*

drives to very narrow errors on the total w at that location, as reflected in Fig. 4.3, where we represent the total w for our best fits and the 1σ error bands. In fact, these two figures serve the additional purpose of illustrating the sort of evolution described by our parametrizations. Nevertheless, as correlation is a topic worth of further consideration, we have elaborated in Section 4.2.

Finally, the last criterion we resort to is the Bayesian deviance information criterion (DIC), see Eq. (1.164). This is a very interesting way to examine results in this context, in particular when one finds marginal differences in the χ^2 values. As it has been previously pointed out, this criterion accounts for the dependence of χ^2 on our parameters, but it also somehow involves the correlation and the percentual errors, thus turning out to be far more informative and having more discerning power. When applied for model selection, as we put forward, the setting with the lowest DIC is in principle the best. In our case, as we are mainly concerned with dark energy issues given that Ω_m is very tightly constrained we construct our DIC starting from a χ^2 marginalized over Ω_m, $\widehat{\chi^2}$. Namely

$$\text{DIC} = 2\overline{\widehat{\chi^2}(\boldsymbol{\theta})} - \widehat{\chi^2}(\boldsymbol{\theta}_{bf}), \tag{4.37}$$

where $\boldsymbol{\theta}_{bf}$ denotes the set of parameters that gives the best fit.

The behaviour of the DIC follows the same pattern as the FoM (although the FoM is not so convenient as a model selection criterion as it does not involve χ^2). Basically, the conventional polynomial model is the best one, then we have the Chebyshev polynomial model, then Wang's scenario, and finally, the CPL model closes the ranking with the highest DIC by far.

Finally, we can see that the FoM values obtained with the mock data are typically better than those for currently available data. This fact proves the capability of the forthcoming surveys to describe the evolutionary features of dark energy.

4.5 Conclusions

Parameterizing dark energy in a phenomenological way offers the possibility of progressing in the characterization of this main component of the Universe, even though its origin has not been yet unveiled from a theoretical perspective. The extensive prior knowledge available on the topic hints that compliance with relevant astrophysical data favours parametrizations which are smooth and have two parameters only. A second order requirement is restraint at high redshifts in the sense that dark energy should never redshift slower than matter, but neither display a significant blueshift.

Given those guidelines, we have presented two new polynomial parametrizations of dark energy and we have payed attention to some particular aspects which are important for model selection. On the one hand we have examined the degree of correlation between the two parameters chosen in our proposal; specifically those are the EOS values at $z = 0$ and $z = 0.5$, which have been already shown to provide a convenient way to revisit and have already been shown to provide a preferred way to reconsider it. On the other hand we have resorted to a genuinely Bayesian model selection criterion, the deviance information criterion (DIC) for a better account of the improvements that our parametrizations represent.

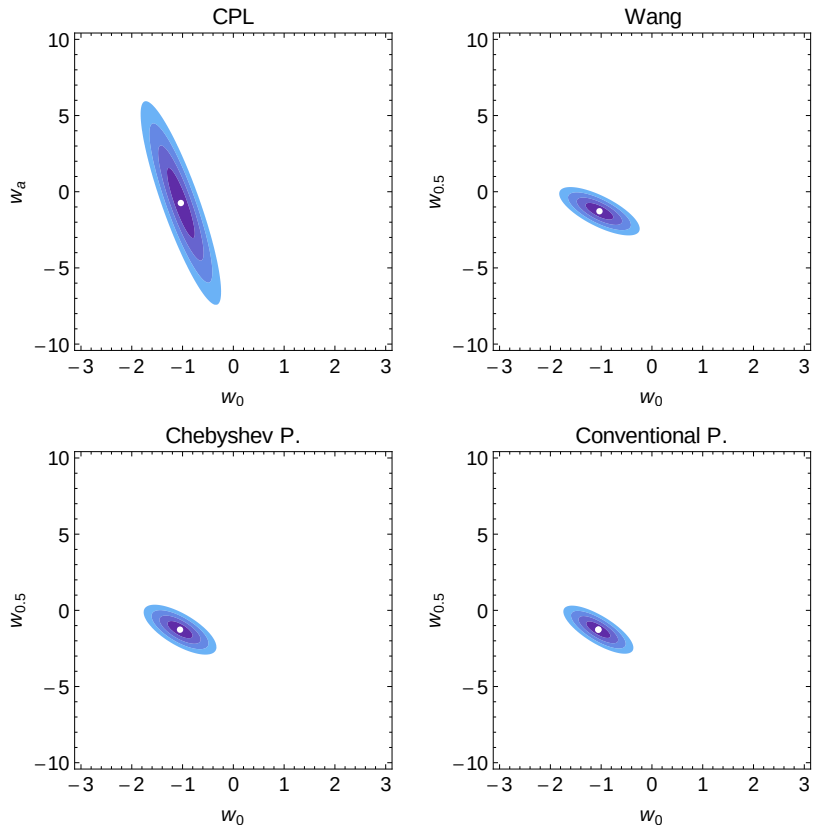

Figure 4.4: *Confidence contours for the four parametrizations using current data.*

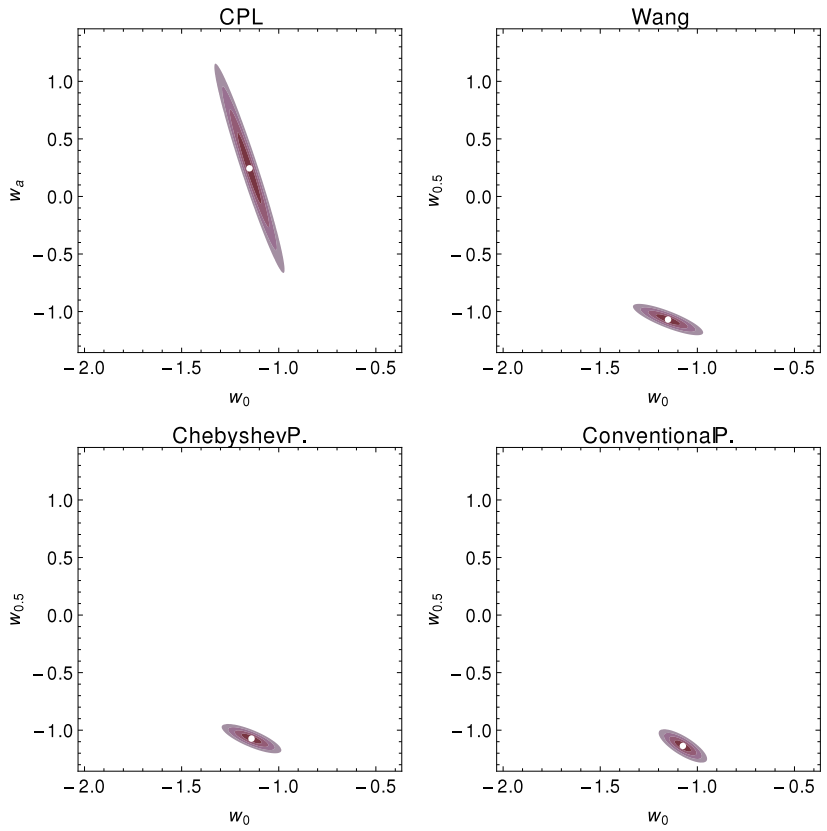

Figure 4.5: *Confidence contours for the four parametrizations using simulated data.*

The astronomical tests we have performed make use of SNeIa luminosity data and the typical BAO related scales, so we have focused on low redshift probes, although our parametrizations are suitable (as they are well behaved at high redshifts) for the analysis of CMB constraints which we hope to address in the future.

The conclusions that have emerged from our analysis is that our new parametrizations perform better in the sense that they allow to obtain tighter constraints on the dark energy EOS at present and its derivative, and they are also favoured by the statistical indicator we mention above (DIC). The main reason why we feel they fare better than their competitors is that they represent rather flexible perturbations of the ΛCDM scenario, which in many respects still remains the best description of the accelerated universe, and not surprisingly is often referred to as the concordance model. In contrast, either CPL or Wang are models which when taken as perturbations of ΛCDM are left with one free parameter only, and then one could expect less ability to accommodate themselves to the data.

Note as well that the datasets we have considered are not only some currently available ones, but we have also simulated surveys to come. Un particular, it is of interest our provision of synthetic measurements of the radial and transversal BAO scales as expected to be obtained with the EUCLID spectroscopic survey, which as expected help us conclude that future surveys will decrease considerably our degree of ignorance about dark energy evolution by providing far tighter constraints that may eventually lead to the conclusion that a cosmological constant is not the preferred candidate for dark energy.

CHAPTER 5

IMPROVED LIMITS ON SHORT-WAVELENGTH GRAVITATIONAL WAVES FROM THE COSMIC MICROWAVE BACKGROUND

A primordial gravitational wave background may have been generated by processes taking place in the early Universe. Given the extremely small cross section of gravitational waves (GWs), they can probe deep into the early Universe, and provide a unique window to explore its evolution. The exact mechanisms of production of primordial GWs are still under investigation. There are many theoretical models that predict them: not only through quantum fluctuations during inflation [2, 43, 226], but also from cosmic strings [74, 75, 196, 245, 246, 253], fragmentation of a scalar condensate in the context of supersymmetry [152], brane inflation [188], causal mechanisms from phase transitions [12, 111, 119, 120, 291], ekpyrotic models [142, 143] or pre big-bang theories [95, 103]. Such backgrounds will involve GWs with wavelengths that extend up to our present cosmological horizon, giving a lowest observable frequency limit of $\sim 10^{-17} - 10^{-16}$ Hz.

A measure of the amplitude of the cosmological gravitational-wave background (CGWB) at low frequencies can be obtained from constraining a possible tensor-mode contribution to the large-scale temperature and polarization fluctuations in the Cosmic Microwave Background [97, 139, 238, 264]. Recent results from the Wilkinson Microwave Anisotropy Probe (WMAP) satellite limit the amplitude of tensor fluctuations, quantified by the tensor-to-scalar ratio, to $r < 0.20$ at the 95% confidence level (C. L.) [147], which translates to an upper bound on the CGWB energy density $\Omega_{\rm gw} h^2 < 10^{-14}$ at frequencies $\sim 10^{-17} - 10^{-16}$ Hz. At higher frequencies, larger than $\sim 10^{-10}$ Hz, a bound on the CGWB can be obtained through big-bang nucleosynthesis (BBN), see Fig. 5.1. Gravitational waves at these frequencies would contribute to the total radiative energy density at the time of nucleosynthesis, thus a measure of the light-element abundances can place a constraint on the CGWB. Current

observations set an upper limit at this frequency range of $10^6\Omega_{\rm gw}h^2 \lesssim 8.0$ [71]. At the same time, pulsars act as natural gravitational wave detectors [132], strongly constraining the amplitude of the GW with the narrow range of frequencies, $f \sim 10^{-9} - 10^{-8}$ Hz, to $10^6\Omega_{\rm gw}h^2 < 10^{-2}$ [281]. Large scale interferometers for gravitational wave detection (e.g., LIGO [3], LISA [243], VIRGO [4]) are also looking for gravitational wave signals. A recent bound of $10^6\Omega_{\rm gw}h^2 < 6.9$ has been obtained at 10^2 Hz from the Laser Interferometer Gravitational Wave Observatory (LIGO) [1].

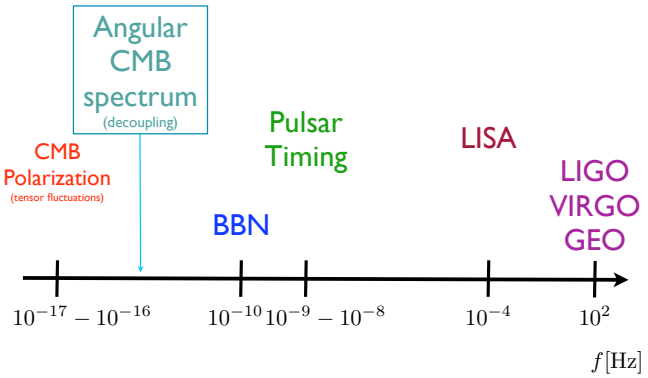

Figure 5.1: *Frequency range of the different CGWB experiments.*

In this work we estimate constraints on the CGWB at frequencies larger than $\sim 10^{-15}$ Hz through their effect on the angular power spectrum of the CMB. This component behaves as a non-interacting relativistic fluid, and so would modify the CMB power spectrum in a similar way to adding extra neutrino species [254]. Given the $\sim 2\sigma$ hint of a neutrino number excess seen by both the South Pole Telescope (SPT) and Atacama Cosmology Telescope (ACT) experiments [83, 141], it is timely to consider alternatives beyond the standard three neutrino species. Constraints on this GW background were first presented in [254], and updated with WMAP 7-year data in [147]. We now make use of the latest CMB data from WMAP and SPT, which currently give the tightest constraints on the number of effective neutrinos [141]. We then use the improved limits to bind the tension of cosmic strings that could generate this gravitational wave background. As in [254], we do not restrict our study to the case where the GW were produced under adiabatic initial conditions, but also study homogeneous initial conditions.

5.1 Theoretical background

5.1.1 Effective number of neutrino species and the Cosmological Microwave Background

As it was previously indicated in Sec. 1.5, the effective number of neutrino species, $N_{\rm eff}$, represents the energy density stored in relativistic components (radiation) as

$$\rho_{\rm rad} = \rho_\gamma + \rho_\nu + \rho_x = \left[1 + \frac{7}{8}\left(\frac{4}{11}\right)^{4/3} N_{\rm eff}\right]\rho_\gamma, \tag{5.1}$$

with ρ_γ, ρ_ν, and ρ_x the energy densities of photons, neutrinos, and possible extra radiation components, respectively. In this expression, all non-photon energy density is expressed in terms of an effective number of neutrino species, $N_{\rm eff}$. Any additional radiation density, ρ_x, would then typically correspond to a non-integer value of $N_{\rm eff}$. The largest effect of increasing the radiation density on the CMB comes from a decrease in the redshift of the matter-radiation equality, z_{eq}, which follows from the relation

$$N_{\rm eff} = 3.04 + 7.44\left(\frac{\Omega_m h^2}{0.1308}\frac{3139}{1+z_{eq}} - 1\right), \tag{5.2}$$

for matter density $\Omega_m h^2$ [146]. An increase in $N_{\rm eff}$ also affects the acoustic oscillations in the primordial photon-baryon plasma, leading to additional damping (early ISW) which will increase the height of the first peak and a phase shift in the acoustic peak positions of the CMB (see Sections 1.5, 1.6.3 and [22]). As noted in [147], the matter density can be better constrained by combining observations of the CMB with late-time distance measurements from BAO data, and a measurement of the Hubble parameter, H_0. These allow the equality redshift to be better measured, improving constraints on $N_{\rm eff}$ from small-scale CMB data.

If we assume that there are three standard neutrino flavors, $N_{\rm eff} = 3.046$ (with the small correction due to finite temperature QED effects and neutrino flavor mixing [185]), and any measured excess would imply an extra relativistic component. Current small-scale CMB data show a slight preference for $N_{\rm eff} > 3$ at 95% C. L., with $N_{\rm eff} = 4.56 \pm 1.5$ measured from the Atacama Cosmology Telescope and $N_{\rm eff} = 3.86 \pm 0.84$ with South Pole Telescope data [141] in combination with WMAP data, measurements of the BAO data, and H_0 [83]. Combining both ACT and SPT (along with WMAP and other probes of large-scale structure) increases the significance to $N_{\rm eff} = 4.0 \pm 0.58$ [255].

5.1.2 CGWB contribution to radiation

In [254] it was proposed that such an excess could be interpreted as a contribution of gravitational waves to the radiation density, instead of neutrinos. As detailed in Sec. 35.7 of [192], it is possible to obtain an effective energy momentum tensor for the gravitational waves as an average of the stress energy carried by several wavelengths

$$T^{GW}_{\mu\nu} = \frac{\langle h_{jk,\mu} h_{jk,\nu}\rangle}{32\pi}. \tag{5.3}$$

For perturbations inside the horizon, gravitational waves can be considered to be propagating in a flat, Minkowski background. In this case, the equation of motion for the tensor perturbation of the metric (see Sec. 1.5.1) becomes, $\partial^\sigma \partial_\sigma h_{\mu\nu} = 0$, whose solution is a plane-wave $h_{\mu\nu} = \mathcal{R}\{A_{\mu\nu} e^{ik_\sigma x^\sigma}\}$, with a wave vector $\mathbf{k}$. It allows us to obtain an expression of the effective energy-momentum tensor:

$$T^{GW}_{\mu\nu} = \frac{A^2 k_\mu k_\nu}{32\pi}, \tag{5.4}$$

which is completely the same as the energy-momentum tensor of a beam of non-interacting massless particles. Thus, the effects on the CMB and the matter power spectra of CGWB are equal to those produced by massless neutrinos.

Since gravitational waves with wavelengths shorter than the sound horizon at decoupling behave as free-streaming massless particles, a limit on additional relativistic radiation can be translated into an upper limit on the energy density of the CGWB for frequencies larger than $\sim 10^{-15}$ Hz. One can relate the effective "number of gravitational-wave" degrees of freedom, $N_{\rm gw} \equiv N_{\rm eff} - 3.046$, to the CGWB energy density [184]:

$$\Omega_{\rm gw} h^2 \equiv \int_0^\infty d\,(\ln f)\, h^2 \Omega_{gw}(f) = 5.6 \times 10^{-6} N_{\rm gw}. \tag{5.5}$$

5.1.3 CGWB production and cosmic string tension

The different processes which may produce a CGWB lead to different initial conditions for perturbations in the CGWB fluid. Adiabatic initial conditions may arise from the incoherent superposition of cusp bursts from a network of cosmic strings or superstrings (see [196, 245] for further details). Bounds on the energy density of this radiation can then be translated into an upper limit on the string tension, $G\mu$, for a given model [74, 75, 196, 245, 246, 284]. Following the procedure given in [196] for the analytical approximation of the CGWB produced by strings, we can relate our limit on the GW energy density to a bound on $G\mu$ and the string reconnection probability, p, which is 1 for cosmic strings and < 1 for superstrings. String loops which are smaller than the causal horizon produce a CGWB with

$$\Omega_{\rm gw}(f) \approx 5 \times 10^{-2} G\mu/p \tag{5.6}$$

whereas the CGWB produced by horizon sized loops scale as

$$\Omega_{\rm gw}(f) \approx 3.2 \times 10^{-4} \sqrt{G\mu}/p. \tag{5.7}$$

An alternative scenario, noted in [254], may arise when the CGWB is produced by quantum fluctuations during a period of inflation. In this case, the perturbations may be non-adiabatic, differing from those of other species produced through the decay of the inflation. We re-examine the dependence on initial conditions by also considering "homogeneous" initial conditions, as in [254]. These have no initial primordial perturbations in the CGWB energy density in the Newtonian gauge, thus the curvature perturbation disappears when the CGWB energy density dominates, and, in addition, it approaches the adiabatic case when the CGWB

energy density vanishes.

5.2 Data and methodology

We use the latest measurements of the CMB power spectrum from the WMAP 7-year data release [153] and SPT [141], which extend the previous set of data to higher multipole moments ($\ell_{\rm max} \sim 3000$). These data considerably improve constraints on $N_{\rm eff}$, which will be translated into tighter bounds on $\Omega_{\rm gw}h^2$. To illustrate the sensitivity of these new data to changes in $N_{\rm eff}$, in Fig. 5.2 we show the difference between a model with $N_{\rm gw} = 0$ and $N_{\rm gw} = 1$ with the other cosmological parameters chosen so that the two models fit the WMAP-7 data equally well. It is clear that the data from SPT covers the range where the power spectrum is sensitive to a variation of $N_{\rm gw}$.

We estimate the bounds on $N_{\rm gw}$ by varying the number of effective gravitational-wave degrees of freedom, $N_{\rm gw}$, imposing a prior that $N_{\rm gw} > 0$ and assuming the standard three non-interacting massless neutrino species and by marginalizing over the standard six ΛCDM parameters: the baryon energy density in units of the critical energy density, $\Omega_{\rm b}h^2$, the energy density in cold dark matter in units of the critical energy density, $\Omega_{\rm DM}h^2$, the angular size of the first acoustic peak θ, the optical depth to the surface of last scattering, τ, the scalar spectral-index, n_s, and the amplitude of the scalar power-spectrum, A_s. To include the SPT data we follow the prescription presented in [141], marginalizing over three additional parameters describing power from foregrounds and the Sunyaev-Zel'dovich effect. We use a Markov Chain Monte Carlo (MCMC) method to estimate the probability distribution, using the CosmoMC[1] software package, see [165, 166] with a modified version of CAMB[2] [167] which includes the homogeneous initial conditions for CGWB perturbations in the conformal Newtonian gauge. We combine these CMB measurements with distance measurements from BAO data measured at $z = 0.2$ and $z = 0.35$ from SDSS and 2dFGRS presented in [209]. We also include a prior of $H_0 = 74.2 \pm 3.6$ km/(s Mpc) on the Hubble constant [223]. The CMB temperature and polarization spectra are obtained with CAMB for each cosmology, and then passed to CosmoMC to obtain the joint likelihood of WMAP, SPT, BAO, and H_0, as described in [141][3].

5.3 Results

As shown in Fig. 5.3 and Table 5.1, the new combination of CMB data gives an upper limit of $N_{\rm gw} < 1.56$, or $10^6\Omega_{\rm gw}h^2 < 8.71$, at 95% C. L. for adiabatic initial conditions which improves the previous upper bounds on $\Omega_{\rm gw}h^2$ given in [147] by a factor of 1.7. A non-zero relativistic excess is weakly favoured at 95% C. L., with the best-fit value $N_{\rm gw} = 0.82 \pm 0.36$. Homogeneous initial conditions for GWs are now more strongly excluded, with $N_{\rm gw} < 0.18$, $10^6\Omega_{\rm gw}h^2 < 1.02$, an improvement on the previous constraint in [253] by a factor of 3.5. In this case, the degeneracy between the effects of CGWB and neutrinos is broken, giving

[1] http://cosmologist.info/cosmomc/
[2] http://camb.info/
[3] Likelihood code is available at http://lambda.gsfc.nasa.gov/

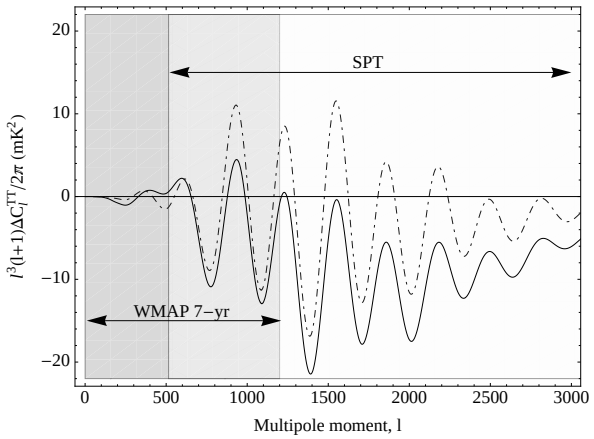

Figure 5.2: *The difference between the temperature power spectrum, ΔC_l^{TT}, between a model with $N_{\rm gw} = 0$ and $N_{\rm gw} = 1$ with the other cosmological parameters chosen so that the two models fit the WMAP-7 data equally well. The thick-line model has adiabatic initial conditions, the dot-dashed homogeneous initial conditions. The angular range of the SPT and WMAP 7-year CMB data are shown.*

us the stronger constraint. These bounds are now competitive with those given by BBN, $10^6\Omega_{\rm gw}h^2 < 8.0$ [71] for $f \gtrsim 10^{-10}$ Hz and LIGO, $10^6\Omega_{\rm gw}h^2 < 6.9$ at $f \approx 10^2$ Hz [1], but with the benefit that this upper bound can be extended to frequencies as low as 10^{-15} Hz.

Our constraint to the integrated CGWB energy density with adiabatic initial conditions can be translated into a constraint on cosmic string networks, as shown in Fig. 5.4. In order to do this we use Eq. (5.5) and integrate the spectra given in Eqs. (5.6) and (5.7). The lower-bound to the CGWB spectrum produced by the string network is $f_{\rm min} \sim 3.6 \times 10^{-18}/(G\mu)$ Hz for horizon-sized string loops, and $f_{\rm min} \sim \alpha^{-1} z_{\rm eq}^{1/2} H_0$ for sub-horizon sized string loops, where $z_{\rm eq} \simeq 3400$ is the redshift at matter-radiation equality [196]. The upper-bound is given by the horizon size at the time of the phase-transition which produced the network, $f_{\rm max} \sim \alpha^{-1} H(T_{\rm pt}) = \alpha^{-1} T_{\rm pt}^2/M_{\rm pl} = \alpha^{-1} M_{\rm pl} G\mu$, where $T_{\rm pt} = \sqrt{G\mu} M_{\rm pl}$ is the temperature of the phase transition, $M_{\rm pl}$ is the Planck mass (see Eq. (1.73)), and $\alpha = 1$ for horizon-sized string loops [196]. With this we find that for subhorizon-sized loops our constraint becomes

$$\frac{G\mu}{p} \ln\left(\frac{G\mu M_{\rm pl}}{H_0 z_{\rm eq}^{1/2}}\right) \lesssim 3 \times 10^{-4}, \tag{5.8}$$

and for horizon-sized loops we have

$$\frac{\sqrt{G\mu}}{p} \ln\left(\frac{(G\mu)^2 M_{\rm pl}}{3.6 \times 10^{-18}\ {\rm Hz}}\right) \lesssim 5 \times 10^{-2}. \tag{5.9}$$

For $p = 1$ we obtain $G\mu \lesssim 2 \times 10^{-7}$ for horizon-sized string loops and $G\mu \lesssim 2.5 \times 10^{-6}$ for subhorizon loops. String tensions this large have already been excluded through directly limiting a string contribution to the CMB power spectrum [27, 40, 83, 85, 279], $G\mu \lesssim 10^{-6} - 10^{-7}$. However, for lower reconnection probability, e.g. $p = 0.1$, the $N_{\rm gw}$ bound tightens to $G\mu \lesssim 2.4 \times 10^{-9}$ for horizon-sized string loops. Further study is required to

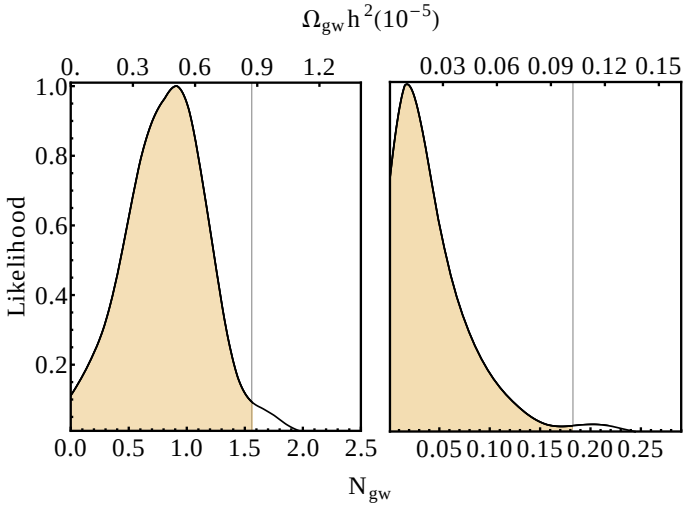

Figure 5.3: *Marginalized likelihoods for $N_{\rm gw}$ and CGWB energy density, $\Omega_{\rm gw}h^2(\times 10^{-5})$, for adiabatic (left) and homogeneous (right) initial conditions, where the horizontal line and the colored/shaded region indicate the 95 % C.L. limit.*

	$N_{\rm gw}$	$10^6\Omega_{\rm gw}h^2$
Adiabatic 95% upper limits	< 1.56	< 8.71
Adiabatic 68% range	0.82 ± 0.36	4.8 ± 0.2
Homogeneous 95% upper limits	< 0.18	< 1.02

Table 5.1: *Upper limits on $N_{\rm gw}$ and $\Omega_{\rm gw}h^2$ at 95% C.L for the adiabatic and homogeneous primordial initial conditions.*

investigate constraints considering both the string contribution to the CMB power spectra, and additional relativistic degrees of freedom.

5.4 Conclusions

We have used recent CMB data at small angular scales from SPT, in combination with data from WMAP-7 year and the latest measures of H_0 and BAO, to constrain a possible cosmological gravitational wave background with frequencies greater than 10^{-15} Hz. Recent measurements of the Silk damping tail from SPT improves limits on the CGWB density by about a factor of two. We note that the inclusion of additional measurements of the small-scale CMB, such as from the Atacama Cosmology Telescope, do not significantly improve the upper-limits presented here [255].

In agreement with other analyses of similar data, we find that a non-zero relativistic energy density with adiabatic initial conditions is preferred at the 95% level [83, 141, 255]. This additional energy density could be attributed to gravitational waves with frequencies greater than $\sim 10^{15}$ Hz, or some other relativistic species (see, e.g., [255]). If we attribute this extra relativistic energy density to gravitational waves produced by a cosmic string network, it is interesting to note that for $p = 1$ the upper limits to the CGWB presented here

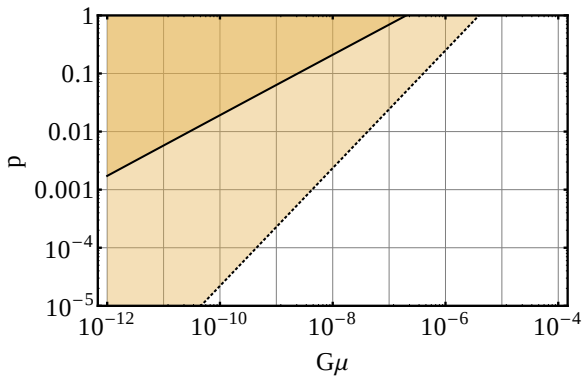

Figure 5.4: *The shaded region shows the 95% C. L. region which is allowed by constraints on the CGWB from the CMB in the $p - G\mu$ plane for horizon-sized (solid), and subhorizon-sized (dashed) cosmic string and superstring models with string tension $G\mu$ and reconnection probability p, given a GW energy density level $\Omega_{\rm gw}h^2 = 8.7 \times 10^{-6}$. For $p = 1$, the CMB power spectrum limits $G\mu \lesssim 10^{-6} - 10^{-7}$.*

are competitive with direct CMB constraints on the the string tension, both now requiring $G\mu \lesssim 10^{-6} - 10^{-7}$.

We have also explored how constraints on the CGWB depend on the initial conditions. Besides the standard adiabatic initial conditions, we placed constraints on the CGWB energy with 'homogenous' initial conditions [253]. The additional information on the small-scale CMB from SPT improves upon the previous upper-limit by more than a factor of 3.5. As opposed to an additional adiabatic relativistic component, the data do not prefer any additional homogeneous relativistic energy density.

Finally, the situation will be greatly improved with near-future CMB observations. For example, the Planck satellite will increase the sensitivity of these constraints by a factor of 5 for adiabatic initial conditions and a factor of 2 for homogeneous initial conditions [253].

CHAPTER 6

OVERALL CONCLUSIONS

The main aim of this thesis has been to go further and obtain some new hints of the nature of dark energy. As a first approach, in Chapter 2 a new unified model for the dark sector has been presented and investigated. In Chapters 3 and 4 the dark energy has been tackled form a new perspective, and new parametrizations of the dark energy equation of state have been proposed. Finally, in Chapter 5, through CMB data, a step further has been given in the physics of the early universe, and constraints on the excess of the radiation energy density have been set. Moreover, an explanation of this effect has been given: this excess can be attributed to the primordial gravitational wave background produced by cosmic strings. In what follows details on the conclusions obtained will be summarized.

Chapter 2 focuses on the study from different views of a new unified model based on a purely kinetic DBI action. This model unifies the dark sector, dark matter and dark energy, in a single fluid. After proving it mimics matter at early times and that a de Sitter regime is recovered at late times, its capability to create structures is studied through a perturbational analysis. An initial domination of the energy density perturbation seeds the initial unstable phase required to initiate the formation of structures. As the Universe becomes dominated by the vacuum or dark energy, these perturbations become negligible. Thus, from the initial perturbation perspective, this model is coherent with what is know nusabout structure formation and evolution. An observational analysis of this model reveals us that, although it is slightly preferred if we compared it with the ΛCDM, it is much better suited to observations that the Chaplygin gas, becoming a potential alternative. A nice feature of this model is that the best fit for the present value of the effective dark energy equation of state is below -1 and this phantom behaviour is achieved without the addition of any special component in the field action. Another remarkable achievement is that we have been able to extend the usage of models based on a DBI action (widely used in inflation) to explain the present acceleration of the Universe. The present work has focused in the case with lowest degrees of freedom, we have considered constant $f(\phi)$ and $V(\phi)$, but it is only a special case and it would be interesting to explore further scenarios and

generalizations. Finally, to get further in the perturbational analysis, it would be convenient to include second order perturbations, because they would help us to obtain a global view of this unified model.

Chapters 3 and 4 detail the results obtained when we perform an observational analysis of different parametrizations of the dark energy equation of state. Specifically, in Chapter 3 a detailed study has been performed to detect an oscillating pattern in the dark energy equation of state and 3 different parametrizations have been proposed: one expressed in terms of the sine and the other two in terms of Struve and Bessel special functions. One of the novelties of this work is that the frequency parameter have not been fixed and the equation of the state has been evaluated at different values. Another novelty is the usage of direct measurements of the Hubble factor and Gamma Ray Bursts data, which widen the redshift range to detect the oscillatory behaviour. The main results obtained are: I. even if constraints on the amplitude are not too strong, we detect a trend of it versus the frequency, i.e. decreasing (and even negatives) amplitudes for higher frequencies; II. the centre of oscillation (which corresponds to the present value of the EoS parameter) is very well constrained, phantom behaviour is excluded at 1σ level and a trend in agreement with the one for the amplitude appears; III. the frequency is hard to constrain, showing similar statistical validity for all the values of the discrete set chosen, but the best fit of all the scenarios considered is associated with a period in the redshift range depicted by our cosmological data. The "best" oscillating models are compared with ΛCDM using a dimensionally consistent Bayesian approach based on information criteria and the conclusion reached is the non existence of significant evidence against dark energy oscillations.

Following the same line as the previous chapter, in Chapter 4 two new parametrizations of the dark energy equation of state have been suggested in order to make the most of the dark energy equation of state parameters and the observational data. This time, the principal goal is to obtain an EoS whose parameters are those least correlated, and at the same time, as ΛCDM is the preferred model by observational data, these parametrizations will represent a perturbation of the ΛCDM scenario. The proposed parametrizations are written in terms of Chebyshev and Conventional polynomials. The astronomical tests we have performed make use of SN luminosity data and the typical BAO related scales of current surveys. But we have also produced mock data to infer the improvement that future experiments as EUCLID will bring us on the constraints of the dark energy equation of state. According to the Bayesian deviance information criterion (DIC), which penalizes large errors and correlations, we show that our models perform better than the famous CPL and its re-parametrization proposed by Wang (in terms of $z = 0$ and $z = 0.5$). This is due to the combination of a lower correlation and smaller relative errors. The same holds for a frequentist perspective: our Figure-of-Merit is larger for our parametrizations.

In the last chapter of this thesis, we have set constraints on the number of effective neutrinos which accounts for the radiation excess. For this purpose, we have used the latest CMB data coming from WMAP7-year and the South Pole Telescope. Then, we have converted these bounds into an energy density of the Cosmological Gravitational Wave Background for two sets of initial conditions: adiabatic and homogeneous. With the inclusion of the data from SPT at small scales the adiabatic bound on the CGWB density is improved by a factor of 1.7 to $10^6\Omega_{gw} < 8.7$ at the 95% confidence level (C.L.), with weak

evidence in favour of an additional radiation component consistent with previous analyses. This constraint has been later converted into an upper limit on the tension of horizon-sized cosmic strings that could generate this gravitational wave component obtaining an upper of limit $G_\mu < 2 \times 10^{-7}$ at 95% C.L. The homogeneous bound improves by a factor of 3.5 to $10^6\Omega_{gw} < 1.0$ at 95% C.L., with no evidence for such a component from current data. It is the first time that a bound on the CGWB coming from the number of effective neutrinos is translated into a string tension, G_μ. As cosmic strings also contribute to the temperature power spectrum of the CMB, a interesting extension of the presented work would be to get further and investigate which would be the constraints considering both the string contribution and additional relativistic degrees of freedom to the CMB power spectra.

BIBLIOGRAPHY

[1] B. P. Abbott et al. An Upper Limit on the Stochastic Gravitational-Wave Background of Cosmological Origin. *Nature*, 460:990, 2009.

[2] L. F. Abbott and M. B. Wise. Constraints on Generalized Inflationary Cosmologies. *Nucl. Phys.*, B244:541–548, 1984.

[3] A. Abramovici et al. LIGO: The Laser interferometer gravitational wave observatory. *Science*, 256:325–333, 1992.

[4] F. Acernese et al. The present status of the VIRGO central interferometer. *Class. Quant. Grav.*, 19:1421–1428, 2002.

[5] H. Akaike. A new look at the statistical model identification. *IEEE Transactions on Automatic Control*, 19:716–723, 1974. ISSN 0018-9286.

[6] A. Albrecht and G. Bernstein. Evaluating dark energy probes using multidimensional dark energy parameters. *Phys. Rev.*, D75:103003, 2007.

[7] A. Albrecht and P. J. Steinhardt. Cosmology for Grand Unified Theories with Radiatively Induced Symmetry Breaking. *Phys. Rev. Lett.*, 48:1220–1223, 1982.

[8] A. Albrecht, L. Amendola, G. Bernstein, D. Clowe, D. Eisenstein, et al. Findings of the Joint Dark Energy Mission Figure of Merit Science Working Group. 2009. URL `http://arxiv.org/abs/0901.0721v1`.

[9] M. Alishahiha, E. Silverstein, and D. Tong. DBI in the sky. *Phys. Rev.*, D70:123505, 2004.

[10] R. Amanullah et al. Spectra and Light Curves of Six Type Ia Supernovae at 0.511¡z¡.12 and the Union2 Compilation. *Astrophys. J.*, 716:712–738, 2010.

[11] Amanullah, R., Stanishev, V., Goobar, A., Schahmaneche, K., Astier, P., Balland, C., Ellis, R. S., Fabbro, S., Hardin, D., Hook, I. M., Irwin, M. J., McMahon, R. G., Mendez, J. M., Mouchet, M., Pain, R., Ruiz-Lapuente, P., and Walton, N. A. Light

curves of five type ia supernovae at intermediate redshift. *Astron. Astrophys.*, 486: 375–382, 2008.

[12] R. Apreda, M. Maggiore, A. Nicolis, and A. Riotto. Gravitational waves from electroweak phase transitions. *Nucl. Phys.*, B631:342–368, 2002.

[13] A. Arbey. Dark fluid: A Complex scalar field to unify dark energy and dark matter. *Phys. Rev.*, D74:043516, 2006.

[14] A. Arbey. Cosmological constraints on unifying Dark Fluid models. *Open Astron. J.*, 1:27–38, 2008.

[15] A. Arbey. Dark Energy vs. Dark Matter: Towards a Unifying Scalar Field? *EAS Publ.Ser.*, 36:161–166, 2009.

[16] P. Astier et al. The Supernova Legacy Survey: Measurement of Ω_M, Ω_Λ and w from the First Year Data Set. *Astron. Astrophys.*, 447:31–48, 2006.

[17] N. A. Bahcall and P. Bode. The Amplitude of Mass Fluctuations. *Astrophys. J.*, 588: L1–L4, 2003.

[18] N. A. Bahcall et al. The Cluster Mass Function from Early SDSS Data: Cosmological Implications. *Astrophys. J.*, 585:182–190, 2003.

[19] E. Barboza, J. Alcaniz, Z.-H. Zhu, and R. Silva. A generalized equation of state for dark energy. *Phys. Rev.*, D80:043521, 2009.

[20] J. Barboza, E.M. and J. Alcaniz. A parametric model for dark energy. *Phys. Lett.*, B666:415–419, 2008.

[21] J. Barboza, E.M., J. Alcaniz, and B. Santos. Scalar field description of a parametric model of dark energy. 2011. URL `http://arxiv.org/abs/1107.2628v1`.

[22] S. Bashinsky and U. Seljak. Neutrino perturbations in CMB anisotropy and matter clustering. *Phys. Rev.*, D69:083002, 2004.

[23] B. A. Bassett and R. Hlozek. Baryon acoustic oscillations. In P. Ruiz-Lapuente, editor, *Dark Energy*. Cambridge University Press, 2010.

[24] B. A. Bassett, M. Kunz, J. Silk, and C. Ungarelli. A Late time transition in the cosmic dark energy? *Mon. Not. Roy. Astron. Soc.*, 336:1217–1222, 2002.

[25] B. A. Bassett, M. Kunz, D. Parkinson, and C. Ungarelli. Condensate cosmology - Dark energy from dark matter. *Phys. Rev.*, D68:043504, 2003.

[26] B. A. Bassett, P. S. Corasaniti, and M. Kunz. The Essence of quintessence and the cost of compression. *Astrophys. J.*, 617:L1–L4, 2004.

[27] R. Battye and A. Moss. Updated constraints on the cosmic string tension. *Phys. Rev.*, D82:023521, 2010.

[28] D. Baumann. TASI Lectures on Inflation. 2009.

[29] D. Baumann and L. McAllister. A Microscopic Limit on Gravitational Waves from D-brane Inflation. *Phys. Rev.*, D75:123508, 2007.

[30] R. Bean and O. Doré. Are chaplygin gases serious contenders for the dark energy? *Phys. Rev.*, D68:023515, 2003.

[31] R. Bean, X. Chen, H. Peiris, and J. Xu. Comparing Infrared Dirac-Born-Infeld Brane Inflation to Observations. *Phys. Rev.*, D77:023527, 2008.

[32] J. P. Beaulieu et al. EUCLID : Dark Universe Probe and Microlensing planet Hunter. 2010.

[33] N. Benitez, E. Gaztanaga, R. Miquel, F. Castander, M. Moles, et al. Measuring Baryon Acoustic Oscillations along the line of sight with photometric redshifs: the PAU survey. *Astrophys. J.*, 691:241–260, 2009.

[34] M. C. Bento, O. Bertolami, and A. A. Sen. Generalized chaplygin gas, accelerated expansion, and dark-energy-matter unification. *Phys. Rev.*, D66:043507, 2002.

[35] M. C. Bento, O. Bertolami, and A. A. Sen. Generalized Chaplygin gas, accelerated expansion and dark energy-matter unification. *Phys. Rev.*, D66:043507, 2002.

[36] B. A. Berg. Introduction to Markov chain Monte Carlo simulations and their statistical analysis. 2004. In Markov Chain Monte Carlo, W.S. Kendall et al. Editors, Lecture Notes Series, Institute for Mathematical Sciences, National University of Singapore, Vol.7, p.1 ff., World Scientific, 2005.

[37] D. Bertacca, N. Bartolo, A. Diaferio, and S. Matarrese. How the Scalar Field of Unified Dark Matter Models Can Cluster. *JCAP*, 0810:023, 2008.

[38] G. Bertone, D. Hooper, and J. Silk. Particle dark matter: Evidence, candidates and constraints. *Phys. Rept.*, 405:279–390, 2005.

[39] E. Bertschinger. Cosmological perturbation theory and structure formation. 2001. URL `http://arxiv.org/abs/astro-ph/0101009v1`.

[40] N. Bevis, M. Hindmarsh, M. Kunz, and J. Urrestilla. Fitting CMB data with cosmic strings and inflation. *Phys. Rev. Lett.*, 100:021301, 2008.

[41] N. Bilic, G. Tupper, and R. Viollier. Unification of dark matter and dark energy: the inhomogeneous chaplygin gas. *Phys. Lett.*, B535:17 – 21, 2002.

[42] N. Bilić, G. B. Tupper, and R. D. Viollier. Cosmological tachyon condensation. *Phy. Rev. D*, 80:023515, 2009.

[43] N. D. Birrell and P. C. W. Davies. *Quantum Fields in Curved Space (Cambridge Monographs on Mathematical Physics)*. Cambridge University Press, 1984.

[44] C. Blake and K. Glazebrook. Probing dark energy using baryonic oscillations in the galaxy power spectrum as a cosmological ruler. *Astrophys. J.*, 594:665–673, 2003.

[45] C. Blake, E. Kazin, F. Beutler, T. Davis, D. Parkinson, et al. The WiggleZ Dark Energy Survey: mapping the distance-redshift relation with baryon acoustic oscillations. *Mon. Not. Roy. Astron. Soc.*, 418:1707–1724, 2011.

[46] C. Blake et al. Universal fitting formulae for baryon oscillation surveys. *Mon. Not. Roy. Astron. Soc.*, 365:255–264, 2006.

[47] J. R. Bond, G. Efstathiou, and M. Tegmark. Forecasting Cosmic Parameter Errors from Microwave Background Anisotropy Experiments. *Mon. Not. Roy. Astron. Soc.*, 291:L33–L41, 1997.

[48] J. H. Brodie and D. A. Easson. Brane inflation and reheating. *JCAP*, 0312:004, 2003.

[49] C. Burigana et al. Forecast for the Planck precision on the tensor to scalar ratio and other cosmological parameters. *Astrophys. J.*, 724:588–607, 2010.

[50] K. P. Burnham, D. R. Anderson, and K. P. Burnham. *Model selection and multimodel inference: A practical information-theoretic approach*. Springer, 2nd edition, 2002.

[51] R. Caldwell. A Phantom menace? *Phys. Lett.*, B545:23–29, 2002.

[52] R. R. Caldwell, M. Kamionkowski, and N. N. Weinberg. Phantom energy and cosmic doomsday. *Phys. Rev. Lett.*, 91:071301, 2003.

[53] X. Chen. Cosmological rescaling through warped space. *Phys. Rev.*, D71:026008, 2005.

[54] X. Chen. Inflation from warped space. *JHEP*, 08:045, 2005.

[55] M. Chevallier and D. Polarski. Accelerating universes with scaling dark matter. *Int. J. Mod. Phys.*, D10:213–224, 2001.

[56] L. P. Chimento, M. Forte, and R. Lazkoz. Dark matter to dark energy transition in k-essence cosmologies. *Mod. Phys. Lett.*, A20:2075, 2005.

[57] J. M. Cline. String cosmology. *Lectures given at Advanced Summer Institute on New Trends in Particle Physics and Cosmology, Sheffield, England, 19-23 Jun 2006 and at Les Houches Summer School - Session 86: Particle Physics and Cosmology: The Fabric of Spacetime, Les Houches, France, 31 Jul - 25 Aug 2006.*, 2006.

[58] A. Clocchiatti et al. Hubble space telescope and ground-based observations of type ia supernovae at redshift 0.5: Cosmological implications. *Astrophys. J.*, 642:1, 2006.

[59] D. Coe. Fisher matrices and confidence ellipses: A quick-start guide and software. URL `http://arxiv.org/abs/0906.4123v1`.

[60] S. Cole et al. The 2dF Galaxy Redshift Survey: Power-spectrum analysis of the final dataset and cosmological implications. *Mon. Not. Roy. Astron. Soc.*, 362:505–534, 2005.

[61] A. Conley et al. Supernova Constraints and Systematic Uncertainties from the First 3 Years of the Supernova Legacy Survey. *Astrophys. J. Suppl.*, 192:1, 2011.

[62] A. Cooray, W. Hu, D. Huterer, and M. Joffre. Measuring angular diameter distances through halo clustering. *Astrophys. J.*, 557:L7, 2001.

[63] A. R. Cooray and D. Huterer. Gravitational lensing as a probe of quintessence. *Astrophys. J.*, 513:L95–L98, 1999.

[64] E. J. Copeland, M. Sami, and S. Tsujikawa. Dynamics of dark energy. *Int. J. Mod. Phys.*, D15:1753–1936, 2006.

[65] P. S. Corasaniti and E. Copeland. A Model independent approach to the dark energy equation of state. *Phys. Rev.*, D67:063521, 2003.

[66] P. S. Corasaniti, M. Kunz, D. Parkinson, E. Copeland, and B. Bassett. The Foundations of observing dark energy dynamics with the Wilkinson Microwave Anisotropy Probe. *Phys. Rev.*, D70:083006, 2004.

[67] R. D. Cousins. Why isn't every physicist a Bayesian? *Am. J. Phys.*, 63:398, 1995.

[68] R. A. C. Croft, W. Hu, and R. Dave. Cosmological Limits on the Neutrino Mass from the Lya Forest. *Phys. Rev. Lett.*, 83:1092–1095, 1999.

[69] A. Cucchiara, A. Levan, D. Fox, N. Tanvir, T. Ukwatta, et al. A Photometric Redshift of z 9.4 for GRB 090429B. *Astrophys. J.*, 736:7, 2011.

[70] J. Cunha and J. Lima. Transition Redshift: New Kinematic Constraints from Supernovae. *Mon. Not. Roy. Astron. Soc.*, 390:210–217, 2008.

[71] R. H. Cyburt, B. D. Fields, K. A. Olive, and E. Skillman. New bbn limits on physics beyond the standard model from 4he. *Astroparticle Phys.*, 23:313–323, 2005.

[72] D.-C. Dai, G. D. Starkman, B. Stojkovic, D. Stojkovic, and A. Weltman. Using quasars as standard clocks for measuring cosmological redshift. 2012.

[73] R. A. Daly, M. P. Mory, C. O'Dea, P. Kharb, S. Baum, et al. Cosmological Studies with Radio Galaxies and Supernovae. *Astrophys. J.*, 691:1058–1067, 2009.

[74] T. Damour and A. Vilenkin. Gravitational wave bursts from cosmic strings. *Phys. Rev. Lett.*, 85:3761–3764, 2000.

[75] T. Damour and A. Vilenkin. Gravitational wave bursts from cusps and kinks on cosmic strings. *Phys. Rev.*, D64:064008, 2001.

[76] W. Davidson. Number count relations in observational cosmology. *Mon. Not. Roy. Astron. Soc*, 119:665, 1959.

[77] T. M. Davis et al. Scrutinizing exotic cosmological models using ESSENCE supernova data combined with other cosmological probes. *Astrophys. J.*, 666:716, 2007.

[78] P. de Bernardis et al. A Flat Universe from High-Resolution Maps of the Cosmic Microwave Background Radiation. *Nature*, 404:955–959, 2000.

[79] W. de Sitter. Einstein's theory of gravitation and its astronomical consequences, Third Paper. *Mon. Not. Roy. Astron. Soc.*, 78:3–28, 1917.

[80] D. T. Denison, C. Holmes, B. Mallick, and S. A.F.M. *Bayesian Methods for Nonlinear Classification and Regression*. Wiley Series in Probability and Statistics. John Wiley & Sons, 2004.

[81] S. Dodelson, M. Kaplinghat, and E. Stewart. Solving the coincidence problem : Tracking oscillating energy. *Phys. Rev. Lett.*, 85:5276–5279, 2000.

[82] J. Dunkley, M. Bucher, P. G. Ferreira, K. Moodley, and C. Skordis. Fast and reliable MCMC for cosmological parameter estimation. *Mon. Not. Roy. Astron. Soc.*, 356: 925–936, 2005.

[83] J. Dunkley, R. Hlozek, J. Sievers, V. Acquaviva, P. Ade, et al. The Atacama Cosmology Telescope: Cosmological Parameters from the 2008 Power Spectra. *Astrophys. J.*, 739:52, 2011.

[84] G. R. Dvali and S. H. H. Tye. Brane inflation. *Phys. Lett.*, B450:72–82, 1999.

[85] C. Dvorkin, M. Wyman, and W. Hu. Cosmic String constraints from WMAP and the South Pole Telescope. *Phys. Rev.*, D84:123519, 2011.

[86] G. Efstathiou. Constraining the equation of state of the universe from distant type ia supernovae and cosmic microwave background anisotropies. *Mon. Not. Roy. Astron. Soc.*, 310:842–850, 1999.

[87] G. Efstathiou and J. R. Bond. Cosmic Confusion: Degeneracies among Cosmological Parameters Derived from Measurements of Microwave Background Anisotropies. *Mon. Not. Roy. Astron. Soc.*, 304:75–97, 1999.

[88] D. J. Eisenstein and W. Hu. Baryonic features in the matter transfer function. *Astrophys. J.*, 496:605, 1998.

[89] D. J. Eisenstein et al. Average spectra of massive galaxies in the SDSS. *Astrophys. J.*, 585:694–713, 2003.

[90] D. J. Eisenstein et al. Detection of the Baryon Acoustic Peak in the Large-Scale Correlation Function of SDSS Luminous Red Galaxies. *Astrophys. J.*, 633:560–574, 2005.

[91] V. R. Eke, S. Cole, C. S. Frenk, and J. P. Henry. Measuring Ω_0 using cluster evolution. *Mon. Not. Roy. Astron. Soc.*, 298:1145, 1998.

[92] O. Elgaroy and T. Multamaki. Bayesian analysis of friedmannless cosmologies. *JCAP*, 0609:002, 2006.

[93] G. Ellis and S. Stoeger, William R. Horizons in inflationary universes. *Class. Quant. Grav.*, 5:207–220, 1988.

[94] G. F. R. Ellis and T. Rothman. Lost horizons. *Am. J. Phys.*, 61:883–893, 1993.

[95] K. Enqvist and M. S. Sloth. Adiabatic CMB perturbations in pre big bang string cosmology. *Nucl. Phys.*, B626:395–409, 2002.

[96] C. Escamilla-Rivera, R. Lazkoz, V. Salzano, and I. Sendra. Tension between SN and BAO: current status and future forecasts. *JCAP*, 1109:003, 2011.

[97] R. Fabbri and M. d. Pollock. The Effect of Primordially Produced Gravitons upon the Anisotropy of the Cosmological Microwave Background Radiation. *Phys. Lett.*, B125: 445–448, 1983.

[98] B. Feng, M. Li, Y.-S. Piao, and X. Zhang. Oscillating quintom and the recurrent universe. *Phys. Lett.*, B634:101 – 105, 2006.

[99] A. V. Filippenko. Optical spectra of supernovae. *Ann. Rev. Astron. Astrophys.*, 35: 309–355, 1997.

[100] A. Friedmann. On the Possibility of a world with constant negative curvature of space. *Z. Phys.*, 21:326–332, 1924. Original in German.

[101] J. A. Frieman, C. T. Hill, A. Stebbins, and I. Waga. Cosmology with ultralight pseudo Nambu-Goldstone bosons. *Phys. Rev. Lett.*, 75:2077–2080, 1995.

[102] J. Garriga and V. F. Mukhanov. Perturbations in k-inflation. *Phys. Lett.*, B458:219 – 225, 1999.

[103] M. Gasperini and G. Veneziano. Pre - big bang in string cosmology. *Astropart. Phys.*, 1:317–339, 1993.

[104] A. Gelman and D. Rubin. Inference from iterative simulation using multiple sequences. *Statistical Science*, 7:457–511, 1992.

[105] M. Giovannini. *A primer on the physics of the cosmic microwave background*. World Scientific, 2009.

[106] F. Gmeiner and C. D. White. DBI Inflation using a One-Parameter Family of Throat Geometries. *JCAP*, 0802:012, 2008.

[107] J. H. Goldstein et al. Estimates of Cosmological Parameters Using the CMB Angular Power Spectrum of ACBAR. *Astrophys. J.*, 599:773–785, 2003.

[108] M. Goliath, R. Amanullah, P. Astier, A. Goobar, and R. Pain. Supernovae and the nature of the dark energy. *Astron. Astrophys.*, 2001.

[109] Y. Gong and A. Wang. Reconstruction of the deceleration parameter and the equation of state of dark energy. *Phys. Rev.*, D75:043520, 2007.

[110] J. Greiner, T. Kruhler, S. McBreen, M. Ajello, D. Giannos, et al. A strong optical flare before the rising afterglow of GRB 080129. *Astrophys. J.*, 693:1912–1919, 2009.

[111] C. Grojean and G. Servant. Gravitational Waves from Phase Transitions at the Electroweak Scale and Beyond. *Phys. Rev.*, D75:043507, 2007.

[112] A. H. Guth. The Inflationary Universe: A Possible Solution to the Horizon and Flatness Problems. *Phys. Rev.*, D23:347–356, 1981.

[113] S. Hannestad and E. Mortsell. Cosmological constraints on the dark energy equation of state and its evolution. *JCAP*, 0409:001, 2004.

[114] W. K. Hastings. Monte Carlo sampling methods using Markov chains and their applications. *Biometrika*, 57:97–109, 1970.

[115] E. Hawkins et al. The 2dF Galaxy Redshift Survey: correlation functions, peculiar velocities and the matter density of the Universe. *Mon. Not. Roy. Astron. Soc.*, 346: 78, 2003.

[116] S. H. Henry Tye. Brane inflation: String theory viewed from the cosmos. *Lect. Notes Phys.*, 737:949–974, 2008.

[117] M. Hicken et al. Improved Dark Energy Constraints from 100 New CfA Supernova Type Ia Light Curves. *Astrophys. J.*, 700:1097–1140, 2009.

[118] W. Hillebrandt and J. C. Niemeyer. Type Ia supernova explosion models. *Ann. Rev. Astron. Astrophys.*, 38:191–230, 2000.

[119] C. Hogan. Nucleation of cosmological phase transitions. *Phys. Lett.*, B133:172–176, 1983.

[120] C. J. Hogan. Gravitational radiation from cosmological phase transitions. *Mon. Not. Roy. Astron. Soc.*, 218:629–636, 1986.

[121] J. A. Holtzman et al. The Sloan Digital Sky Survey-II Photometry and Supernova IA Light Curves from the 2005 Data. *Astron. J.*, 136:2306–2320, 2008.

[122] W. Hu and Z. Haiman. Redshifting Rings of Power. *Phys. Rev.*, D68:063004, 2003.

[123] W. Hu and B. Jain. Joint galaxy - lensing observables and the dark energy. *Phys. Rev.*, D70:043009, 2004.

[124] W. Hu and N. Sugiyama. Small scale cosmological perturbations: An analytic approach. *Astrophys. J.*, 471:542, 1996.

[125] M.-x. Huang, G. Shiu, and B. Underwood. Multifield DBI Inflation and Non-Gaussianities. *Phys. Rev.*, D77:023511, 2008.

[126] E. Hubble. A relation between distance and radial velocity among extra-galactic nebulae. *Proceedings of the National Academy of Sciences*, 15:168–173, 1929.

[127] D. Huterer and M. S. Turner. Probing the dark energy: Methods and strategies. *Phys. Rev.*, D64:123527, 2001.

[128] M. Ishak. Remarks on the formulation of the cosmological constant/dark energy problems. *Found. Phys.*, 37:1470–1498, 2007.

[129] D. Jain, A. Dev, and J. Alcaniz. Cosmological bounds on oscillating dark energy models. *Phys. Lett.*, B656:15 – 18, 2007. ISSN 0370-2693.

[130] H. Jassal, J. Bagla, and T. Padmanabhan. WMAP constraints on low redshift evolution of dark energy. *Mon. Not. Roy. Astron. Soc.*, 356:L11–L16, 2005.

[131] H. Jeffreys. *Theory of Probability, Oxford University Press*. Oxford University Press, Oxford, 3rd edition, 1961.

[132] F. A. Jenet, G. B. Hobbs, W. van Straten, R. N. Manchester, M. Bailes, J. P. W. Verbiest, R. T. Edwards, A. W. Hotan, J. M. Sarkissian, and S. M. Ord. Upper bounds on the low-frequency stochastic gravitational wave background from pulsar timing observations: Current limits and future prospects. *Astrophys. J.*, 653:1571, 2006.

[133] R. Jimenez and A. Loeb. Constraining cosmological parameters based on relative galaxy ages. *Astrophys. J.*, 573:37–42, 2002.

[134] R. Jimenez, L. Verde, T. Treu, and D. Stern. Constraints on the equation of state of dark energy and the Hubble constant from stellar ages and the CMB. *Astrophys. J.*, 593:622–629, 2003.

[135] R. Jimenez, J. MacDonald, J. S. Dunlop, P. Padoan, and J. A. Peacock. Synthetic stellar populations: Single stellar populations, stellar interior models and primordial proto-galaxies. *Mon. Not. Roy. Astron. Soc.*, 349:240, 2004.

[136] S. Kachru et al. Towards inflation in string theory. *JCAP*, 0310:013, 2003.

[137] R. Kallosh. On Inflation in String Theory. *Lect. Notes Phys.*, 738:119–156, 2008.

[138] A. Y. Kamenshchik, U. Moschella, and V. Pasquier. An alternative to quintessence. *Phys. Lett.*, B511:265–268, 2001.

[139] M. Kamionkowski, A. Kosowsky, and A. Stebbins. A probe of primordial gravity waves and vorticity. *Phys. Rev. Lett.*, 78:2058–2061, 1997.

[140] S. Kecskemeti, J. Maiden, G. Shiu, and B. Underwood. DBI inflation in the tip region of a warped throat. *JHEP*, 09:076, 2006.

[141] R. Keisler, C. Reichardt, K. Aird, B. Benson, L. Bleem, et al. A Measurement of the Damping Tail of the Cosmic Microwave Background Power Spectrum with the South Pole Telescope. *Astrophys. J.*, 743:28, 2011.

[142] J. Khoury, B. A. Ovrut, P. J. Steinhardt, and N. Turok. The ekpyrotic universe: Colliding branes and the origin of the hot big bang. *Phys. Rev.*, D64:123522, 2001.

[143] J. Khoury, B. A. Ovrut, P. J. Steinhardt, and N. Turok. Density perturbations in the ekpyrotic scenario. *Phys. Rev.*, D66:046005, 2002.

[144] A. G. Kim, E. V. Linder, R. Miquel, and N. Mostek. Effects of Systematic Uncertainties on the Supernova Determination of Cosmologial Parameters. *Mon. Not. Roy. Astron. Soc.*, 347:909–920, 2004.

[145] Y. Kodama, D. Yonetoku, T. Murakami, S. Tanabe, R. Tsutsui, and T. Nakamura. Gamma-ray bursts in 1.8 ¡ z ¡ 5.6 suggest that the time variation of the dark energy is small. *Mon. Not. Roy. Astron. Soc.: Letters*, 391:L1–L4, 2008. ISSN 1745-3933.

[146] E. Komatsu et al. Five-Year Wilkinson Microwave Anisotropy Probe (WMAP) Observations:Cosmological Interpretation. *Astrophys. J. Suppl.*, 180:330–376, 2009.

[147] E. Komatsu et al. Seven-Year Wilkinson Microwave Anisotropy Probe (WMAP) Observations: Cosmological Interpretation. *Astrophys. J. Suppl.*, 192:18, 2011.

[148] M. Kowalski et al. Improved cosmological constraints from new, old and combined supernova datasets. *Astrophys. J.*, 686:749–778, 2008.

[149] A. Krause. Large Gravitational Waves and Lyth Bound in Multi Brane Inflation. *JCAP*, 0807:001, 2008.

[150] K. Krisciunas. Type ia supernovae and the acceleration of the universe: results from the essence supernova survey. *International Astronomical Union*, 2008.

[151] A. Kurek, O. Hrycyna, and M. Szydlowski. From model dynamics to oscillating dark energy parametrisation. *Phys. Lett.*, B690:337–345, 2010.

[152] A. Kusenko and A. Mazumdar. Gravitational waves from fragmentation of a primordial scalar condensate into Q-balls. *Phys. Rev. Lett.*, 101:211301, 2008.

[153] D. Larson, J. Dunkley, G. Hinshaw, E. Komatsu, M. Nolta, et al. Seven-Year Wilkinson Microwave Anisotropy Probe (WMAP) Observations: Power Spectra and WMAP-Derived Parameters. *Astrophys. J. Suppl.*, 192:16, 2011.

[154] R. Lazkoz and E. Majerotto. Cosmological constraints combining h(z), cmb shift and snia observational data. *JCAP*, 2007:015, 2007.

[155] R. Lazkoz, S. Nesseris, and L. Perivolaropoulos. Exploring cosmological expansion parametrizations with the gold snia data set. *JCAP*, 2005:010, 2005.

[156] O. Le Fevre, G. Vettolani, B. Garilli, L. Tresse, D. Bottini, et al. The VIMOS VLT Deep Survey - First epoch VVDS-deep survey: 11564 spectra with 17.5¡=IAB¡=2, and the redshift distribution over 0¡z¡=5. *Astron. Astrophys.*, 439:845–862, 2005.

[157] H. S. Leavitt. 1777 variables in the Magellanic Clouds. *Annals of Harvard College Observatory*, 60:87–108, 1908.

[158] O. Lechtenfeld, A. D. Popov, and S. Uhlmann. Exact solutions of berkovits' string field theory. *Nuclear Physics B*, 637:119 – 142, 2002. ISSN 0550-3213.

[159] B. Leibundgut. Cosmological Implications from observations of Type Ia supernovae. *Ann. Rev. Astron. Astrophys.*, 39:67–98, 2001.

[160] R. G. Leigh. Dirac-Born-Infeld Action from Dirichlet Sigma Model. *Mod. Phys. Lett.*, A4:2767, 1989.

[161] G. Lemaitre. A homogeneous Universe of constant mass and growing radius accounting for the radial velocity of extragalactic nebulae. *Annales Soc. Sci. Brux. Ser. I Sci. Math. Astron. Phys.*, A47:49–59, 1927.

[162] C. Leng. The residual information criterion, corrected. 2007. URL `http://arxiv.org/abs/0711.1918v1`.

[163] J. Lesgourgues. The Cosmic Linear Anisotropy Solving System (CLASS) I: Overview. 2011. URL `http://arxiv.org/abs/1104.2932v2`.

[164] A. Lewis. CAMB Notes. `http://cosmologist.info/notes/CAMB.pdf`.

[165] A. Lewis and S. Bridle. CosmoMC Notes. `http://cosmologist.info/notes/CosmoMC.pdf`.

[166] A. Lewis and S. Bridle. Cosmological parameters from cmb and other data: A monte carlo approach. *Phys. Rev.*, D66:103511, 2002.

[167] A. Lewis, A. Challinor, and A. Lasenby. Efficient computation of CMB anisotropies in closed FRW models. *Astrophys. J.*, 538:473–476, 2000.

[168] M. Li. A model of holographic dark energy. *Phys. Lett.*, B603:1, 2004.

[169] A. R. Liddle. Acceleration of the universe. *New Astron.Rev.*, 45:235–253, 2001. Companion paper to astro-ph/0009492 by Pedro Viana.

[170] A. R. Liddle, P. Mukherjee, and D. Parkinson. Cosmological model selection. *Astron. Geophys.*, 47:4.30–4.33, 2006.

[171] A. R. Liddle, P. S. Corasaniti, M. Kunz, P. Mukherjee, D. Parkinson, and R. Trotta. Comment on 'tainted evidence: cosmological model selection versus fitting', by eric v. linder and ramon miquel (astro-ph/0702542v2). 2007. URL `http://arxiv.org/abs/astro-ph/0703285`.

[172] J. E. Lidsey and D. Seery. Primordial Non-Gaussianity and Gravitational Waves: Observational Tests of Brane Inflation in String Theory. *Phys. Rev.*, D75:043505, 2007.

[173] A. D. Linde. A New Inflationary Universe Scenario: A Possible Solution of the Horizon, Flatness, Homogeneity, Isotropy and Primordial Monopole Problems. *Phys. Lett.*, B108:389–393, 1982.

[174] E. V. Linder. Exploring the expansion history of the universe. *Phys. Rev. Lett.*, 90: 091301, 2003.

[175] E. V. Linder. On oscillating dark energy. *Astroparticle Physics*, 25:167 – 171, 2006. ISSN 0927-6505.

[176] E. V. Linder. Biased Cosmology: Pivots, Parameters, and Figures of Merit. *Astropart.Phys.*, 26:102–110, 2006.

[177] E. V. Linder and D. Huterer. How many dark energy parameters? *Phys. Rev. D*, 72: 043509, 2005.

[178] J. Liu, H. Li, J. Xia, and X. Zhang. Testing Oscillating Primordial Spectrum and Oscillating Dark Energy with Astronomical Observations. *JCAP*, 0907:017, 2009.

[179] D. H. Lyth and A. R. Liddle. *The Primordial Density Perturbation: Cosmology, Inflation and the Origin of Structure*. Cambridge University Press, 2009.

[180] C.-P. Ma and E. Bertschinger. Cosmological perturbation theory in the synchronous and conformal newtonian gauges. *Astrophys. J.*, 455:7, 1995.

[181] J.-Z. Ma and X. Zhang. Probing the dynamics of dark energy with novel parametrizations. *Phys. Lett.*, B699:233–238, 2011.

[182] R. Maartens. Brane cosmology, 2004. Talk given at 39th Rencontres de Moriond Workshop on Exploring the Universe: Contents and Structures of the Universe, La Thuile, Italy, 28 Mar - 4 Apr 2004.

[183] D. J. C. MacKay. *Information Theory, Inference and Learning Algorithms*. Cambrdige University Press, 2003.

[184] M. Maggiore. Gravitational wave experiments and early universe cosmology. *Phys. Rept.*, 331:283–367, 2000.

[185] G. Mangano, G. Miele, S. Pastor, T. Pinto, O. Pisanti, et al. Relic neutrino decoupling including flavor oscillations. *Nucl. Phys.*, B729:221–234, 2005.

[186] D. Martin and A. Albrecht. Talk about Pivots. 2006. URL `http://arxiv.org/abs/astro-ph/0604401v1`.

[187] J. Martin and M. Yamaguchi. Dbi-essence. *Phys. Rev.*, D77:123508, 2008.

[188] A. Mazumdar and H. Stoica. Exciting gauge field and gravitons in a brane-anti-brane annihilation. *Phys. Rev. Lett.*, 102:091601, 2009.

[189] P. McDonald et al. The Linear Theory Power Spectrum from the Lyman-alpha Forest in the Sloan Digital Sky Survey. *Astrophys. J.*, 635:761–783, 2005.

[190] P. Meszaros. Gamma Ray Bursts. 2012. URL `http://arxiv.org/abs/1204.1897v2`.

[191] N. Metropolis, A. Rosenbluth, M. Rosenbluth, A. Teller, and E. Teller. Equation of state calculations by fast computing machines. *J. Chem. Phys.*, 21:1087–1092, 1953.

[192] C. W. Misner, K. Thorne, and J. Wheeler. *Gravitation*. W.H Freeman and Company, San Francisco, 1974.

[193] R. M. Neal. Probabilistic inference using markov chain Monte Carlo methods. (CRG-TR-93-1), 1993. URL `http://www.cs.utoronto.ca/~radford/papers-online.html`.

[194] S. Nesseris and L. Perivolaropoulos. Comparison of cosmological models using recent supernova data. *Phys. Rev.*, D70:043531, 2004.

[195] S. Nojiri and S. D. Odintsov. The oscillating dark energy: future singularity and coincidence problem. *Phys. Lett.*, B637:139 – 148, 2006. ISSN 0370-2693.

[196] S. Olmez, V. Mandic, and X. Siemens. Gravitational-Wave Stochastic Background from Kinks and Cusps on Cosmic Strings. *Phys. Rev.*, D81:104028, 2010.

[197] J. Oort. The force exerted by the stellar system in the direction perpendicular to the galactic plane and some related problems. *Bulletin of the Astronomical Institutes of the Netherlands*, 6:249, 1932.

[198] J. H. Oort. Some problems concerning the distribution of luminosities and peculiar velocities of extragalactic nebulae. *Bulletin of the Astronomical Institutes of the Netherlands*, 6:155, 1931.

[199] T. Padmanabhan. Cosmological constant: The Weight of the vacuum. *Phys. Rept.*, 380:235–320, 2003.

[200] T. Padmanabhan and T. R. Choudhury. Can the clustered dark matter and the smooth dark energy arise from the same scalar field? *Phys. Rev.*, D66:081301, 2002.

[201] J. A. Peacock and S. J. Dodds. Nonlinear evolution of cosmological power spectra. *Mon. Not. Roy. Astron. Soc.*, 280:L19, 1996.

[202] P. Peebles and B. Ratra. The Cosmological constant and dark energy. *Rev.Mod.Phys.*, 75:559–606, 2003.

[203] H. V. Peiris, D. Baumann, B. Friedman, and A. Cooray. Phenomenology of D-Brane Inflation with General Speed of Sound. *Phys. Rev.*, D76:103517, 2007.

[204] A. A. Penzias and R. W. Wilson. A Measurement of excess antenna temperature at 4080- Mc/s. *Astrophys. J.*, 142:419–421, 1965.

[205] W. Percival. Geometrical constraints from galaxy clustering measurements based on euclid spectroscopy. URL `http://sci.esa.int/science-e/www/object/doc.cfm?fobjectid=46450`.

[206] W. Percival. Baryon acoustic oscillations. In H. K. Klckner, S. Rawlings, M. Jarvis, and T. A., editors, *Cosmology, Galaxy Formation and Astroparticle Physics on the Pathway to the SKA*, page 187. ASTRON, 2006.

[207] W. J. Percival et al. The 2dF Galaxy Redshift Survey: The Power spectrum and the matter content of the Universe. *Mon. Not. Roy. Astron. Soc.*, 327:1297, 2001.

[208] W. J. Percival et al. Measuring the baryon acoustic oscillation scale using the sdss and 2dfgrs. *Mon. Not. Roy. Astron. Soc*, 381:1053–1066, 2007.

[209] W. J. Percival et al. Baryon Acoustic Oscillations in the Sloan Digital Sky Survey Data Release 7 Galaxy Sample. *Mon. Not. Roy. Astron. Soc.*, 401:2148–2168, 2010.

[210] S. Perlmutter et al. Measurements of omega and lambda from 42 high-redshift supernovae. *Astrophy. J.*, 517:565–586, 1999.

[211] M. Phillips. The absolute magnitudes of Type IA supernovae. *Astrophys. J.*, 413: L105–L108, 1993.

[212] A. C. Pope et al. Cosmological Parameters from Eigenmode Analysis of Sloan Digital Sky Survey Galaxy Redshifts. *Astrophys. J.*, 607:655–660, 2004.

[213] W. Press, S. Teukolsky, W. Vetterling, and B. Flannery. *Numerical Recipes in C*. Cambridge University Press, Cambridge, UK, 2nd edition, 1992.

[214] F. Quevedo. Phenomenological aspects of D-branes. 2002. Prepared for ICTP Spring School on Superstrings and Related Matters, Trieste, Italy, 18-26 Mar 2002.

[215] A. C. S. Readhead et al. Extended Mosaic Observations with the Cosmic Background Imager. *Astrophys. J.*, 609:498–512, 2004.

[216] A. Refregier. Weak Gravitational Lensing by Large-Scale Structure. *Ann. Rev. Astron. Astrophys.*, 41:645–668, 2003.

[217] A. Refregier, A. Amara, T. Kitching, and A. Rassat. iCosmo: an Interactive Cosmology Package. *Astron. Astrophys.*, 528:A33, 2011.

[218] A. Refregier et al. Euclid Imaging Consortium Science Book. 2010.

[219] M. B. Ribeiro and W. R. Stoeger. Relativistic cosmology number counts and the luminosity function. *Astrophys. J.*, 592:1–16, 2003.

[220] A. G. Riess et al. Observational Evidence from Supernovae for an Accelerating Universe and a Cosmological Constant. *Astron. J.*, 116:1009–1038, 1998.

[221] A. G. Riess et al. Type Ia Supernova Discoveries at z¿1 From the Hubble Space Telescope: Evidence for Past Deceleration and Constraints on Dark Energy Evolution. *Astrophys. J.*, 607:665–687, 2004.

[222] A. G. Riess et al. New Hubble Space Telescope Discoveries of Type Ia Supernovae at z¿1: Narrowing Constraints on the Early Behavior of Dark Energy. *Astrophys. J.*, 659:98–121, 2007.

[223] A. G. Riess et al. A Redetermination of the Hubble Constant with the Hubble Space Telescope from a Differential Distance Ladder. *Astrophys. J.*, 699:539–563, 2009.

[224] W. Rindler. Visual horizons in world-models. *Gen. Rel. Grav.*, 34:133–153, 2002. Original Mon. Not. Roy. Astron. Soc. article reprinted in Gen. Rel. Grav.

[225] S. A. Rodney, A. G. Riess, T. Dahlen, L.-G. Strolger, H. C. Ferguson, et al. A Type Ia Supernova at Redshift 1.55 in Hubble Space Telescope Infrared Observations from CANDELS. *Astrophys. J.*, 746:5, 2012.

[226] V. A. Rubakov, M. V. Sazhin, and A. V. Veryaskin. Graviton Creation in the Inflationary Universe and the Grand Unification Scale. *Phys. Lett.*, B115:189–192, 1982.

[227] D. Saez-Gomez. Oscillating Universe from inhomogeneous EoS and coupled dark energy. *Grav. Cosmol.*, 15:134–140, 2009.

[228] V. Sahni. Dark matter and dark energy. *Lect. Notes Phys.*, 653:141–180, 2004.

[229] V. Sahni and L.-M. Wang. A New cosmological model of quintessence and dark matter. *Phys. Rev.*, D62:103517, 2000.

[230] V. Sahni, T. D. Saini, A. A. Starobinsky, and U. Alam. Statefinder: A New geometrical diagnostic of dark energy. *JETP Lett.*, 77:201–206, 2003.

[231] T. D. Saini, S. Raychaudhury, V. Sahni, and A. A. Starobinsky. Reconstructing the cosmic equation of state from supernova distances. *Phys. Rev. Lett.*, 85:1162–1165, 2000.

[232] R. Salvaterra, M. Della Valle, S. Campana, G. Chincarini, S. Covino, et al. GRB 090423 reveals an exploding star at the epoch of re-ionization. *Nature*, 461:1258–1260, 2009.

[233] A. G. Sanchez, C. M. Baugh, W. Percival, J. Peacock, N. Padilla, et al. Cosmological parameters from CMB measurements and the final 2dFGRS power spectrum. *Mon. Not. Roy. Astron. Soc.*, 366:189–207, 2006.

[234] R. J. Scherrer. Purely kinetic k-essence as unified dark matter. *Phys. Rev. Lett.*, 93: 011301, 2004.

[235] D. Schlegel et al. The BigBOSS Experiment. 2011. URL http://arxiv.org/abs/1106.1706v1.

[236] D. J. Schlegel, C. Bebek, H. Heetderks, S. Ho, M. Lampton, et al. BigBOSS: The Ground-Based Stage IV Dark Energy Experiment. 2009. URL http://arxiv.org/abs/0904.0468v1.

[237] G. Schwarz. Estimating the Dimension of a Model. *The Annals of Statistics*, 6: 461–464, 1978.

[238] U. Seljak and M. Zaldarriaga. Signature of gravity waves in polarization of the microwave background. *Phys. Rev. Lett.*, 78:2054–2057, 1997.

[239] U. Seljak et al. Cosmological parameter analysis including SDSS Ly-alpha forest and galaxy bias: Constraints on the primordial spectrum of fluctuations, neutrino mass, and dark energy. *Phys. Rev.*, D71:103515, 2005.

[240] I. Sendra and R. Lazkoz. Supernova and baryon acoustic oscillation constraints on (new) polynomial dark energy parametrizations: current results and forecasts. *Mon. Not. Roy. Astron. Soc.*, 422:776–793, 2012.

[241] H.-J. Seo and D. J. Eisenstein. Probing Dark Energy with Baryonic Acoustic Oscillations from Future Large Galaxy Redshift Surveys. *Astrophys. J.*, 598:720–740, 2003.

[242] H.-J. Seo and D. J. Eisenstein. Improved forecasts for the baryon acoustic oscillations and cosmological distance scale. *Astrophys. J.*, 665:14–24, 2007.

[243] D. A. Shaddock. An overview of the Laser Interferometer Space Antenna. *Publ. Astron. Soc. Austral.*, 26:128–132, 2009.

[244] A. Shafieloo, V. Sahni, and A. A. Starobinsky. Is cosmic acceleration slowing down? *Phys. Rev.*, D80:101301, 2009.

[245] X. Siemens, V. Mandic, and J. Creighton. Gravitational-wave stochastic background from cosmic strings. *Phys. Rev. Lett.*, 98:111101, 2007.

[246] X. Siemens et al. Gravitational wave bursts from cosmic (super)strings: Quantitative analysis and constraints. *Phys. Rev.*, D73:105001, 2006.

[247] J. Silk. Cosmic black body radiation and galaxy formation. *Astrophys. J.*, 151:459–471, 1968.

[248] E. Silverstein and D. Tong. Scalar Speed Limits and Cosmology: Acceleration from D- cceleration. *Phys. Rev.*, D70:103505, 2004.

[249] J. Simon, L. Verde, and R. Jimenez. Constraints on the redshift dependence of the dark energy potential. *Phys. Rev.*, D71:123001, 2005.

[250] V. M. Slipher. Spectrographic Observations of Nebulae. *Popular Astronomy*, 23: 21–24, 1915.

[251] A. Slosar. A New Figure of Merit for Dark Energy Studies. 2010. URL `http://arxiv.org/abs/1003.5959v1`.

[252] I. Smail, R. S. Ellis, and M. J. Fitchett. Gravitational Lensing of Distant Field Galaxies by Rich Clusters - Part One - Faint Galaxy Redshift Distributions. *Mon. Not. Roy. Astron. Soc.*, 270:245–270, 1994.

[253] T. L. Smith, M. Kamionkowski, and A. Cooray. Direct detection of the inflationary gravitational wave background. *Phys. Rev.*, D73:023504, 2006.

[254] T. L. Smith, E. Pierpaoli, and M. Kamionkowski. A new cosmic microwave background constraint to primordial gravitational waves. *Phys. Rev. Lett.*, 97:021301, 2006.

[255] T. L. Smith, S. Das, and O. Zahn. Constraints on neutrino and dark radiation interactions using cosmological observations. *Phys. Rev.*, D85:023001, 2012.

[256] G. F. Smoot, C. Bennett, A. Kogut, E. Wright, J. Aymon, et al. Structure in the COBE differential microwave radiometer first year maps. *Astrophys. J.*, 396:L1–L5, 1992.

[257] T. P. Sotiriou and V. Faraoni. f(R) Theories Of Gravity. *Rev. Mod. Phys.*, 82:451–497, 2010.

[258] M. Spalinski. On Power Law Inflation in DBI Models. *JCAP*, 0705:017, 2007.

[259] M. Spalinski. On the Slow Roll Expansion for Brane Inflation. *JCAP*, 0704:018, 2007.

[260] M. Spalinski. A consistency relation for power law inflation in DBI models. *Phys. Lett.*, B650:313–316, 2007.

[261] D. N. Spergel et al. First Year Wilkinson Microwave Anisotropy Probe (WMAP) Observations: Determination of Cosmological Parameters. *Astrophys. J. Suppl.*, 148: 175–194, 2003.

[262] D. N. Spergel et al. Wilkinson Microwave Anisotropy Probe (WMAP) three year results: Implications for cosmology. *Astrophys. J. Suppl.*, 170:377, 2007.

[263] D. J. Spiegelhalter, N. G. Best, B. P. Carlin, and A. Van Der Linde. Bayesian measures of model complexity and fit. *Journal of the Royal Statistical Society - Series B: Statistical Methodology*, 64:583–639, 2002.

[264] A. A. Starobinsky. Cosmic Background Anisotropy Induced by Isotropic Flat- Spectrum Gravitational-Wave Perturbations. *Sov. Astron. Lett.*, 11:133, 1985.

[265] D. Stern, A. Connolly, P. Eisenhardt, R. Elston, B. Holden, et al. First results from the spices survey. 2000. URL `http://arxiv.org/abs/astro-ph/0012146v1`.

[266] D. Stern, R. Jimenez, L. Verde, M. Kamionkowski, and S. A. Stanford. Cosmic Chronometers: Constraining the Equation of State of Dark Energy. I: H(z) Measurements. *JCAP*, 1002:008, 2010.

[267] D. Stern, R. Jimenez, L. Verde, S. A. Stanford, and M. Kamionkowski. Cosmic Chronometers: Constraining the Equation of State of Dark Energy. II. A Spectroscopic Catalog of Red Galaxies in Galaxy Clusters. *Astrophys. J. Suppl.*, 188:280–289, 2010.

[268] M. Sullivan et al. SNLS3: Constraints on Dark Energy Combining the Supernova Legacy Survey Three Year Data with Other Probes. *Astrophys. J.*, 737:102, 2011.

[269] S. Sullivan, D. Sarkar, S. Joudaki, A. Amblard, D. E. Holz, et al. Beyond two dark energy parameters. *Phys. Rev. Lett.*, 100:241302, 2008.

[270] N. Suzuki, D. Rubin, C. Lidman, G. Aldering, R. Amanullah, et al. The Hubble Space Telescope Cluster Supernova Survey: V. Improving the Dark Energy Constraints Above z>1 and Building an Early-Type-Hosted Supernova Sample. *Astrophys. J.*, 746:85, 2012.

[271] T. T. Takeuchi. Application of the information criterion to the estimation of galaxy luminosity function. *Astrophys. Space Sci.*, 271:213–226, 2000.

[272] N. Tanvir, D. Fox, A. Levan, E. Berger, K. Wiersema, et al. A gamma-ray burst at a redshift of z 8.2. *Nature*, 461:1254–1257, 2009.

[273] A. N. Taylor and T. D. Kitching. Analytic methods for cosmological likelihoods. *Mon. Not. Roy. Astron. Soc.*, 408:865–875, 2010. ISSN 1365-2966.

[274] M. Tegmark et al. Cosmological parameters from sdss and wmap. *Phys. Rev. D*, 69: 103501, 2004.

[275] R. Trotta. private comunication.

[276] R. Trotta. *Cosmic microwave background anisotropies: Beyond standard parameters*. PhD thesis, 2004. Ph.D.Thesis Advisor: (Ruth Durrer).

[277] R. Trotta. Forecasting the Bayes factor of a future observation. *Mon. Not. Roy. Astron. Soc.*, 378:819–824, 2007.

[278] A. Upadhye, M. Ishak, and P. J. Steinhardt. Dynamical dark energy: Current constraints and forecasts. *Phys. Rev.*, D72:063501, 2005.

[279] J. Urrestilla, N. Bevis, M. Hindmarsh, and M. Kunz. Cosmic string parameter constraints and model analysis using small scale Cosmic Microwave Background data. *JCAP*, 1112:021, 2011.

[280] J. Väliviita. *The Nature of Primordial Perturbations in Light of CMB Observations*. PhD thesis, Helsinki Institute of Physics, 2005.

[281] R. Van Haasteren et al. *Mon. Not. Roy. Astron. Soc.*, 414:3117, 2011.

[282] L. Van Waerbeke et al. Cosmic Shear Statistics and Cosmology. *Astron. Astrophys.*, 374:757–769, 2001.

[283] P. T. P. Viana, R. C. Nichol, and A. R. Liddle. Constraining the Matter Power Spectrum Normalization using the SDSS/RASS and REFLEX Cluster surveys. *Astrophys. J.*, 569:L75, 2002.

[284] A. Vilenkin. GRavitational Radiation from cosmic strings . *Phys. Lett.*, B107:47–50, 1981.

[285] F. Y. Wang and Z. G. Dai. Constraining dark energy and cosmological transition redshift with type ia supernovae. *Chin. J. Astron. Astrophys.*, 6:561–571, 2006.

[286] Y. Wang. Figure of merit for dark energy constraints from current observational data. *Phys. Rev. D*, 77:123525, 2008.

[287] Y. Wang and P. Mukherjee. Observational Constraints on Dark Energy and Cosmic Curvature. *Phys. Rev.*, D76, 2007.

[288] Y. Wang, W. Percival, A. Cimatti, P. Mukherjee, L. Guzzo, et al. Designing a space-based galaxy redshift survey to probe dark energy. *Mon. Not. Roy. Astron. Soc.*, 409:737, 2010.

[289] J. Weller and A. Albrecht. Future supernovae observations as a probe of dark energy. *Phys. Rev.*, D65:103512, 2002.

[290] C. Wetterich. Phenomenological parameterization of quintessence. *Phys. Lett.*, B594: 17–22, 2004.

[291] E. Witten. Cosmic Separation of Phases. *Phys. Rev.*, D30:272–285, 1984.

[292] W. M. Wood-Vasey et al. Observational Constraints on the Nature of the Dark Energy: First Cosmological Results from the ESSENCE Supernova Survey. *Astrophys. J.*, 666:694–715, 2007.

[293] A. Wright. Nobel Prize 2011: Perlmutter, Schmidt & Riess. *Nature Physics*, 7:833, 2011.

[294] J.-Q. Xia, B. Feng, and X. Zhang. Constraints on oscillating quintom from supernova, microwave background and galaxy clustering. *Mod. Phys. Lett.*, A20:2409, 2005.

[295] J.-Q. Xia, G.-B. Zhao, H. Li, B. Feng, and X. Zhang. Features in the dark energy equation of state and modulations in the hubble diagram. *Phys. Rev.*, D74:083521, 2006.

[296] J.-Q. Xia, H. Li, G.-B. Zhao, and X. Zhang. Probing for the Cosmological Parameters with PLANCK Measurement. *Int. J. Mod. Phys.*, D17:2025–2048, 2008.

[297] L.-I. Xu, C.-W. Zhang, B.-R. Chang, and H.-Y. Liu. Reconstruction of Deceleration Parameters from Recent Cosmic Observations. 2007.

[298] D. Yonetoku, T. Murakami, T. Nakamura, R. Yamazaki, A. Inoue, et al. Gamma-ray burst formation rates inferred from the spectral peak energy-peak luminosity relation. *Astrophys. J.*, 609:935, 2004.

[299] I. Zlatev, L.-M. Wang, and P. J. Steinhardt. Quintessence, Cosmic Coincidence, and the Cosmological Constant. *Phys. Rev. Lett.*, 82:896–899, 1999.

[300] F. Zwicky. Die Rotverschiebung von extragalaktischen Nebeln. *Helv. Phys. Acta*, 6: 110, 1933.

[301] F. Zwicky. On the Masses of Nebulae and of Clusters of Nebulae. *Astrophys. J.*, 86: 217+, 1937.